Totally Asymmetric Simple Exclusion Process With Finite Resources

Larry Jonathan Cook

Dissertation submitted to the Faculty of the
Virginia Polytechnic Institute and State University
in partial fulfillment of the requirements for the degree of

Doctor of Philosophy
in
Physics

Royce K. P. Zia, Chair
Beate Schmittmann, co-Chair
Michel J. F. Pleimling
Rahul V. Kulkarni

December 4, 2009
Blacksburg, Virginia

Keywords: TASEP, open-boundary, protein synthesis

Totally Asymmetric Simple Exclusion Processes With Finite Resources

Larry Jonathan Cook

(ABSTRACT)

In many situations in the world, the amount of resources available for use is limited. This statement is especially true in the cells of living organisms. During the translation process in protein synthesis, ribosomes move along the mRNA strand constructing proteins based on the sequence of codons that form a gene. The totally asymmetric simple exclusion process (TASEP) models well the translation process. However, these genes are constantly competing for ribosomes and other resources in the cell. To see how finite resources and competition affects such a system, we must construct a simple model to account for the limited resources.

We consider coupling multiple TASEPs to a finite reservoir of particles where the entry rate of particles into the TASEPs depends on the number of particles left in the reservoir. Starting with a single TASEP connected to the reservoir, we study the system using both Monte Carlo simulations and theoretical approaches. We explore how the average overall density, density profile, and current change as a function of the number of particles initially in the reservoir for various parameters. New features arise not seen in the ordinary TASEP model, even for a single TASEP connected to the pool of particles. These features include a localized shock in the density profile. To explain what is seen in the simulations, we use an appropriately generalized version of a domain wall theory.

The dynamics of the TASEPs with finite resources are also studied through the power spectra associated with the total particle occupancy of each TASEP and the reservoir. Again, we find new phenomena not seen in the power spectrum of the ordinary TASEP. For a single constrained TASEP, we find a suppression at low frequencies when compared to the power spectrum of the ordinary TASEP. The severity of this suppression is found to depend on how the entry rate changes with respect to the number of particles in the pool. For two TASEPs of different lengths, we find an enhancement of the power spectrum of the smaller TASEP when compared to the ordinary TASEP's power spectrum. We explain these findings using a linearized Langevin equation.

Finally, we model competition between ten genes found in Escherichia coli using a modified version of the TASEP. This modified version includes extended objects and inhomogeneous internal hopping rates. We use the insight gained from the previous studies of finite resources and competition as well as other studies to gain some insight into how competition affects protein production.

This work is supported by the NSF through Grant No. DMR-0705152.

Dedication

I dedicate this work to my wife, Emily.

Acknowledgments

I first and foremost would like to acknowledge my adviser Dr. Royce Zia, who has great enthusiasm for research and knowledge. He has assisted me greatly in getting to this point in my academic career. He is an excellent mentor and teacher. I would also like to thank my committee members Dr. Beate Schmittmann, Dr. Michel Pleimling, and Dr. Rahul Kulkarni for their insightful feedback and assistance in my research.

I would also like to acknowledge my wife, Emily, who has supported me through everything. She read my thesis and gave many helpful comments. Thank you for all you have done for me.

I would like to thank Chris Thomas as well. She always knows what to do when dealing with the graduate school.

Contents

List of Figures

Chapter 1

Introduction

Equilibrium statistical mechanics is one of the great achievements of the twentieth century physics. It connects the microscopic description of the world to the macroscopic view of thermodynamics quantities. While describing the dynamics of one or two particles in a box is simple, keeping track of 10^{24} particles individually is impossible (unless they are non-interacting), even with modern computers. Yet, a comprehensive framework has been developed to successfully describe the probability of finding a system in a particular configuration. From the microscopic description, macroscopic quantities such as the average energy, temperature, entropy, and magnetization are calculated. It has been successfully used to describe certain gases and magnetic materials.

However, equilibrium statistical mechanics has its limitations. For one, the system has to be in equilibrium, i. e. not changing, and with its environment. Many systems in the world are not in an equilibrium state, especially in biology. For instance, a human cannot be described by equilibrium statistical mechanics (unless they are dead). Humans consume food which provide a source of energy for their bodies and expend energy through exercise and other activities. As a result, the environment is constantly changing and a human cannot be regarded as an equilibrium state. Given the abundance of such systems in nature, it is recognized that one of the main challenges in condensed matter physics is to understand non-equilibrium processes [1] and that a new framework be developed which can successfully describe systems far from thermal equilibrium.

In non-equilibrium systems, detailed balance is violated at the microscopic level. Consequently, even stationary distributions are unknown in general, in contrast the Boltzmann distribution which proves to be adequate for *all* systems in thermal equilibrium. While no comprehensive theory has been discovered [2], the study of simple models can serve as a starting point for our attempts at understanding this subject. The classic example of this approach is the Lenz-Ising model [3]. Despite its simplicity, the research on it since 1925 yielded invaluable insights into the existence and the nature of phase transitions in many physical systems [4, 5, 6]. For non-equilibrium systems, a similar class of simple models that

can provide insight is driven diffusive systems [7]. In particular, the Totally Asymmetric Simple Exclusion Process (TASEP) is such a paradigmatic model.

The TASEP is a simple model, yet it displays a rich variety of phenomena. The stationary states and dynamics of this system are well studied [8, 9, 10, 11, 12, 13]. Two types of boundary conditions are usually studied, periodic and open boundary conditions. With periodic boundary conditions, the stationary distribution is trivial, much like the microcanonical ensemble [8]. But, due to the violation of detailed balance, much of the dynamics is non-trivial [14, 15, 16, 17, 18, 19, 20, 21, 22]. For the open TASEP, even the stationary state is non-trivial, displaying three distinct phases [23]. In addition to theoretical interest, the TASEP has been used to model a wide range of physical processes, with potential applications in many fields of science and engineering.

The components and rules of the TASEP are simple. It consists of a one-dimensional lattice with open or periodic boundary conditions. Particles can move to the next site only if that site is empty. The particles move in one direction and cannot move backwards or jump over other particles. For the open TASEP, particles can enter the lattice with a particular probability and leave with another probability. The entry and exit rates determine which of the three phases the system reaches at steady state [23]. This dissertation will focus on modified versions of the open TASEP. The motivation is to use it as a simple model for translation during protein synthesis, a process we briefly review here.

According to the central dogma of molecular biology [24], the general transfer of genetic information in a cell consists of three steps: replication, transcription, and translation. These steps occur in most living organisms [25]. During replication, the DNA molecule makes copies of itself. The genetic information is transferred from the DNA to the messenger RNA (mRNA) through transcription. Finally, a protein is produced from the mRNA sequence during translation. It is the final step, translation, on which we will focus on modeling.

Translation is the process of creating proteins from a mRNA codon sequence [25]. This process consists of three steps – initiation, elongation, and termination [25]. During initiation, the ribosomes assemble on the mRNA before the start codon for the gene. At the start codon, the elongation step begins where the ribosomes move along the mRNA and build a chain of amino acids. The amino acids are brought to the ribosomes by the tRNA, which have a corresponding anti-codon to the codon of the mRNA [25]. The sequence of amino acids for a particular protein is stored as a sequence of codons along the mRNA. Each codon consists of three nucleotides [25]. Since only four nucleotides exist on the mRNA [25], there are 64 possible codons. The rate of an amino acid is added to the chain is proportional to the concentration of the corresponding tRNA [26, 27]. Once the ribosome reaches the stop codon, the protein is complete and the ribosomes are released and can be reused again.

Typically, a mRNA – or gene – is a sequence of up to 1000 codons. Naturally, one question is the rates of production of the proteins. Factors that can affect these rates include initiation time, rarity of the transfer RNA (tRNA) anti-codon corresponding to the mRNA codon, abundance of ribosomes, and ribosome recycling [26, 28]. Many of the factors fall into the

broad category of limiting resources. Since there are only a finite amount of resources in a cell, competition for these resources is ongoing and can be important.

In order to begin to understand how translation works in a cell, we attempt to model the process using the TASEP. It has already been used to model protein synthesis for many decades [29, 30, 31, 32, 33, 34, 35]. The mapping from the translation process to the TASEP is simple – ribosomes are represented by the particles and the mRNA molecule is represented by the one-dimensional lattice. Initiation is modeled through an entry rate probability and termination is modeled through an exit rate probability. While the simplest model consists of constant entry and exit rate along with a homogeneous lattice, many modifications have been studied, which include inhomogeneous hopping rates [32, 33] and large particles [34, 35]. Particles covering more than one site are used to model the large size of the ribosomes covering more than one codon. Since the rate an amino acid is added to the chain is proportional to the tRNA concentration for the particular codon [26, 27], inhomogeneous hopping rates are needed to model the various gene sequences found in nature. Since the rate of expression depends on the resources available in the cell [26], competition for particles is a natural extension of the TASEP model in this context.

Besides translation in protein synthesis, the TASEP has been used to model other systems, some outside the context of biology. These systems include traffics flow [36, 37], surface growth [38, 39], bio-molecular motors [40, 41, 42, 43, 44, 45], and the parking garage problem [46]. In particular, the parking garage problem [46] deals with finite resources. Therefore, a deeper understanding of how limiting the amount of resources and competition for these resources affects a system will increase our knowledge on a wider variety of problems.

This dissertation is structured as follows: In the next chapter, we will present background material and previous results for the TASEP model to lay the foundation for the work in the remainder of the dissertation. In Chapter 3, we discuss the effect of having finite resources and present a theoretical approach to dealing with these effects. In Chapter 4, competition for the resources is introduced into the model by having multiple TASEPs connected to a finite reservoir of particles. In Chapter 5, we present results for competition between ten real genes of Escherichia coli (E. Coli). We conclude with a summary and outlook in Chapter 6.

Chapter 2

Background and Previous Results

In this chapter, we wish to give background information about the TASEP and previously discovered results. The model has been studied over the past couple of decades [8, 9, 10, 11, 12, 13]. It consists of a one-dimensional lattice of length L on which particles move uni-directionally. A particle may move to the next site with rate γ only if that site is empty. Two types of boundary conditions are usually studied, periodic and open. In the periodic boundary case, the number of particles in the TASEP is fixed. The periodic boundary condition gives rise to a trivial stationary state in which all configurations are equally probable [8]. However, the dynamics of the steady state are non-trivial [14, 15, 16, 17, 18, 19, 20, 21, 22]. For the open boundary conditions, particles can enter the lattice at site 1 with a rate α and leave at site L with a rate β. As a result, the number of particles on the lattice fluctuates. A non-trivial phase diagram for α and β is found [23]. There are three different phases consisting of a low density (LD), high density (HD), and maximal current (MC) phase shown in Figure 2.1. Along the coexistence line (red in Fig. 2.1) between the HD and LD phases ($\alpha = \beta$), a shock forms between the high and low density regions and performs a random walk along the entire lattice. For this reason, the coexistence line is sometimes referred to as the "shock phase" (SP). The exact solution is known for all α and β for the open TASEP [9, 10, 11]. While the exact solution exists, other approximations have been formulated to give a similar result, specifically domain wall theory [12, 47, 48]. Reviews on the TASEP model include [49, 50].

2.1 Open TASEP Results

In this dissertation, we will mainly study the TASEP with the open boundary conditions in the steady state. Therefore, a review of the major results is in order. First, we will discuss the average density profile. Examples of typical profiles are shown in Fig. 2.2. We will separate this discussion into two parts: the bulk density and the boundary density profile of

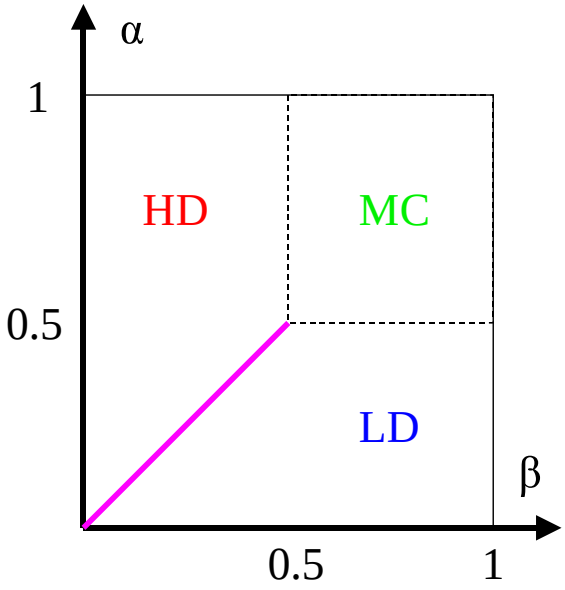

Figure 2.1: Phase diagram for the open TASEP.

the TASEP. In the bulk, the density profile is constant and depends on the phase the system is in [9, 10, 11]. When in the LD phase, particles leave faster than they enter with $\alpha < \beta$ and $\alpha < 1/2$. Thus, the bulk density will be the entry rate α. For the HD phase, particles enter faster than they leave with $\alpha > \beta$ and $\beta < 1/2$. The particles pile up at the exit and into the bulk. Particles leave at a rate β, so they stay on the lattice at a rate $1 - \beta$. Thus, the bulk density is $1 - \beta$. Particle-hole symmetry can also be used to explain the HD phase. Holes enter for the exit site L at a rate β and leave at the entrance with rate α. Therefore the density of holes is β and the density of particles is $1 - \beta$. For the MC phase, both α and β are greater than $1/2$. In this phase, the current is a maximum and the bulk density is $1/2$. For large system sizes, the average overall density ρ is approximately the bulk density value. In the SP, the density profile is linear with an average density of $1/2$. So, to summarize [9, 10, 11]:

$$\rho = \begin{cases} \alpha & \text{LD} & \alpha < \beta; \alpha < 1/2 \\ 1-\beta & \text{HD} & \beta < \alpha; \beta < 1/2 \\ 1/2 & \text{SP} & \alpha = \beta < 1/2 \\ 1/2 & \text{MC} & \alpha, \beta > 1/2 \end{cases} \tag{2.1}$$

Near the boundaries, a different decay to the bulk value is seen for the different phases [9, 10, 11]. In the LD (HD) phase, the density profile decays exponentially from β (α) at exit (entrance) boundary to the bulk value. The localization length for the decay is given by [11]:

$$\xi^{-1} = |\xi_\alpha^{-1} - \xi_\beta^{-1}| \tag{2.2}$$

with

$$\xi_\sigma^{-1} = -\ln[4\sigma(1-\sigma)] \tag{2.3}$$

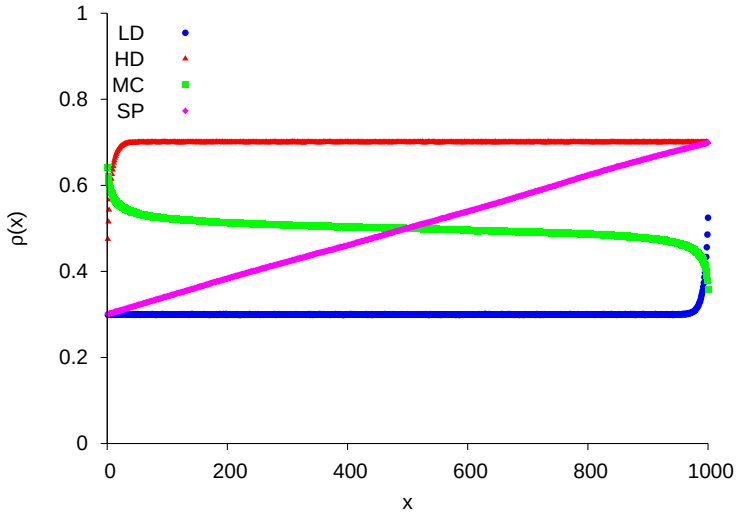

Figure 2.2: Typical average density profiles for the TASEP in the LD, HD, MC, and SP phases.

For the MC phase, there is an algebraic decay of the profile to the bulk value at both the entrance and exit. ξ is divergent in this phase. The SP has no decay since linear profile extends to the boundary.

We now turn our attention to the current J of the system. This quantity has also been computed exactly [9, 10, 11]. In the thermodynamic limit for the LD, HD, and MC phases, the expression for the current in the stationary state is:

$$J = \rho(1 - \rho) \tag{2.4}$$

where ρ is the average overall density given above. The expression has a single maximum at $\rho = 1/2$, which corresponds to a current $J = 1/4$. The maximum only occurs in the MC phase, hence its name. For the SP, the current is given by:

$$J = \alpha(1 - \alpha) = \beta(1 - \beta) \tag{2.5}$$

For systems with a finite length, corrections to J can be calculated from the exact result for any α and β [9, 10].

2.2 Domain Wall Theory

While the exact solution is known for the open TASEP [9, 10, 11], there is a phenomenological theory that reproduces the results called domain wall theory [12, 13, 47, 48]. The domain wall theory assumes a domain wall, or shock, forms between a high density region with density $\rho_+ = 1 - \beta$ near the exit and a low density region with density $\rho_- = \alpha$ near the

entrance. It also assumes that the shock must be located at some point on the lattice and cannot leave. The master equation for the probability of finding the shock at position k, $P(k)$, is given by [13, 47]:

$$\partial_t P(k,t) = D_- P(k+1,t) + D_+ P(k-1,t) - (D_- + D_+)P(k,t) \tag{2.6}$$

The assumption that the shock is located on the lattice gives us reflecting boundary conditions for $P(k)$ [13, 47]:

$$\partial_t P(0,t) = D_- P(1,t) - D_+ P(0,t) \tag{2.7}$$
$$\partial_t P(L,t) = D_+ P(L-1,t) - D_- P(L,t) \tag{2.8}$$

The D_- and D_+ are the hopping rates for the domain wall to move toward the entrance or exit respectively. The rate at which the shock moves is related to the current of the particles or holes in the TASEP. The height of the domain wall also is a factor in the hopping rates. If the difference in the high density and low density is large, then the shock will be less likely to move due to the large number of particles/holes needed to shift the wall in either direction. Thus, the hopping rates are given by [12, 13, 47]:

$$D_- = \frac{\rho_-(1-\rho_-)}{\rho_+ - \rho_-} \tag{2.9}$$
$$D_+ = \frac{\rho_+(1-\rho_+)}{\rho_+ - \rho_-} \tag{2.10}$$

The numerator is the particle/hole current and the denominator is the wall height. For steady state, the master equation can be solved to give [13]:

$$P^*(k) \propto \left(\frac{D_-}{D_+}\right)^{-k} \tag{2.11}$$

The time dependence of the master equation has also been studied [13, 47]. From the quantity $P^*(k)$, the average density profile and average overall density can be calculated in the steady state. The expression for the average overall density is [13]:

$$\rho = \rho_- \frac{\delta}{L}\left[\frac{r}{1-r} - (L+1)\frac{r^{L+1}}{1-r^{L+1}}\right] \tag{2.12}$$

where $\delta = \rho_+ - \rho_- = (1-\beta) - \alpha$ and

$$r = \frac{\rho_-(1-\rho_-)}{\rho_+(1-\rho_+)} = \frac{\alpha(1-\alpha)}{\beta(1-\beta)} \tag{2.13}$$

The average density profile is found using:

$$\rho(x) = \sum_{k=0}^{x}(1-\beta)P^*(k) + \sum_{k=x+1}^{L}\alpha P^*(k) \tag{2.14}$$

The profiles from the domain wall theory are similar to those shown in Fig. 2.2 for the LD, HD, and SP. In [13], the authors show how the profile changes in time when β is suddenly changed forcing the system to go from the LD phase to the HD phase, and vice versa. While the domain wall picture approximates the LD, HD, and SP density profiles well, it fails to quantitatively capture the features of the MC phase. In this phase, the assumption of a single shock forming between a high and low density region is no longer valid. However in [47], the authors use site dependent hopping rates that are derived from the exact solution in the MC phase to correctly account for the algebraic decay at the boundaries. On the other hand, this approach requires the exact solution to be known, which defeats the purpose of using an approximation like DW theory to obtain the density profile.

The localization length of the decay of the density profile in the steady state can also be calculated using the DW theory [12]. The length is given by[12]:

$$\xi = -\ln\left(\frac{D_-}{D_+}\right) = -\ln\left(\frac{\rho_-(1-\rho_-)}{\rho_+(1-\rho_+)}\right) \tag{2.15}$$

This result is the same as the result from the exact solution in Eqn. (2.2) [11]. Thus, the DW theory produces the exact expression for the localization length of the decay of the density profile near the boundaries.

2.3 Power spectrum

The dynamics of the open TASEP have also been studied [12, 13, 47, 51, 52, 53, 54, 55]. In [47, 51, 52], the largest relaxation times and dynamical exponents are calculated in the various phases for different system sizes. The power spectrum $I(\omega)$ associated with the autocorrelation function has been studied in [53, 54]. In [55], the power spectrum associated with the total occupancy N is studied. It is defined to be [55]:

$$I(\omega) = \langle |\tilde{N}(\omega)|^2 \rangle \tag{2.16}$$

where

$$\tilde{N}(\omega) = \sum_t e^{i\omega t} N(t) \tag{2.17}$$

and the bracket indicates an average over configurations. Typical time traces of the total occupancy are shown in Fig. 2.3. For the total occupancy, oscillations are observed in the power spectrum $I(\omega)$ for the LD and HD phases [55]. These oscillations are shown in Fig. 2.4(a). A linear stochastic equation of motion is solved to analytically understand the Monte Carlo simulation results in these two phases. The solution is [55]:

$$I(\omega) = \frac{8ADT}{V^3} Re\left[\frac{e^{ik_+L}-1}{R(1-R)^2} + \frac{e^{ik_-^*L}-1}{R^*(1+R^*)^2}\right] \tag{2.18}$$

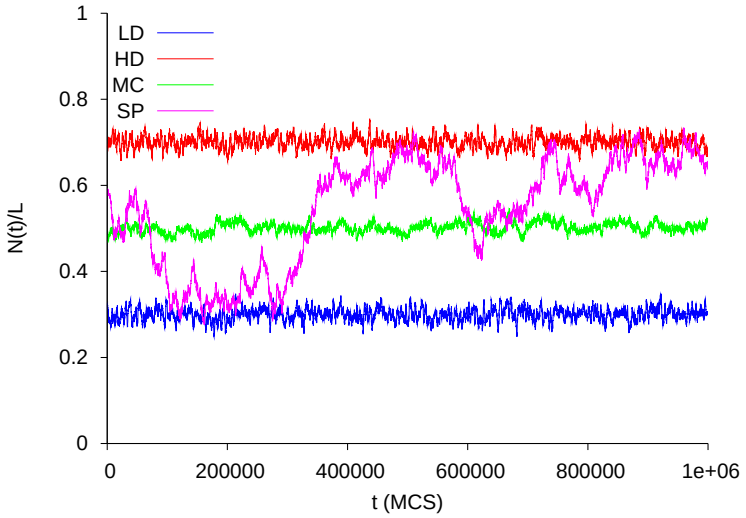

Figure 2.3: Typical time traces for total occupancy $N(t)$ for the TASEP in the LD, HD, MC, and SP phases.

where A is the variance in the noise, D is the diffusion coefficient, $v = 1 - 2\rho$ is the group velocity, $R = \sqrt{1 - 4iD\omega/v^2}$, and $k_\pm = iv(-1 \pm R)/2D$. A and D are both fit parameters in the theory. The authors in [55] found that the oscillations where due, in part, to the finite size of the system by looking at the low ω regime. Then in this regime, Eqn. (2.18) becomes [55]:

$$I(\omega) \approx \frac{2AvT}{D\omega^2}\left[1 - e^{-\frac{D\omega^2 L}{v^3}}\cos(\omega L/v)\right] \tag{2.19}$$

The minima of the oscillations occur every $m = vT/L$ [55], which agree with the simulation results shown in Fig. 2.4(a). To fit the simulation data, the authors use a D value that is much larger than the naive value of $1/2$ [55]. Such a large renormalization of the diffusion coefficient is unexpected. This issue has recently been explored in [56].

For the SP and MC phase, $I(\omega)$ has a power law behavior: $I \sim \omega^p$, where $p = -2$ and $p = -5/3$ for the SP and MC phase respectively [55]. These two phases are shown in Fig. 2.4(b). The exponent in the SP is simply due to the shock performing a random walk on the lattice [55]. Since the shock performs a random walk, so will the total occupancy. Thus for a large system, we have:

$$\partial_t N(t) = \eta(t) \tag{2.20}$$

where $\eta(t)$ is Gaussian noise with zero mean and variance A. The solution of this equation in Fourier space is:

$$\tilde{N}(\omega) = \frac{\tilde{\eta}(\omega)}{-i\omega} \tag{2.21}$$

The power spectrum is then:

$$I(\omega) = \frac{A}{\omega^2} \tag{2.22}$$

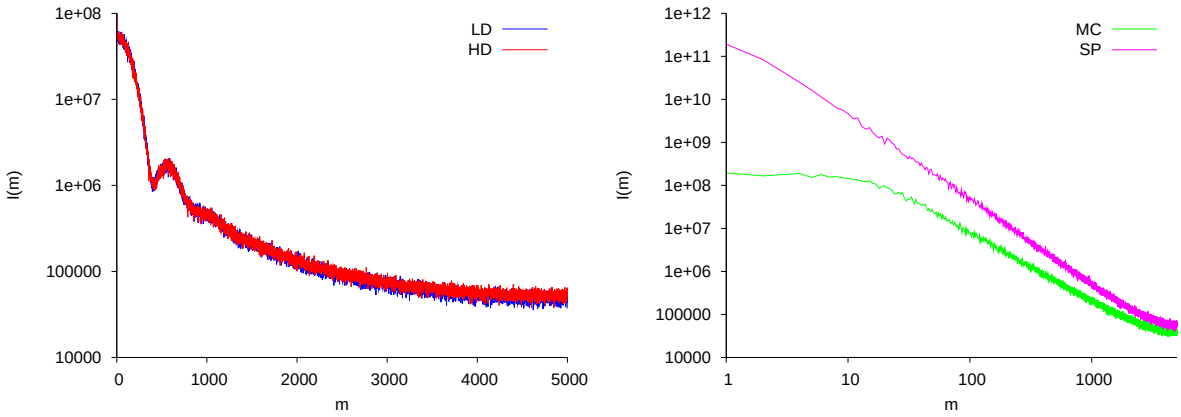

(a) (b)

Figure 2.4: Typical power spectra $I(\omega)$ as a function of $m = \omega T/2\pi$ for the TASEP in the (a) LD, HD, (b) MC, and SP phases.

For the MC phase, the authors in [55] look at the scaling function's two-point correlation in an infinitely long system of the noisy Burgers equation. The two-point correlation is translationally invariant and has a scaling form [55]:

$$C(\xi, \tau) = \xi^{-1} f\left(\xi/\tau^{2/3}\right) \tag{2.23}$$

where $\xi = x - x^{'}$ and $\tau = t - t^{'}$. By using this form to approximate the two-point function in a finite system of length L, the power spectrum becomes [55]:

$$I(\omega) = \omega^{-5/3} G(L\omega^{2/3}) \tag{2.24}$$

If $G(L\omega^{2/3})$ approaches a constant for $\omega \gg L^{-3/2}$, then $I(\omega) \propto \omega^{-5/3}$ [55]. The theoretical results for the SP and MC phase power spectra agree with the simulation data seen in Fig. 2.4(b).

2.4 Constrained TASEP

In this dissertation, we will focus on competition for resources which is closely related to the studies of finite resources in [46, 57]. In [46], the authors study the parking garage problem where cars leave the garage, travel on the road, and re-renter the garage. In [57], the authors are motivated by translation during protein synthesis to study how a fluctuating entry rate that is based on the number of particles remaining in a reservoir affect the overall density and current of the TASEP in the different phases. Since we are also motivated by translation during protein synthesis in a cell, we will review the results in [57]. In [57], a TASEP is modified by connecting it to a reservoir, or "pool", with a finite number of particles. The

entry rate is also modified to depend on the number of particles left in the pool, creating an effective entry rate α_{eff}. It has the form [57]:

$$\alpha_{eff} = \alpha f(N_p) \tag{2.25}$$

where α is a constant, N_p is the number of particles in the pool, and f returns a value between zero and 1 for all N_p. If no particles are in the pool, then nothing can enter the TASEP, so $f(0) = 0$. For a large pool size, we should recover the ordinary TASEP results for a constant entry rate α. Therefore, we have $f(N_p \to \infty) = 1$. To model mRNA and ribosomes, the entry rate should depend linearly on the amount of available resources for a small amount of resources [57]. Thus, f is chosen to be [57]:

$$f(N_p) = \tanh\left(\frac{N_p}{N^*}\right) \tag{2.26}$$

where N^* is a crossover scale chosen to be the number of particles in the ordinary TASEP. Explicitly, we have [57]:

$$N^* = \begin{cases} L/2 & \text{MC; SP} \quad \alpha, \beta \geq 1/2;\ \alpha = \beta \leq 1/2 \\ \alpha L & \text{LD} \qquad \alpha \leq \min(\beta, 1/2) \\ (1-\beta)L & \text{HD} \qquad \beta \leq \min(\alpha, 1/2) \end{cases} \tag{2.27}$$

Simulation results are presented in [57] for α and β chosen to be in the LD, HD, SP, and MC phases, the most interesting of which are the HD phase and SP. In [57], the authors study the average overall density ρ and current J as a function of the total number of particles in the pool and TASEP (N_{tot}). In the LD case in Fig. 2.5(a), they find that the density rises linearly at small N_{tot} and gradually levels off to α for large N_{tot}. In this case, the density is

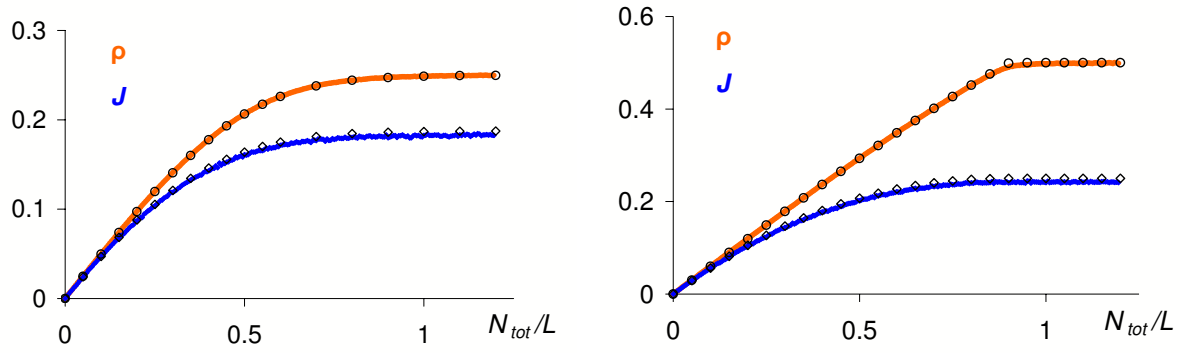

(a) (b)

Figure 2.5: Average overall density ρ as a function of N_{tot} for $L = 1000$ with (a) $\alpha = 0.25$ and $\beta = 0.75$ and (b) $\alpha = \beta = 0.75$. Originally published in [57].

simply the average α_{eff} and can be found using [57]:

$$\rho = \alpha \tanh\left(\frac{N_{tot} - \rho L}{\alpha L}\right) \tag{2.28}$$

From this equation, the small N_{tot} limit give [57]:

$$\rho = \frac{N_{tot}}{2L} \tag{2.29}$$

which is the linear rise seen at small N_{tot}. For the MC case, a similar linear rise in the density is seen, but then quickly levels off to a value of 1/2 when the average α_{eff} approaches 1/2. For both cases, the current is given by $J = \rho(1 - \rho)$.

In the HD phase, the authors find three regions appear when the density ρ is studied as a function of N_{tot} [57], as shown in Fig. 2.6. The linear region at low N_{tot} values corresponds

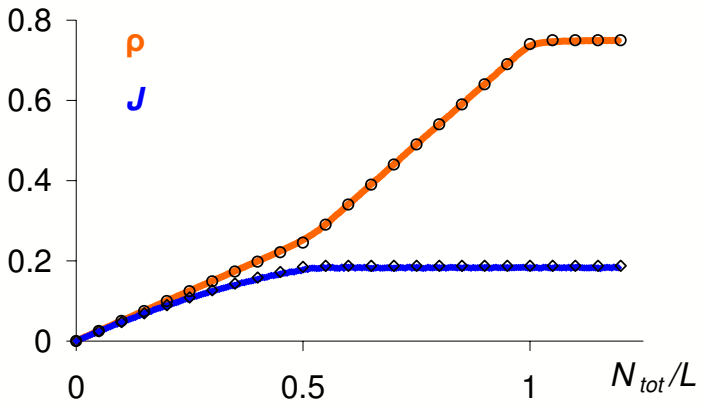

Figure 2.6: Average overall density ρ as a function of N_{tot} for $L = 1000$ with $\alpha = 0.75$ and $\beta = 0.25$. Originally published in [57].

to the TASEP being in a LD state due to the limited number of particles in the system [57]. The flat region at large N_{tot} is where the TASEP is in the HD state. Here, the system has enough particles for both the TASEP and the pool, making $\alpha_{eff} = \alpha$ and $\rho = 1 - \beta$ [57]. In the remaining crossover region between the LD and HD states, the constrained TASEP is crossing the coexistence line between the LD and HD phases with $\alpha_{eff} = \beta$ and entering the SP. Here, the number of particles in the pool remain relatively constant as N_{tot} is increased [57]. The extra particles from the increase in N_{tot} are absorbed into the TASEP, which gives the linear rise seen in Fig. 2.6 for this region. The N_{tot} values at which the system enters and leaves the crossover region are also found in [57]. For the lower N_{tot} value, we have $\alpha_{eff} = \rho = \beta$. This relation leads to [57]

$$N_{tot} = (1 - \beta)L \tanh^{-1}\left(\frac{\beta}{\alpha}\right) + \beta L \tag{2.30}$$

For the upper N_{tot} value, we have $\alpha_{eff} = \beta$ and $\rho = 1 - \beta$. These relations lead to [57]

$$N_{tot} = (1 - \beta)L \tanh^{-1}\left(\frac{\beta}{\alpha}\right) + (1 - \beta)L \tag{2.31}$$

In between these two N_{tot} values, the density goes as [57]

$$\rho = \frac{N_{tot}}{L} - (1-\beta)\tanh^{-1}\left(\frac{\beta}{\alpha}\right) \tag{2.32}$$

The slope of the density is greater in the crossover regime than the slope of the LD state [57], which is what is seen in Fig. 2.6. In contrast to the density, the current does not change at the higher N_{tot} value. The reason for this lack of change is because the current has already reached its final value of $\beta(1-\beta)$ [57]. Before entering the crossover region, the current is given by $J = \rho(1-\rho) = \alpha_{eff}(1-\alpha_{eff})$. Once $\alpha_{eff} = \beta$ and the system enters what would normally be the SP, then $J = \alpha_{eff}(1-\alpha_{eff}) = \beta(1-\beta)$, and it is independent of the density. After leaving the crossover region, the current returns to $J = \rho(1-\rho)$. However, $\rho = 1-\beta$ which leads to $J = \beta(1-\beta)$. Therefore, the current does not change as the system leaves the crossover region [57].

For the SP, the authors find that the density as a function N_{tot} displays a complex transition from the LD state to the SP [57], shown in Fig. 2.7. To explain this result, the authors

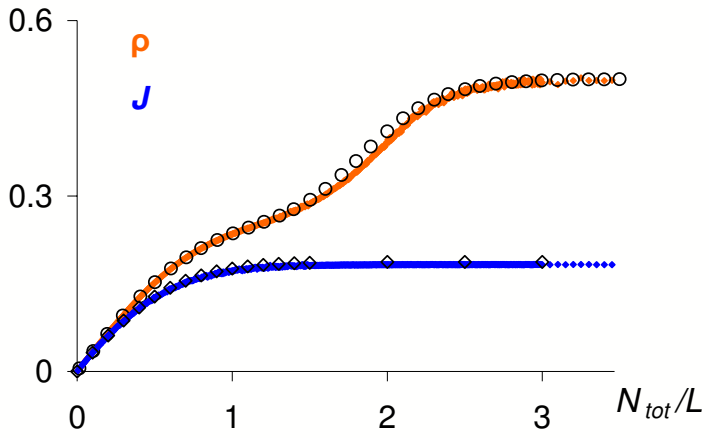

Figure 2.7: Average overall density ρ as a function of N_{tot} for $L = 1000$ with $\alpha = \beta = 0.25$. Originally published in [57].

use the results for the DW theory from [13] by replacing α with α_{eff} in the expression for the average overall density ρ given above in Eqn. (2.12) and solving self-consistently for ρ. The theoretical results agree well with the simulation data as shown in Figs. 2.6 and 2.7, except in the transition region for the SP case [57]. As we will see in the next chapter, this difference along with the density profiles can be better explained by generalizing the DW theory to include the fluctuating α_{eff} in the hopping rates.

2.5 Other modifications to the TASEP model

Besides having finite resources, other modifications to the simple TASEP model have also been studied [31, 32, 33, 34, 35, 40, 41, 42, 43, 44, 45, 46, 57]. Modifications include slow sites [32, 33], large particles [34, 35, 31], and creation and annihilation of particles in the bulk [40, 41, 42, 43, 44, 45]. Since we have in mind protein synthesis as a potential application, there are other aspects of TASEP besides finite resources, which require attention. In particular, we will look at particles covering more than one site and inhomogeneous hopping rates in the interior of the TASEP. The combined effects of large particles and a few slow sites are studied in [34]. Later, we will combine these two extensions with finite resources in order to model competition between 10 genes found in E. coli.

For translation during protein synthesis, ribosomes cover more than one codon [25] and can be modeled in the TASEP using particles that cover more than one site. The effect of extended objects on the open TASEP is an increase of the size of the maximal current phase boundary in Fig. 2.1 [34, 35, 31]. To be in the MC phase, α and β must be greater than $\hat{\chi}$ where

$$\hat{\chi} = \frac{1}{1+\sqrt{\ell}} \tag{2.33}$$

and ℓ is the length of the particle [31, 35]. In terms of the coverage density, the maximum current is reached at a higher coverage density than in the TASEP with $\ell = 1$. This result will be useful when trying to explain how the current changes as a function of the coverage density for the competing real genes.

In addition to extended particles, inhomogeneous hopping rates are used to model the various binding rates of amino acids associated with different codons [26, 27]. In the simplest situation of a TASEP with a few slow sites and $\ell = 1$, the location and distance between the slow sites affects the overall current [32, 33]. However, a real gene has multiple transfer rates, so more than a few slow sites are needed. The more complex case of a TASEP with quenched random disorder in the hopping rates has also been studied [58, 59, 60]. The effect of disorder is the expansion of the MC on the phase diagram in Fig. 2.1. The new boundaries for the MC phase depend on the distribution from which the hopping rates are taken [59, 60]. In [58], the authors accurately predict the current through TASEP using a mean field approach. How the random disorder relates to the rates in real gene is unclear; however, the study of such systems should give insight into the effects of inhomogeneous hopping rates on protein production.

Chapter 3

Single TASEP with Finite Resources

The TASEP with finite resources has been studied previously in [57]. In this chapter, we wish to expand the results presented in [57]. We will investigate the average density profile, which was not studied in [57]. We will also extend the domain wall theory for the ordinary TASEP to include the effects of the finite resources. In [57], the fluctuating entry rate α_{eff} is not taken into account in the domain wall theory. Here, we will add this fluctuation into the master equation for the domain wall. As we will soon see, this fluctuation is needed to account for the average density profile, which exhibits shock localization.

The second part of this chapter will include the simulation and theoretical results for the power spectra of the total occupancy of the constrained TASEP. When only a small amount of particles are available to the TASEP, we see a difference in power spectrum when compared to the ordinary TASEP's power spectra that is studied in [55]. We will explore how the constrained TASEP power spectra relates to the ordinary TASEP power spectra through both simulation and theoretical considerations. The constrained power spectrum can be explained using linearized, discrete Langevin equations for each site on the lattice. The effect of the finite number of particles are taken into account in these equations. Even though we have neglected all quadratic terms, the linear theory gives an explanation for the difference in the two power spectra for a small reservoir size.

For the Monte Carlo simulations, we use a similar method to the one described in [57]. We choose a site at random to update. If the site is occupied and the next site is empty, then the particle moves to the next site. If the last site is chosen and occupied, then the particle leaves the system and returns to the pool with probability β. If the pool is chosen, then a particle can enter the TASEP with probability α_{eff}, provided the first site is empty. One Monte Carlo step (MCS) consists of $L+1$ updates. Data for the overall density and density profile is taken every 100 MCS after the system reaches steady state. The simulation is typically run for 1M MCS. The overall density and density profile are typically averaged over 100 runs.

3.1 Extending domain wall theory

In this section, we wish to extend the domain wall theory to include the effects of the finite number of particles in the pool. While the theoretical results in [57] agree well with the simulation data, there is room for improvement, especially for the SP case. As shown in Fig. 3.1, the overall density from the simple domain wall (SDW) theory used by the authors in [57] slightly differs from the simulation results for $L = 100$ and $L = 1000$. Originally in

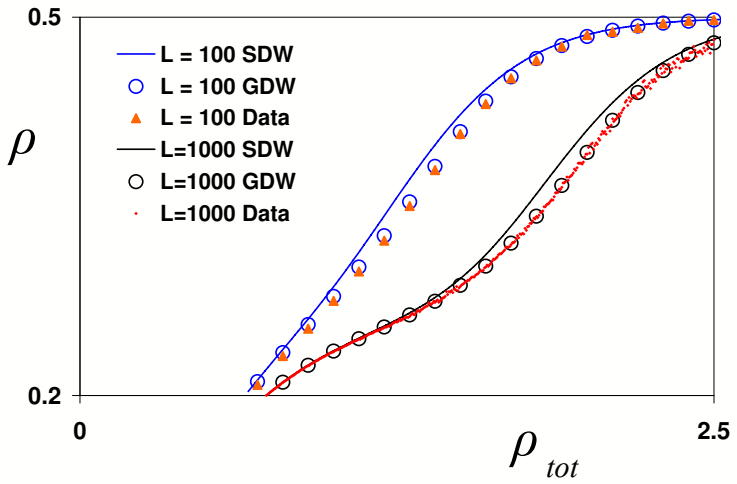

Figure 3.1: Average overall density as a function of $\rho_{tot} = N_{tot}/L$ in the SP ($\alpha = \beta = 0.25$) for $L = 100$ and $L = 1000$. Originally published in [61].

[57], the authors replace α with α_{eff} into the result for the density in [13] given in Eqn. (2.12). By using this equation, the substitution amounts to using the average α_{eff} and does not take into account that the entry rate fluctuates. Therefore, we need to generalize the domain wall theory to include these fluctuations in the entry rate α_{eff} in order to improve upon the theoretical results presented in [57].

The fluctuation in α_{eff} is due to the changing number of particles in the pool. In the model, we specify the total number of particles N_{tot} in the system (pool + TASEP). Using a domain wall approach with a given shock position k, we can estimate the number of particles in the TASEP by using [61]:

$$N = \rho_- k + \rho_+(L-k) = \alpha_{eff} k + (1-\beta)(L-k) \tag{3.1}$$

We can use this information to write

$$\alpha_{eff} = \alpha f(N_{tot} - \alpha_{eff} k - (1-\beta)(L-k)) \tag{3.2}$$

Through this expression, we can solve self-consistently for α_{eff} as a function of k which we will denote $\alpha_{eff,k}$. Previously, the hopping rate in the master equation for the simple domain

wall theory depended upon the ordinary TASEP entry rate α. By replacing α with $\alpha_{eff,k}$ in the expressions for the hopping rate, we obtain a new master equation where the hopping rates depend on where the domain wall is located. The effect of the site dependence is simple to understand. As the wall moves closer to the entrance, less particles will enter into the lattice than leave, thereby forcing the wall to move toward the exit. On the other hand, if the wall moves closer to the exit, then more particles will enter than leave and force the wall to move back toward the entrance. For small N_{tot}, the pool always has a small number of particles. This limit will push the domain wall toward the exit since α_{eff} is small for any k value. Therefore the TASEP will be in the LD phase regardless of the α chosen. Also in this expression for α_{eff}, we are ignoring the time it takes for the fluctuations in the entry rate to reach the domain wall. This omission does not affect the results as long as we are in the steady state, where average quantities are independent of time.

Since we are limiting the number of particles in the system, the domain wall cannot move along the entire lattice if N_{tot} is too small. If all the particles are found in the lattice, then $N = N_{tot}$. The position of the shock associated with this value will be denoted k_{min} and is given by [61]:

$$k_{min} = L - \frac{N_{tot}}{1-\beta} \tag{3.3}$$

At this value, there are no particles left in the pool so the domain wall cannot move toward the entrance anymore. The only direction left for the wall to travel is back toward the exit. This creates a reflecting boundary at k_{min}. This boundary replaces the entrance reflecting boundary condition from the simple domain wall theory. As a result, the probability for finding the shock past this point is zero.

The master equation for this system is given by [61]:

$$\partial_t P(k,t) = D^+_{k-1}P(k-1,t) + D^-_{k+1}P(k+1,t) - (D^-_k + D^+_k)P(k,t) \tag{3.4}$$

with boundary conditions:

$$\partial_t P(k_{min},t) = D^-_{k_{min}+1}P(k_{min}+1,t) - D^+_{k_{min}}P(k_{min},t) \tag{3.5}$$

$$\partial_t P(L,t) = D^+_{L-1}P(L-1,t) - D^-_L P(L,t) \tag{3.6}$$

where

$$D^+_k = \frac{\beta(1-\beta)}{1-\beta-\alpha_{eff,k}} \tag{3.7}$$

$$D^-_k = \frac{\alpha_{eff,k}(1-\alpha_{eff,k})}{1-\beta-\alpha_{eff,k}} \tag{3.8}$$

Both hopping rates now depend on the DW position k. We are interested in the steady state solution $P^*(k)$ of these equations with $\partial_t P(k,t) = 0$. Starting from either boundary, we construct a recursion relation that satisfies detailed balance, namely:

$$D^+_k P^*(k) = D^-_{k+1}P^*(k+1) \tag{3.9}$$

Then the solution is easily found to be:

$$P^*(k) \propto \prod_{\ell=k}^{L-1} \frac{D_{\ell+1}^-}{D_\ell^+} \tag{3.10}$$

and using proper normalization, we get [61]:

$$P^*(k) = \left(\sum_{m=k_{min}}^{k-1} \prod_{\ell=m+1}^{k} \frac{D_{\ell+1}^-}{D_\ell^+} + 1 + \sum_{m=k+1}^{L} \prod_{\ell=k+1}^{m} \frac{D_{\ell+1}^-}{D_\ell^+} \right)^{-1} \tag{3.11}$$

With $P^*(k)$, we can compute the density profile:

$$\rho_i = \sum_{k=k_{min}}^{i} (1-\beta) P^*(k) + \sum_{k=i+1}^{L} \alpha_{eff,k} P^*(k) \tag{3.12}$$

and the overall density $\rho = \sum \rho_i / L$. As mentioned before, there is a slight deviation of the simple DW theory from the simulation data in the SP [57]. However, the generalized domain wall (GDW) theory, which includes the feedback from α_{eff}, has a much better agreement with the simulation data as seen in Fig. 3.1 [61].

Only the overall average density is considered in [57]. Since the domain wall theory also predicts the density profiles, Monte Carlo simulations were run with the same parameters as in [57]. As seen in Fig. 3.2, the GDW theory agrees better with the simulation results for the profile than the SDW theory does in the SP case [61].

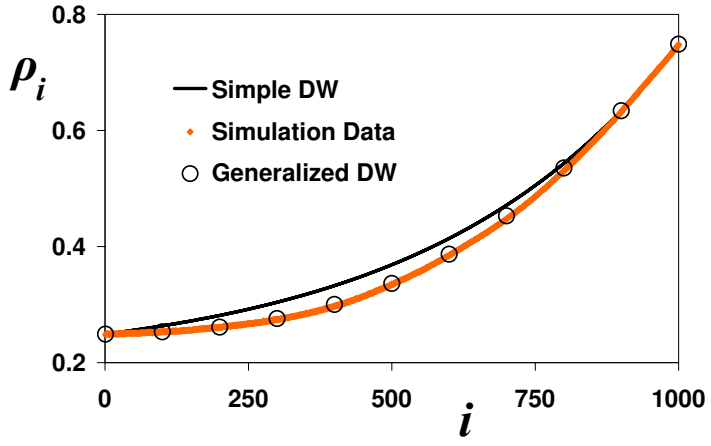

Figure 3.2: Average density profile for $L = 1000$ with $N_{tot} = 2000$ and $\alpha = \beta = 0.25$. Originally published in [61].

The most surprising result came from the density profile in the HD case. During the crossover regime from LD to HD, we find the shock becomes localized to a certain region of the lattice

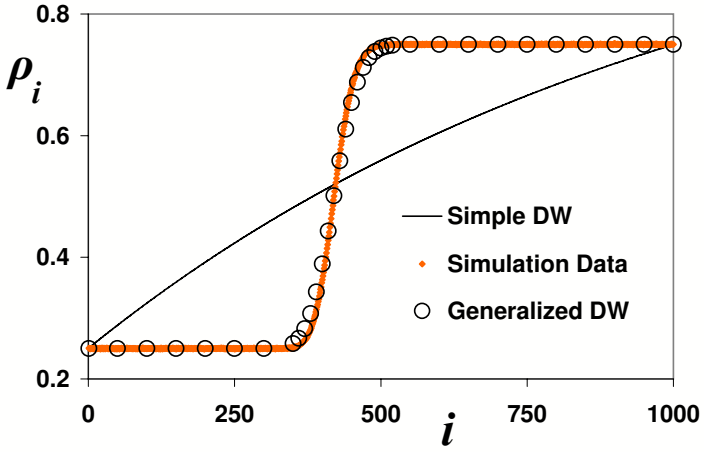

Figure 3.3: Average density profile for $L = 1000$ with $N_{tot} = 800$, $\alpha = 0.75$, and $\beta = 0.25$. Originally published in [61].

as shown in Fig. 3.3. The GDW theory captures this phenomenon while the SDW theory fails. The physical explanation is simple. As the shock wanders toward the entrance, α_{eff} becomes lower. This decrease causes the hopping rate D^- to become smaller than D^+, thereby making it easier for the shock to move toward the exit. A similar argument can be made for the shock wandering toward the exit. As it approaches the exit, α_{eff} becomes larger, which in turn causes D^- to become larger than D^+. The shock is then more likely to move toward the entrance. This entire argument depends on the hopping rates changing with the shock position. The SDW has no mechanism to produce such an effect. It will always predict an exponential decay for the density profile as seen in Fig. 3.3. However, the GDW theory produces the localized shock and agrees well with the simulation data in Fig. 3.3 due to the hopping rates being site dependent [61].

To understand how $P(k)$ can predict the exponential decays found in the HD and LD phases as well as the localized shock for the crossover region in the HD case, we use a Taylor expansion for $\ln P(k)$ about the average k-value $\bar{k}$:

$$\ln[P(k)] = \ln[P(\bar{k})] + (k-\bar{k})\frac{\partial \ln[P(k)]}{\partial k}|_{k=\bar{k}} + \frac{(k-\bar{k})^2}{2}\frac{\partial^2 \ln[P(k)]}{\partial k^2}|_{k=\bar{k}} + \ldots \tag{3.13}$$

For $\partial_k \ln[P(k)]$,

$$\begin{aligned} \frac{\partial \ln[P(k)]}{\partial k}|_{k=\bar{k}} &= \ln[P(\bar{k})] - \ln[P(\bar{k}-1)] \\ &= \ln\left[\frac{D^+_{\bar{k}-1}}{D^-_{\bar{k}}}\right] \end{aligned} \tag{3.14}$$

and for $\partial_{\bar{k}}^2 \ln[P(k)]$,

$$\begin{aligned} \frac{\partial^2 \ln[P(k)]}{\partial k^2}|_{k=\bar{k}} &= \ln[P(\bar{k}-1)] - 2\ln[P(\bar{k})] + \ln[P(\bar{k}+1)] \\ &= \ln\left[\frac{D_{\bar{k}}^-}{D_{\bar{k}-1}^+}\frac{D_{\bar{k}}^+}{D_{\bar{k}+1}^-}\right] \end{aligned} \tag{3.15}$$

For the ordinary TASEP, $P(k)$ is an exponential [13], thus $\ln[P(k)]$ contains up to the term linear in k. We recover that result here since the hopping rates of the ordinary TASEP do not depend on k and the quadratic term vanishes. For the constrained TASEP, the higher order terms do not vanish for all k, but one term may dominate over the others. For example, the coefficient of the linear term is much larger in the HD and LD regimes than the other terms. However, the coefficient of the linear term is approximately zero for the crossover region in the HD case, where the quadratic and cubic terms dominate. The fact that all higher order terms are included in $P(k)$ is the reason for the excellent agreement with the simulation data, especially in these crossover regimes.

To understand the effects of the feedback on the domain wall better, let us look at the gradient of the profile, specifically in the SP and HD phase. We define the lattice gradient to be:

$$\Delta\rho_i = \rho_{i+1} - \rho_i \tag{3.16}$$

The gradient is directly related to $P(k)$:

$$\Delta\rho_i = (\rho_+ - \alpha_{eff,i})P(i) \tag{3.17}$$

The gradient of the simulation data appears to be close to a Gaussian, as well as from the theory (Fig. 3.4). Yet, the width of the theory curve is larger than the simulation data. This difference can be traced back to how the number of particles N is related to the DW position k. In the simulation, N is an integer, however, that is not the case in general when computing it from the DW picture since k is an integer while ρ_+ and ρ_- are not. In fact, the DW must move multiple sites in a single direction in order to increase or decrease N by 1. Therefore, $\partial\alpha_{eff}/\partial N$ is greater than $\partial\alpha_{eff}/\partial k$. The larger derivative for N will confine the DW more about its average position in the simulation than in the DW theory. One possible way of improving this GDW approach would be to only change α_{eff} when the DW has moved far enough to change N by an integer value. Since this new approach will only marginally improve the previous result and not advance our understanding of the underlying physics greatly, we will not explore this idea further at this time.

Another quantity of interest is the probability of finding a given number of particles on the TASEP, $P(N)$. This quantity gives us information about the size of the fluctuations of the total number of particles. First, let us compare the constrained TASEP to the ordinary, unconstrained TASEP in the LD phase. As we see in Fig. 3.5, both distributions are close to a Gaussian. The width of the constrained TASEP is smaller than that of the ordinary

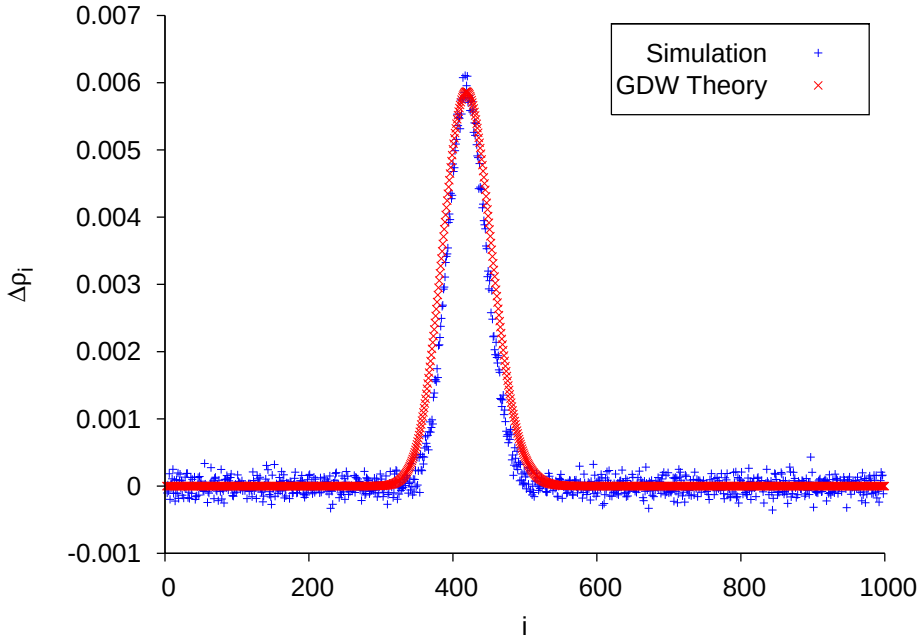

Figure 3.4: Gradient of the average density profile for $L = 1000$ with $N_{tot} = 800$, $\alpha = 0.75$, and $\beta = 0.25$.

one. Again, this difference has to do with the changing of α_{eff}. As N moves away from its average value, the α_{eff} acts as a restoring force by making easier or more difficult for a new particle to enter to replace the ones leaving the lattice. The ordinary TASEP does not have this "restoring force," so there is a greater probability of finding a N value that is further away from its average.

The GDW theory could be used to predict $P(N)$ for the constrained TASEP. However, one immediate difficultly is that the entire range of possible N values is not captured by the relationship between N and k. The minimum number of particles on the lattice that the GDW theory allows is when the DW is located at the exit with $N_{min} = \alpha_{eff,L}L$. Similarly, the maximum number of particles occurs when the wall is located at the entrance with $N_{max} = (1 - \beta)L$. Thus, the probability of finding a N that occurs outside of this range is zero in the DW picture. The second shortcoming comes from the previously mentioned problems with N and k both being integer values. Since this correspondence is not one-to-one, a direct comparison of $P(k)$ and $P(N)$ is not possible even if the N values are between N_{min} and N_{max}. Thus, using the GDW to find $P(N)$ through $P(k)$ is not feasible.

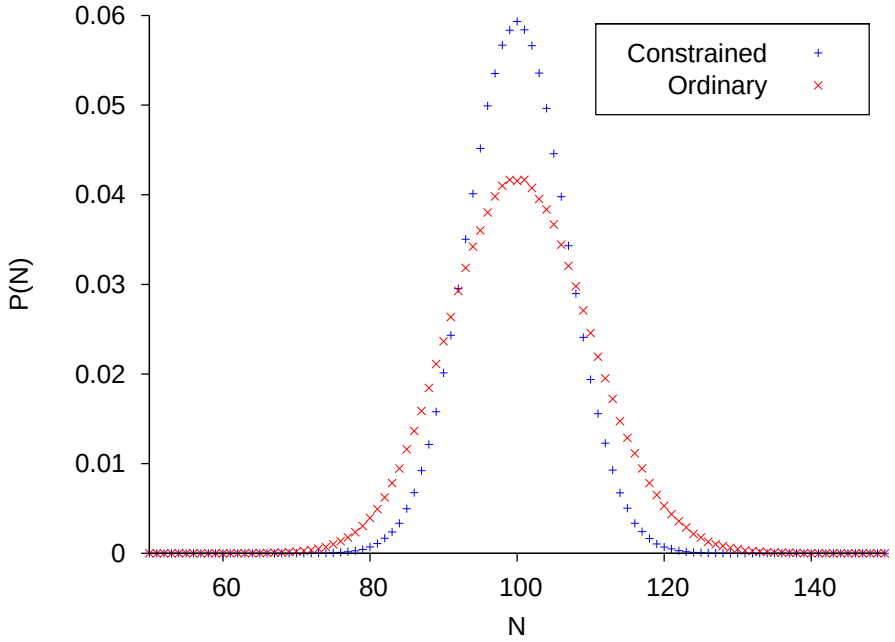

Figure 3.5: Distribution of the total occupancy N for $L = 1000$ with an average density of $\rho = 0.1$.

3.2 Power spectrum of a single TASEP with finite resources

In this section, we wish to look at the power spectrum of the total occupancy of the TASEP. This quantity has already been studied in the case of the ordinary TASEP in [55]. The constrained TASEP's power spectrum does contain new features not seen in the power spectrum of the ordinary TASEP. As we will see, these new features are due to the feedback effect of the pool on α_{eff}. We will explore the differences between the two models' power spectra and present a theory to explain them. We will first look at the power spectrum in the crossover regime in the HD case. Later, we will study the power spectrum in the LD state.

To calculate the power spectrum in the simulations, we use the same approach as [55]. We record the number of particles $N(t)$ on the TASEP every 100 MCS giving T data points. We define the Fourier transform to be

$$\tilde{N}(t) = \sum_{t=0}^{T-1} e^{i\omega t} N(t) \tag{3.18}$$

where

$$\omega = \frac{2\pi m}{T} \tag{3.19}$$

and m is an integer. The power spectrum is then given by

$$I(\omega) = \langle |\tilde{N}(\omega)|^2 \rangle \tag{3.20}$$

where the bracket indicates an average over the configurations. Typically, $T = 10k$ and $m \in [0, 10k]$ for the simulations and the power spectrum is averaged over 100 configurations.

3.2.1 Crossover regime in the HD case

Simulation results

Monte Carlo simulation results are shown in Fig. 3.6 for the crossover regime in the HD case. In this regime, the average α_{eff} is equal to β. Since the entry and exit rates are equal, one would expect to see a power spectrum similar to the power spectrum of the ordinary TASEP in the SP. However, a suppression at low ω is present that is not seen in the power spectrum of the ordinary TASEP in the SP. As shown previously, the DW is localized to a small region on the lattice while the average value of α_{eff} is equal to β [61]. In the ordinary TASEP with $\alpha = \beta$, a shock forms and performs a random walk over the entire length of the lattice, which gives rise to a power law decay of ω^{-2} for the power spectrum. The constrained TASEP in the crossover regime also has an ω^{-2} decay and the suppression near $\omega = 0$ as seen in Fig. 3.6. The suppression is due to the feedback effect of α_{eff}. The shock in the

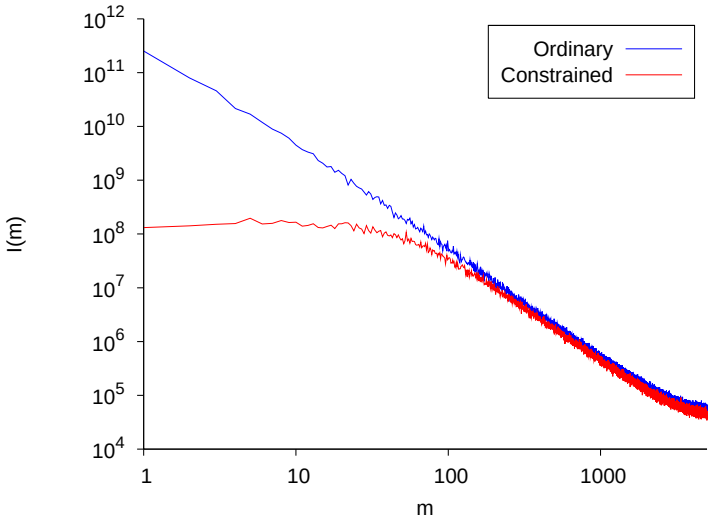

Figure 3.6: Constrained TASEP power spectra for $\bar{\alpha}_{eff} = \beta = 0.3$ and ordinary TASEP power spectrum for $\alpha = \beta = 0.3$ with $L = 1000$ plotted as a function of m.

ordinary TASEP has an equal probability to be found anywhere on the lattice. In contrast, the shock is localized to a specific location and the probability of finding it away from its

average location decreases as the shock moves further away. The restoring aspect of α_{eff} keeps $N(t)$ near its average value over long time periods, which in turn decreases the power spectrum for small ω. Therefore, the fluctuating α_{eff} is the source of the suppression of the power spectrum at low ω.

Theoretical considerations

To understand the simulation results better, we will consider a simple theory that incorporates the feedback effects of α_{eff}. We begin with the continuity equation:

$$\partial_t \rho(x,t) = \partial_x J(x) + \partial_x \eta(x,t) \tag{3.21}$$

where $\rho(x,t)$ is the local density, $J(x)$ is the local current, and $\eta(x,t)$ is a noise term that accounts for the local fluctuations in time in the current. Integrating over the length of the system, we have:

$$\partial_t N(t) = J(L) - J(1) + \eta(L,t) - \eta(1,t) \tag{3.22}$$

with the currents given by:

$$J(1) = \alpha_{eff}(1-\alpha_{eff}) \tag{3.23}$$

$$J(L) = \beta(1-\beta) \tag{3.24}$$

We expand α_{eff} about the average number of particles $\bar{N}$:

$$\alpha_{eff} = \bar{\alpha}_{eff} + (N(t)-\bar{N})\frac{\partial \alpha_{eff}}{\partial N}|_{N=\bar{N}} + (O)(N-\bar{N})^2 \tag{3.25}$$

and the current $J(1)$ becomes:

$$J(1) = \bar{\alpha}_{eff} - \bar{\alpha}_{eff}^2 + (N-\bar{N})(1-2\bar{\alpha}_{eff})\frac{\partial \alpha_{eff}}{\partial N}|_{N=\bar{N}} + (O)(N-\bar{N})^2 \tag{3.26}$$

Since $\bar{\alpha}_{eff} = \beta$, the first two terms in the expression for $J(1)$ are equal to $J(L)$. The equation for $\partial_t N(t)$ becomes:

$$\partial_t (N(t)-\bar{N}) = (N(t)-\bar{N})(1-2\bar{\alpha}_{eff})\frac{\partial \alpha_{eff}}{\partial N}|_{N=\bar{N}} + \eta(t) \tag{3.27}$$

where terms $(O)(N(t)-\bar{N})^2$ have been dropped and $\eta(L,t) - \eta(1,t) = \eta(t)$. The solution to this equation in Fourier space is simple ($\omega > 0$):

$$\tilde{N}(\omega) = \frac{\tilde{\eta}}{-i\omega - \gamma} \tag{3.28}$$

where

$$\gamma = (1-2\beta)\frac{\partial \alpha_{eff}}{\partial N}|_{N=\bar{N}} \tag{3.29}$$

The power spectrum is then:

$$I(\omega) = \langle |\tilde{N}(\omega)|^2 \rangle = \frac{A}{\omega^2 + \gamma^2} \tag{3.30}$$

where $\langle \tilde{\eta}(\omega)\tilde{\eta}(\omega') \rangle = A\delta(\omega - \omega')$ with A being the variance of the noise.

This theory has only one fit parameter A with which we can use to match the data. The γ is completely determined by the form of α_{eff} and $\bar{N}$. Also, note that γ does not depend explicitly on the system size L or the total number of particles in the system N_{tot}, however, such a dependence could be hidden in the form of α_{eff}. Once the parameter A is fit to the data, we see in Fig. 3.7 for $L = 1000$ with $\alpha = 0.7$, $\beta = 0.3$, and $N_{tot} = 800$ that the agreement is quite good.

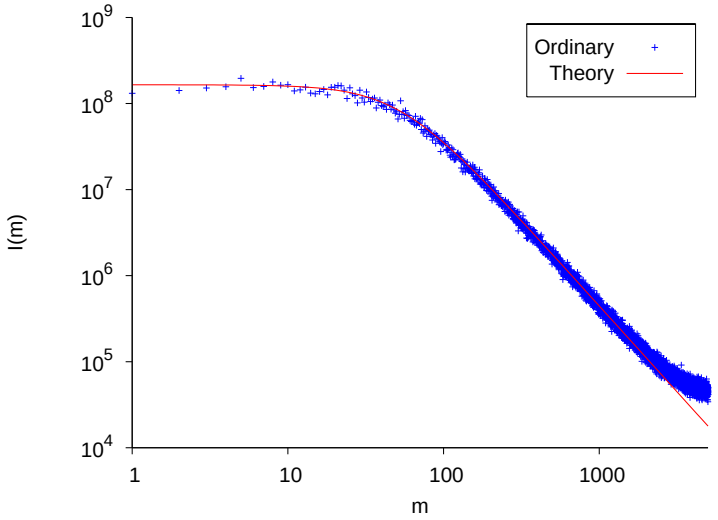

Figure 3.7: Simulation data and theory for the constrained TASEP power spectrum for $\alpha = 0.7$, $\beta = 0.3$ and $N_{tot} = 800$ with $L = 1000$ and $A = 17.6$ plotted as a function of m.

To check the dependence on N_{tot} and L of γ, we will vary these parameters and compare the results to the theory. While not shown here, all of the power spectra within the crossover regime for the parameters shown in Fig. 3.7 follow the same curve, regardless of the N_{tot} value. This confirms the theoretical result that the power spectrum should not depend on the total number of particles in the system. We explore the dependence on L by increasing the system size. In Fig. 3.8, we show that the suppression of the power spectrum in this regime does not depend on L.

On the other hand, decreasing the system size introduces finite size effects. Even at $L = 100$, the power spectrum of the ordinary TASEP deviates significantly at low ω from the ω^{-2} decay. The small size plays a similar role as α_{eff} in the constrained TASEP by limiting the

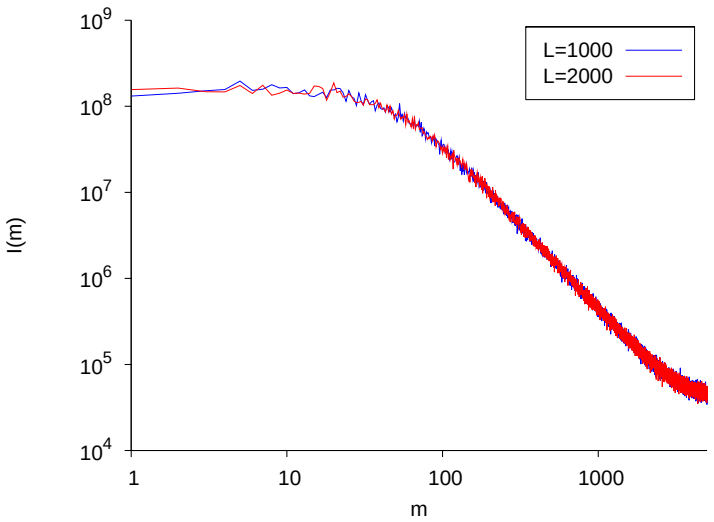

Figure 3.8: Simulation data for the constrained TASEP power spectrum for $\alpha = 0.7$, $\beta = 0.3$ with $L = 1000$ for $N_{tot} = 800$ and $L = 2000$ for $N_{tot} = 1300$ plotted as a function of m.

fluctuations in $N(t)$. A form similar to Eqn. (3.30) can be used to fit the data for small L, where γ is replaced by a length dependent quantity. The details of the fit are presented in Appendix B. For the constrained TASEP for small L, the finite size and α_{eff} effects both contribute to the low ω suppression from the ω^{-2} provided $\partial_{N_p}\alpha_{eff}$ is not too large. Therefore, the γ in Eqn. (3.30) will contain two terms, one from the fluctuating α_{eff} and another that depends on L.

3.2.2 LD state

Simulation results

Results from Monte Carlo simulations for the LD state are presented here. As previously found [55], oscillations in the power spectra $I(\omega)$ occur in the LD and HD phases. We find the same oscillation here as well (Fig. 3.9(a)). However, we also see a suppression of the power spectrum near $\omega = 0$ when the constrained TASEP is compared to the ordinary TASEP. The value at which the two curves meet does depend on the length of the lattice. As seen in Fig. 3.9(b) for $L = 32000$, the intersection occurs at a much lower ω value than in the $L = 1000$ case. The time it takes for a fluctuation to enter and leave the TASEP increases as the length of the lattice increases. The feedback effect from the fluctuating value of α_{eff} takes more time to travel through the system when the length is increased from 1000 to 32000, which is why we see the intersection value of ω decrease.

The magnitude of the suppression of the power spectrum for the constrained TASEP depends

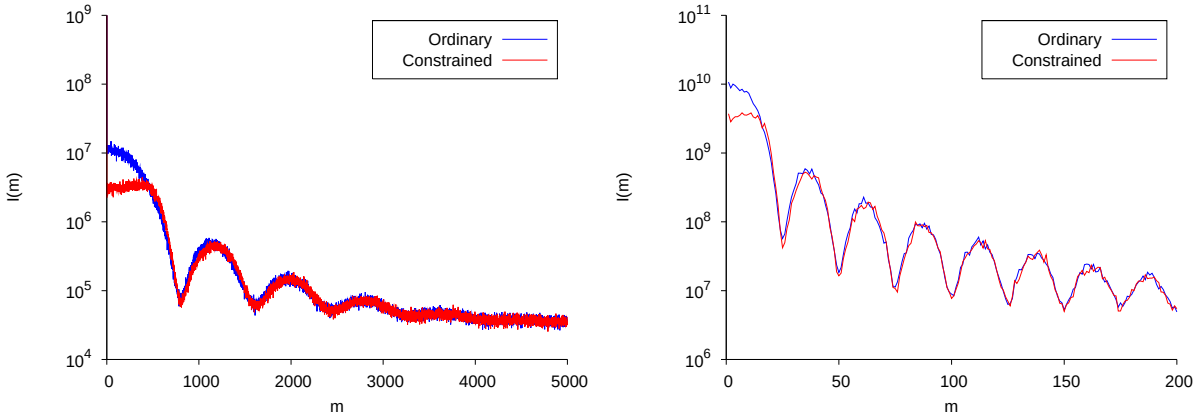

(a) (b)

Figure 3.9: Constrained and ordinary power spectra for $\rho = 0.1$ plotted as a function of $m = \omega T/2\pi$. For the constrained TASEP, $\alpha = 0.3$, $\beta = 0.9$, and (a) $N_{tot} = 205$ with $L = 1000$, and (b) $N_{tot} = 6527$ with $L = 32000$. For the ordinary TASEP, $\alpha = 0.1$ and $\beta = 0.9$.

on how much α_{eff} changes when the number of particles in the pool N_p changes. For the ordinary TASEP, α is a constant and $\partial_{N_p}\alpha = 0$. For the constrained TASEP, α_{eff} fluctuates and $\partial_{N_p}\alpha_{eff} \neq 0$. At small N_{tot}, the TASEP is effectively in a LD state regardless of the values of α and β chosen. However, we find a slightly greater suppression at larger N_{tot} values when comparing the power spectrum with α and β in the LD phase and α and β in the HD phase at the same density. One difference is that the N^* and α values are larger in the HD than in the LD case. This difference leads to $\partial_{N_p}\alpha_{eff}$ being larger at a given overall density in the HD case than in the LD case as N_{tot} increases. The suppression of the power spectra is shown in Fig. 3.10 for $L = 1000$ and an average overall density of $\rho = 0.1$ with $N^* = 150, 300, 600$ for the constrained TASEP. These different N^* values give rise to the different $\partial_{N_p}\alpha_{eff}$ values shown in the figure.

Another piece of evidence supporting this claim that the suppression depends on $\partial_{N_p}\alpha_{eff}$ is how the suppression depends on N_{tot}. As N_{tot} is increased in either the HD or LD case, the suppression of the power spectrum decreases. For the form of α_{eff} chosen here, $\partial_{N_p}\alpha_{eff}$ approaches zero as N_{tot} becomes large. For large enough N_{tot}, the ordinary and constrained TASEPs' power spectra are the same (Fig. 3.11). Again, we see that the magnitude of the suppression is related to the change in α_{eff}.

Theoretical considerations

To understand the power spectrum in the LD state better, we construct a theory that incorporates the feedback effects of α_{eff}. We begin with the Langevin equations for the

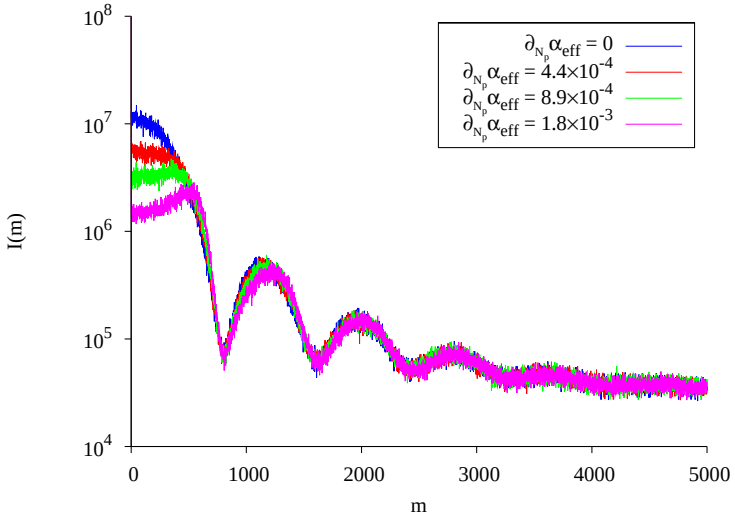

Figure 3.10: Constrained power spectra for $\rho = 0.1$ with $L = 1000$ with different $\partial\alpha_{eff}/\partial N_p$. The $\partial\alpha_{eff}(N_p)/\partial N_p = 0$ line corresponds to the ordinary TASEP with a constant α.

density:

$$\partial_t\rho(x,t) = \rho(x-1,t)[1-\rho(x,t)] - \rho(x,t)[1-\rho(x+1,t)] + \xi(x-1,t) - \xi(x,t) \tag{3.31}$$

where $\xi(x,t)$ is the noise associated with site x. For a finite system of size L, we include two boundary equations:

$$\begin{aligned} \partial_t\rho(1,t) &= \alpha_{eff}[1-\rho(1,t)] - \rho(1,t)[1-\rho(2,t)] + \xi(0,t) - \xi(1,t) && (3.32)\\ \partial_t\rho(L,t) &= \rho(L-1,t)[1-\rho(L,t)] - \rho(L,t)\beta + \xi(L-1,t) - \xi(L,t) && (3.33) \end{aligned}$$

For the constrained TASEP, the TASEP and the pool may be thought of as a ring with $L+1$ sites where the $x = 0$ site does not have a restriction on the number of particles it can hold. Then to complete the ring, we also write an equation for the pool at site $x = 0$:

$$\partial_t\rho(0,t) = \rho(L,t)\beta - \alpha_{eff}[1-\rho(1,t)] + \xi(L,t) - \xi(0,t) \tag{3.34}$$

To simplify the remaining parts of the calculation, we choose α and β such that the average density profile is flat with:

$$\begin{aligned} \rho(x) &= \bar{\rho} && (3.35)\\ \langle N\rangle &= \bar{\rho}L && (3.36)\\ \beta &= 1-\bar{\rho} && (3.37)\\ \alpha f(\bar{\rho}L) &= \bar{\rho} && (3.38)\\ \bar{f} &= \frac{\bar{\rho}}{\alpha} && (3.39) \end{aligned}$$

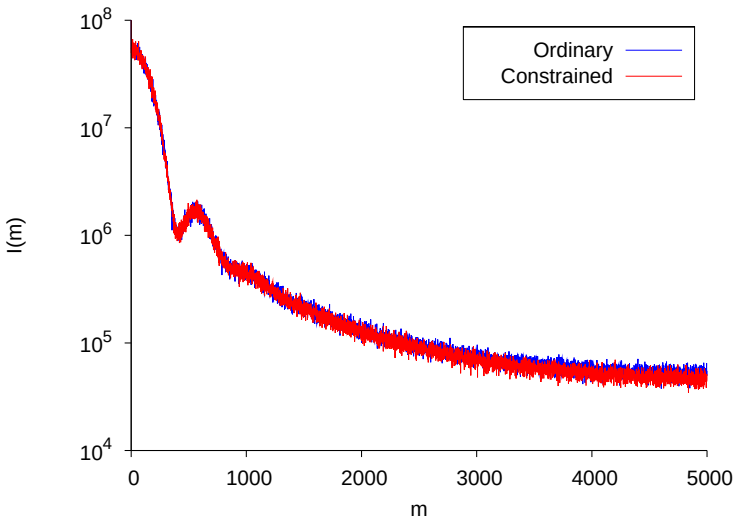

Figure 3.11: Constrained and ordinary power spectra for $\rho = 0.7$ with $L = 1000$ plotted as a function of m. The ordinary TASEP has $\alpha = 0.7$ and $\beta = 0.3$. The constrained TASEP has $\alpha = 0.7$, $\beta = 0.3$, and $N_{tot} = 1400$.

We define the fluctuation of $\rho(x,t)$ about its average $\bar{\rho}$ to be:

$$\varphi(x,t) = \rho(x,t) - \bar{\rho} \tag{3.40}$$

and for the fluctuation of N_p about its average, we have

$$\varphi_0(t) = \bar{\rho}L - N(t) \tag{3.41}$$

We also define for the $f(N_p)$ given above

$$\partial_N f|_{\bar{\rho}L} = f' = -\frac{1-\bar{f}^2}{N^*} \tag{3.42}$$

Our goal is to solve the linearized Langevin equation in Fourier space. In order to linearize the equations, we must first expand α_{eff} about $\bar{\rho}L$ to first order in φ_0. We have then

$$\begin{aligned} \alpha_{eff} &= \alpha\left[\bar{f} + (N(t) - \bar{\rho}L)f' + \ldots\right] \\ &= \bar{\rho} - \alpha f' \varphi_0(t) + \ldots \end{aligned} \tag{3.43}$$

with the ... being the higher order terms in the expansion. We are now ready to write the linearized Langevin equations for the TASEP:

$$\begin{aligned}
\Delta_t\varphi_0(t) &= (1-\bar{\rho})\varphi(L,t) + \alpha f^{'}(1-\bar{\rho})\varphi_0(t) + \bar{\rho}\varphi(1,t) && \text{(3.44a)}\\
&\quad +\xi(L,t) - \xi(0,t) \\
\Delta_t\varphi(1,t) &= -\alpha f^{'}(1-\bar{\rho})\varphi_0(t) - \varphi(1,t) + \bar{\rho}\varphi(2,t) && \text{(3.44b)}\\
&\quad +\xi(0,t) - \xi(1,t) \\
\Delta_t\varphi(x,t) &= (1-\bar{\rho})\varphi(x-1,t) - \varphi(x,t) + \bar{\rho}\varphi(x+1,t) && \text{(3.44c)}\\
&\quad +\xi(x-1,t) - \xi(x,t) \\
\Delta_t\varphi(L,t) &= (1-\bar{\rho})\varphi(L-1,t) - \varphi(L,t) + \xi(L-1,t) - \xi(L,t) && \text{(3.44d)}
\end{aligned}$$

We now separate out the parts that violate translational invariance in the $x = 0$, $x = 1$, and $x = L$ equations and combine all four into one single equation for all x.

$$\begin{aligned}
\Delta_t\varphi(x,t) &= (1-\bar{\rho})\varphi(x-1,t) - \varphi(x,t) + \bar{\rho}\varphi(x+1,t) && \text{(3.45)}\\
&\quad +\xi(x-1,t) - \xi(x,t) + \ldots \\
&= \frac{1}{2}\left[\varphi(x-1,t) - 2\varphi(x,t) + \varphi(x+1,t)\right] \\
&\quad +\frac{1-2\bar{\rho}}{2}\left[\varphi(x-1,t) - \varphi(x+1)\right] \\
&\quad +\xi(x-1,t) - \xi(x,t) + \ldots
\end{aligned}$$

where the ... represent the part that violates translational invariance. Before proceeding, we need to say a few words about this equation. The coefficient in front of the first term in the square bracket becomes the diffusion coefficient in the continuum limit. However, we expect from previous studies [55, 62] that this diffusion coefficient will be "renormalized." To deal with the renormalization, we will multiply this term by an effective diffusion coefficient D_{eff}, which will be a free parameter in this theory. The coefficient for the second term in square brackets is related to the bias $v = 1 - 2\bar{\rho}$ in the continuum limit. We will now use D_{eff} and v explicitly for the rest of the calculation. For the part that violates translational invariance, we have

$$\begin{aligned}
\ldots &= \delta_{x,0}\left[\alpha f^{'}(\frac{D_{eff}}{2} + \frac{v}{2})\varphi_0(t) + D_{eff}\varphi_0(t)\right] && \text{(3.46)}\\
&\quad +\delta_{x,1}\left[-\alpha f^{'}(\frac{D_{eff}}{2} + \frac{v}{2})\varphi_0(t) - \left(\frac{D_{eff}}{2} + \frac{v}{2}\right)\varphi_0(t)\right] && \text{(3.47)}\\
&\quad +\delta_{x,L}\left[-\left(\frac{D_{eff}}{2} - \frac{v}{2}\right)\varphi_0(t)\right] && \text{(3.48)}
\end{aligned}$$

Note that the inhomogeneities only depend on $\varphi_0(t)$. This result comes as no surprise since the $x = 0$ site is the only site that is different from the others. We now use the Fourier

transform

$$\varphi(x,t) = \sum_k \sum_\omega e^{i(kx+\omega t)} \tilde{\varphi}(k,\omega) \tag{3.49}$$

$$\tilde{\varphi}(k,\omega) = \frac{1}{(L+1)T} \sum_x \sum_t e^{-i(kx+\omega t)} \varphi(x,t) \tag{3.50}$$

with

$$k = \frac{2\pi j}{L+1} \quad j \in [0, L] \tag{3.51}$$

$$\omega = \frac{2\pi m}{T} \quad m \in [1, T] \tag{3.52}$$

to solve this equation. The solution to the translationally invariant part of the equation is

$$\tilde{\varphi}(k,\omega) = \frac{e^{-ik}-1}{P(k,\omega)} \tilde{\xi}(k,\omega) + \ldots \tag{3.53}$$

where $P(k,\omega)$ is given by

$$P(k,\omega) = e^{i\omega} - 1 + D_{eff}(1-\cos k) + iv \sin k \tag{3.54}$$

and the remaining part is

$$\begin{aligned} \ldots = \frac{1}{(L+1)TP(k,\omega)} \Bigg\{ & \left[\alpha f'(\frac{D_{eff}}{2} + \frac{v}{2}) + D_{eff} \right] \\ & + \left[-\alpha f'(\frac{D_{eff}}{2} + \frac{v}{2}) - \frac{D_{eff}}{2} - \frac{v}{2} \right] e^{-ik} \\ & + \left[-\frac{D_{eff}}{2} + \frac{v}{2} \right] e^{ik} \Bigg\} \sum_t e^{-i\omega t} \varphi_0(t) \end{aligned} \tag{3.55}$$

But,

$$\varphi_0(t) = \sum_k \sum_\omega e^{i(k(0)+\omega t)} \tilde{\varphi}(k,\omega) \tag{3.56}$$

$$\frac{1}{T} \sum_t e^{-i\omega t} \varphi_0(t) = \sum_k \tilde{\varphi}(k,\omega) \tag{3.57}$$

So, we can replace the sum over t with the one over k. We can now sum over k to get:

$$\sum_k \tilde{\varphi}(k,\omega) = \frac{1}{Q(\omega)} \sum_k \frac{e^{-ik}-1}{P(k,\omega)} \tilde{\xi}(k,\omega) \tag{3.58}$$

where

$$Q(\omega) = \sum_q \frac{e^{i\omega} - 1 + \alpha f' \left(\frac{D_{eff}}{2} + \frac{v}{2}\right)(1 - e^{-iq})}{(L+1)P(q,\omega)} \tag{3.59}$$

From this point, we could solve for $\tilde{\varphi}(k,\omega)$ in terms of the noise. Instead, let us write the Fourier transform of the total occupancy

$$\begin{aligned} \tilde{N}(\omega) &= \frac{1}{T}\sum_t e^{-i\omega} N(t) && (3.60)\\ &= \frac{1}{T}\sum_t e^{-i\omega}[-\varphi_0(t)] && (3.61)\\ &= \sum_k \tilde{\varphi}(k,\omega) && (3.62) \end{aligned}$$

So, we do not need the expression $\tilde{\varphi}(k,\omega)$, but just the sum over k of the expression. The power spectrum is easily computed from the above

$$I(\omega) = \langle |\tilde{N}(\omega)|^2 \rangle = \sum_k \frac{2A(1-\cos k)}{|Q(\omega)P(k,\omega)|^2} \tag{3.63}$$

where we have assumed to have Gaussian noise with zero mean value and a variance of A. In other words, $\langle \tilde{\xi}(k,\omega)\tilde{\xi}(k',\omega')\rangle = A\delta_{k,k'}\delta_{\omega,\omega'}$.

This result could be used to match the simulation data, except we took data every 100 MCS instead of at every MCS. The relationship between $I(\omega)$ and the Monte Carlo simulation result is detailed in Appendix A. If we define the interval between the measurements to be ℓ, then we find the simulation power spectrum is given by

$$I(m) = \frac{1}{\ell^2}\sum_{n=0}^{\ell-1}\sum_k \frac{2(1-\cos k)}{|Q(\omega_{m,n})P(k,\omega_{m,n})|^2} \tag{3.64}$$

where

$$\omega_{m,n} = 2\pi\left(\frac{m}{T} + \frac{n}{\ell}\right) \tag{3.65}$$

Here we are simply summing over the nT/ℓ harmonics.

The theory has two fit parameters – A and D_{eff}. The D_{eff} parameter controls how much the amplitude of the oscillations are damped as ω is increased, while the A parameter sets the value that $I(\omega)$ approaches as $\omega \to 0$. Unfortunately, there is no set of A and D_{eff} that agrees with the simulation data over the entire range of ω. The theory does capture the suppression at small ω and the values of ω for the minima of the oscillations as shown in Fig. 3.12.

This fitting problem occurs for both the ordinary and constrained TASEP power spectra. Instead, let us look at the ratio of the ordinary TASEP's power spectrum I_0 to the constrained

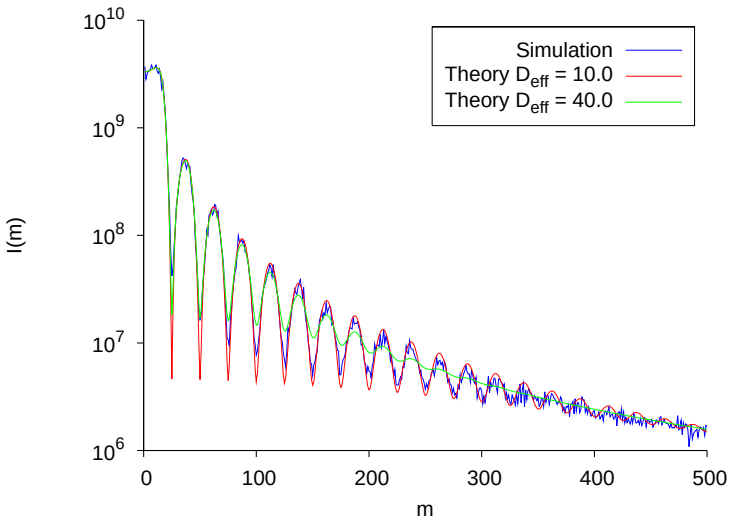

Figure 3.12: Simulation data and theory for the constrained TASEP power spectrum for $\bar{\rho} = 0.1$ with $L = 32000$ for various D_{eff} plotted as a function of m.

TASEP's power spectrum I_c. In (3.64), the only term that depends on $f^{'}$ is $Q(\omega_{m,n})$. Let us define $Q_0(\omega_{m,n})$ as $Q(\omega_{m,n})$ with $f^{'} = 0$, which corresponds to the ordinary TASEP case. We can write $Q(\omega_{m,n})$ in terms of $Q_0(\omega_{m,n})$:

$$Q(\omega_{m,n}) = Q_0 + f^{'} B(\omega_{m,n}) \tag{3.66}$$

where

$$B(\omega_{m,n}) = \sum_q \frac{\alpha \left(\frac{D_{eff}}{2} + \frac{v}{2} \right) (1 - e^{iq})}{(L+1) P(q, \omega_{m,n})} \tag{3.67}$$

Then,

$$\frac{I_0(m)}{I_c(m)} = 1 + f^{'} C_1(m) + (f^{'})^2 C_2(m) \tag{3.68}$$

where $C_1(m)$ and $C_2(m)$ are real functions that include the sum over the nT/ℓ harmonics. Without the sum over the harmonics, the ratio is simply:

$$\frac{I_0(\omega)}{I_c(\omega)} = \frac{Q(\omega)}{Q_0(\omega)} \tag{3.69}$$

However, the extra sum over the harmonics does not allow for the cancellation of the sum over k in (3.64). Yet, when the ratio of the theories is compared to the simulation data, the agreement is quite remarkable even with $D_{eff} = 1$ for $L = 1000$ (Fig. 3.13). This agreement between the theory and simulation means that the impact of effective diffusion coefficient is decreased when the ratio is taken. While the two quantities are in good agreement for

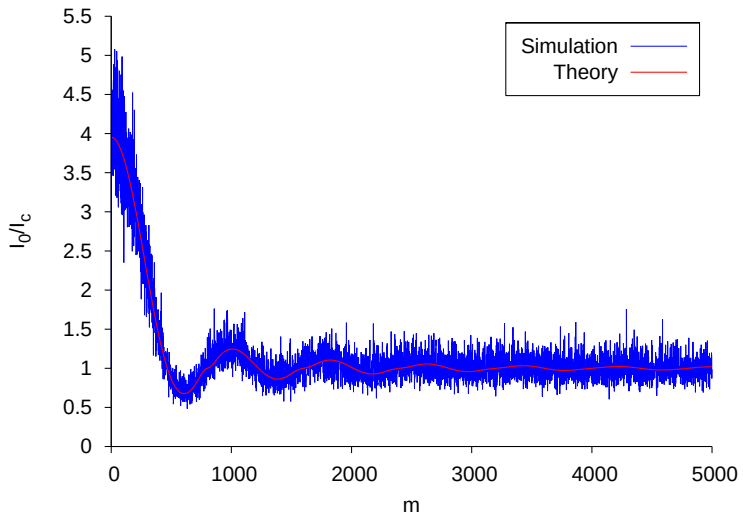

Figure 3.13: Simulation data and theory for the ratio of the ordinary TASEP power spectrum to the constrained TASEP power spectrum for $\bar{\rho} = 0.1$ with $L = 1000$ and $D_{eff} = 1$ plotted as a function of m.

$L = 1000$, the agreement is not as good for the $L = 32000$ in Fig. 3.14. This disagreement is due to the value of the diffusion coefficient increasing as the length increases [55].

While the agreement is good between the simulation and theory, the theory curve in Fig. 3.13 shows additional structure after the first oscillation. In order to see if these structures are real or simply artifacts of the numerical calculation, we calculate the power spectrum using a different method. Instead of performing a Fourier transform on the spatial coordinate, we sum over x to get $N(\omega)$. This method follows more closely what is done in the simulation where the total occupancy is found by summing the occupancy for each site. Again, we start from the Langevin equations and keep only the terms linear in φ. We Fourier transform the equations in time to get:

$$\begin{aligned}
(e^{i\omega} - 1 - \alpha f'(1-\bar{\rho}))\tilde{\varphi}(0,\omega) &= (1-\bar{\rho})\tilde{\varphi}(L,\omega) + \bar{\rho}\tilde{\varphi}(1,\omega) \qquad (3.70a)\\
&\quad +\tilde{\xi}(L,\omega) - \tilde{\xi}(0,\omega)\\
e^{i\omega}\tilde{\varphi}(1,\omega) &= -\alpha f'(1-\bar{\rho})\tilde{\varphi}(0,\omega) + \bar{\rho}\tilde{\varphi}(2,\omega) \qquad (3.70b)\\
&\quad +\tilde{\xi}(0,\omega) - \tilde{\xi}(1,\omega)\\
e^{i\omega}\tilde{\varphi}(x,\omega) &= \bar{\rho}\tilde{\varphi}(x+1,\omega) + (1-\bar{\rho})\tilde{\varphi}(x-1,\omega) \qquad (3.70c)\\
&\quad +\tilde{\xi}(x-1,\omega) - \tilde{\xi}(x,\omega)\\
e^{i\omega}\tilde{\varphi}(L,\omega) &= (1-\bar{\rho})\tilde{\varphi}(L-1,\omega) \qquad (3.70d)\\
&\quad +\tilde{\xi}(L-1,t) - \tilde{\xi}(L,t)
\end{aligned}$$

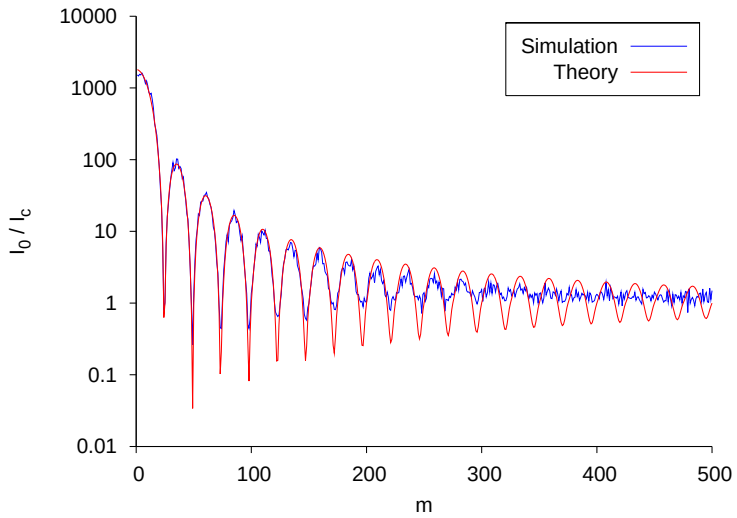

Figure 3.14: Simulation data and theory for the ratio of the ordinary TASEP power spectrum to the constrained TASEP power spectrum for $\bar{\rho} = 0.1$ with $L = 32000$ and $D_{eff} = 1$ plotted as a function of m.

We need $\tilde{N}(\omega)$, which is $-\tilde{\varphi}(0,\omega)$ (for $\omega > 0$):

$$(e^{i\omega} - 1 - \alpha f'(1-\bar{\rho}))\tilde{N}(\omega) = -\bar{\rho}\tilde{\varphi}(1,\omega) - (1-\bar{\rho})\tilde{\varphi}(L,\omega) + \tilde{\xi}(0,\omega) - \tilde{\xi}(L,\omega) \tag{3.71}$$

If we define:

$$\tilde{\xi}_0(\omega) = \tilde{\xi}(0,\omega) \tag{3.72}$$
$$\tilde{\xi}_L(\omega) = \tilde{\xi}(L,\omega) \tag{3.73}$$
$$\tilde{\varphi}_1(\omega) = \tilde{\varphi}(1,\omega) \tag{3.74}$$
$$\tilde{\varphi}_L(\omega) = \tilde{\varphi}(L,\omega) \tag{3.75}$$

Then,

$$\tilde{N}(\omega) = \frac{\bar{\rho}\tilde{\varphi}_1(\omega) + (1-\bar{\rho})\tilde{\varphi}_L(\omega) + \tilde{\xi}_L(\omega) - \tilde{\xi}_0(\omega)}{1 - e^{i\omega} - \alpha f'(1-\bar{\rho})} \tag{3.76}$$

Here, the solution depends on both $\tilde{\varphi}_1$ and $\tilde{\varphi}_L$. In order to find those expressions, we need to solve the full set of $\tilde{\varphi}$ equations. The equations in (3.70) form a linear system and can be solved directly, but before doing so, we need to add in an effective diffusion coefficient D_{eff}. The D_{eff} will again be a fit parameter. We can rewrite (3.70) in the following form:

$$\mathbb{M}\tilde{\varphi} = \tilde{\eta} \tag{3.77}$$

where,

$$\tilde{\varphi} = \begin{pmatrix} \tilde{\varphi}(0,\omega) \\ \tilde{\varphi}(1,\omega) \\ \tilde{\varphi}(2,\omega) \\ \vdots \\ \tilde{\varphi}(L,\omega) \end{pmatrix} \tag{3.78}$$

$$\tilde{\eta} = \begin{pmatrix} \tilde{\xi}(L,\omega) - \tilde{\xi}(0,\omega) \\ \tilde{\xi}(0,\omega) - \tilde{\xi}(1,\omega) \\ \tilde{\xi}(1,\omega) - \tilde{\xi}(2,\omega) \\ \vdots \\ \tilde{\xi}(L-1,\omega) - \tilde{\xi}(L,\omega) \end{pmatrix} \tag{3.79}$$

and the matrix $\mathbb{M}$ has non-zero elements:

$$\begin{aligned}
\mathbb{M}_{01} &= e^{i\omega} - 1 - (D_{eff}/2 + v/2)\alpha f^{'} && (3.80)\\
\mathbb{M}_{02} &= -D_{eff}/2 + v/2 && (3.81)\\
\mathbb{M}_{0L} &= -D_{eff}/2 - v/2 && (3.82)\\
\mathbb{M}_{10} &= (D_{eff}/2 + v/2)\alpha f^{'} && (3.83)\\
\mathbb{M}_{ii} &= e^{i\omega} - 1 + D_{eff} \quad i \in [1, L] && (3.84)\\
\mathbb{M}_{ii+1} &= -D_{eff}/2 + v/2 \quad i \in [1, L-1] && (3.85)\\
\mathbb{M}_{i+1i} &= -D_{eff}/2 - v/2 \quad i \in [1, L-1] && (3.86)
\end{aligned}$$

To find $\tilde{N}$, we only need the $\mathbb{M}^{-1}_{0i}$ components of the inverse. Since $\mathbb{M}$ is almost a tridiagonal matrix with constant values along those diagonals, we can write the solution in terms of its cofactors M_n:

$$\begin{aligned}
\tilde{\varphi}(0,\omega) &= \frac{1}{Det(\mathbb{M})}\Bigg[Det(M_L)\tilde{\eta}_0 \\
&\quad + \sum_{x=1}^{L} \{ (D_{eff}/2 + v/2)^{L-x+1} Det(M_{x-1}) \\
&\quad + (D_{eff}/2 - v/2)^{x} Det(M_{L-x}) \} \tilde{\eta}_x \Bigg]
\end{aligned} \tag{3.87}$$

where M_n is the n by n lower right block (nth principle minor) of $\mathbb{M}$ and $\tilde{\eta}_x(\omega) = \tilde{\xi}(x-1,\omega) - \tilde{\xi}(x,\omega)$. The determinants have the recursion relation:

$$\begin{aligned}
Det(M_n) &= (e^{i\omega} - 1 + D_{eff}) Det(M_{n-1}) \\
&\quad - (D_{eff}/2 - v/2)(D_{eff}/2 + v/2) Det(M_{n-2})
\end{aligned} \tag{3.88}$$

with

$$
\begin{aligned}
Det(M_0) &= 1 && (3.89)\\
Det(M_1) &= e^{i\omega} - 1 + D && (3.90)\\
Det(\mathbb{M}) &= (e^{i\omega} - 1 - (D_{eff}/2 + v/2)\alpha f^{'})Det(M_L) && (3.91)\\
&\quad -(D_{eff}/2 + v/2)(D_{eff}/2 - v/2)\alpha f^{'} Det(M_{L-1})\\
&\quad -(D_{eff}/2 + v/2)^{L+1}\alpha f^{'}
\end{aligned}
$$

The solution for $\tilde{\varphi}(0,\omega)$ is:

$$
\begin{aligned}
\tilde{\varphi}(0,\omega) &= \frac{1}{Det(\mathbb{M})}\Bigg[Det(M_L)\tilde{\eta}_0 && (3.92)\\
&\quad + \sum_{x=1}^{L}\{(D_{eff}/2 + v/2)^{L-x+1} Det(M_{x-1})\\
&\quad + (D_{eff}/2 - v/2)^{x} Det(M_{L-x})\}\tilde{\eta}_x\Bigg]
\end{aligned}
$$

The power spectrum (for $\omega > 0$) is then given by $I(\omega) = \langle|\tilde{\varphi}(0,\omega)|^2\rangle$. To calculate this quantity, we will need:

$$
\begin{aligned}
\langle\tilde{\eta}_x\tilde{\eta}^*_{x'}\rangle &= \langle(\tilde{\xi}(x-1) - \tilde{\xi}(x))(\tilde{\xi}^*(x'-1) - \tilde{\xi}^*(x')) && (3.93)\\
&= \langle\tilde{\xi}(x-1)\tilde{\xi}^*(x'-1)\rangle - \langle\tilde{\xi}(x-1)\tilde{\xi}^*(x')\rangle\\
&\quad -\langle\tilde{\xi}(x)\tilde{\xi}^*(x'-1)\rangle + \langle\tilde{\xi}(x)\tilde{\xi}^*(x')\rangle\\
&= \frac{A}{T}(\delta_{x-1,x'-1} - \delta_{x-1,x'} - \delta_{x,x'-1} + \delta_{x,x'})
\end{aligned}
$$

Thus, we have:

$$\begin{aligned}\langle\tilde{\varphi}_0\tilde{\varphi}_0^*\rangle &= \frac{1}{|Det(\mathbb{M})|^2}\Bigg[|Det(M_L)|^2\langle\tilde{\eta}_0\tilde{\eta}_0^*\rangle \\ &+\sum_{x=1}^{L}\sum_{x'=1}^{L}\{(D_{eff}/2+v/2)^{L-x+1}Det(M_{x-1}) \\ &+(D_{eff}/2-v/2)^{x}Det(M_{L-x})\} \\ &\times\{(D_{eff}/2+v/2)^{L-x'+1}Det(M_{x'-1}) \\ &+(D_{eff}/2-v/2)^{x'}Det(M_{L-x'})\}^*\langle\tilde{\eta}_x\tilde{\eta}_{x'}^*\rangle \\ &+\sum_{x=1}^{L}Det(M_L)\{(D_{eff}/2+v/2)^{L-x+1}Det(M_{x-1}) \\ &+(D_{eff}/2-v/2)^{x}Det(M_{L-x})\}^*\langle\tilde{\eta}_0\tilde{\eta}_x^*\rangle \\ &+\sum_{x=1}^{L}Det(M_L)^*\{(D_{eff}/2+v/2)^{L-x+1}Det(M_{x-1}) \\ &+(D_{eff}/2-v/2)^{x}Det(M_{L-x})\}\langle\tilde{\eta}_x\tilde{\eta}_0^*\rangle\Bigg]\end{aligned} \tag{3.94}$$

The first term is:

$$|Det(M_L)|^2\langle\tilde{\eta}_0\tilde{\eta}_0^*\rangle = \frac{2A|Det(M_L)|^2}{T} \tag{3.95}$$

The second term is:

$$\begin{aligned}&\sum_{x=1}^{L}\sum_{x'=1}^{L}\{(D_{eff}/2+v/2)^{L-x+1}Det(M_{x-1}) \\ &+(D_{eff}/2-v/2)^{x}Det(M_{L-x})\} \\ &\times\{(D_{eff}/2+v/2)^{L-x'+1}Det(M_{x'-1})+(D_{eff}/2-v/2)^{x'}Det(M_{L-x'})\}^*\langle\tilde{\eta}_x\tilde{\eta}_{x'}^*\rangle \\ =&\frac{A}{T}\Bigg[\sum_{x=1}^{L}2|(D_{eff}/2+v/2)^{L-x+1}Det(M_{x-1})+(D_{eff}/2-v/2)^{x}Det(M_{L-x})|^2 \\ &-\sum_{x=2}^{L}\Big\{[(D_{eff}/2+v/2)^{L-x+1}Det(M_{x-1})+(D_{eff}/2-v/2)^{x}Det(M_{L-x})] \\ &\times[(D_{eff}/2+v/2)^{L-x+2}Det(M_{x-2})+(D_{eff}/2-v/2)^{x-1}Det(M_{L-x+1})]^* \\ &+[(D_{eff}/2+v/2)^{L-x+1}Det(M_{x-1})+(D_{eff}/2-v/2)^{x}Det(M_{L-x})]^* \\ &\times[(D_{eff}/2+v/2)^{L-x+2}Det(M_{x-2})+(D_{eff}/2-v/2)^{x-1}Det(M_{L-x+1})]\Big\}\Bigg]\end{aligned} \tag{3.96}$$

The third term is:

$$\begin{aligned}
&\sum_{x=1}^{L} Det(M_L)\{(D_{eff}/2+v/2)^{L-x+1}Det(M_{x-1}) \\
&+(D_{eff}/2-v/2)^{x}Det(M_{L-x})\}^*\langle\tilde{\eta}_0\tilde{\eta}_x^*\rangle \\
= \;& \frac{A}{T}\big\{Det(M_L)[(D_{eff}/2+v/2)^{L}Det(M_0)+(D_{eff}/2-v/2)^{1}Det(M_{L-1})]^* \\
&+Det(M_L)[(D_{eff}/2+v/2)^{1}Det(M_{L-1})+(D_{eff}/2-v/2)^{L}Det(M_0)]^*\big\}
\end{aligned} \tag{3.97}$$

The last term is:

$$\begin{aligned}
&\sum_{x=1}^{L} Det(M_L)^*\{(D_{eff}/2+v/2)^{L-x+1}Det(M_{x-1}) \\
&+(D_{eff}/2-v/2)^{x}Det(M_{L-x})\}\langle\tilde{\eta}_x\tilde{\eta}_0^*\rangle \\
=& \frac{A}{T}\big\{Det(M_L)^*[(D_{eff}/2+v/2)^{L}Det(M_0)+(D_{eff}/2-v/2)^{1}Det(M_{L-1})] \\
&+Det(M_L)^*[(D_{eff}/2+v/2)^{1}Det(M_{L-1})+(D_{eff}/2-v/2)^{L}Det(M_0)]\big\}
\end{aligned} \tag{3.98}$$

To connect to the simulation data, we again sum over the harmonics as we did in Eqn. (3.64). The numerical results for the two theories are the same for all ω. Therefore, the ratio of the ordinary and constrained TASEPs using this "matrix" approach will give the same ratio as the previous theory. This result is shown in Fig. 3.15.

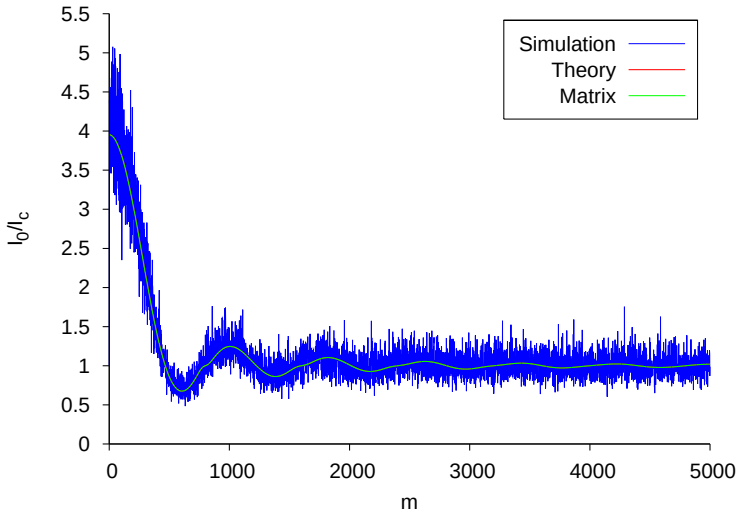

Figure 3.15: Simulation data and theory for the ratio of the ordinary TASEP power spectrum to the constrained TASEP power spectrum for $\bar{\rho}=0.1$ with $L=1000$ and $D_{eff}=1$ plotted as a function of m.

From this information, we conclude that these substructures are real and not an artifact of the numerical calculations. However, it should be noted that the non-linearities have not been fully taken into account. The non-linear terms could possibly remove or alter these additional structures in the oscillations. Exactly how these terms affect the power spectrum could be quantitatively found using a field theory approach. However, such an approach is beyond the scope of this dissertation.

3.3 Summary

In summary, we have studied how to generalize the domain wall theory to include the feedback effect due to having finite resources. The effective entry rate α_{eff}, the value of which depends on the shock location, was incorporated into the hopping rates in the master equation for the domain wall. The GDW theory better predicts the $\rho(N_{tot})$ curve in the SP case [57, 61]. While this improvement is minor, the GDW theory is essential to capture the features seen the in density profiles for both the HD and SP case [61]. In the HD case, we see shock being localized to a region on the TASEP as the system crosses over from a LD state to a HD one. The simple DW theory fails to capture this new feature [61]. The GDW theory utilizes the feedback effect of α_{eff} to correctly predict the density profiles.

We have also explored the power spectrum of the total occupancy for the constrained TASEP. Through Monte Carlo simulations, we saw oscillations in the LD states that were similar to those seen in the ordinary TASEP [55]. A new feature appeared near $\omega = 0$ where the power spectrum of constrained TASEP was suppressed when compared to the power spectrum of the ordinary TASEP. We presented a linear theory that included how α_{eff} changed with N_p to explain this suppression. While the result for the power spectrum did not match the simulation data in absolute terms, the ratio of power spectra of the ordinary to the constrained TASEP did agree between the theory and the simulation. A similar suppression was found in the crossover regime in the HD case when compared to the ordinary TASEP's power spectrum in the SP. Here again, the changing α_{eff} was incorporated into a theory to correctly predict the suppression.

Chapter 4

Multiple TASEPs with Finite Resources

In this chapter, we wish to extend the constrained TASEP to include additional TASEPs connected to the same reservoir of particles. For each TASEP, the entry rate α_{eff} and the exit rate β are the same, however, they can have different lengths. An arbitrary number of TASEPs can be connected to the pool of particles, but we will start with the simplest case of just two TASEPs. We will be presenting both Monte Carlo simulation data and theoretical considerations. Later, we will look at the power spectrum of the total occupancy of each TASEP.

4.1 Model

The model we are considering consists of multiple TASEPs connected to a single reservoir with a finite number of particles. For a single constrained TASEP, a particle leaving the pool only had one site, namely the first site on the lattice, to move to. This situation is different in the multiple TASEP case. A particle leaving the pool can move to the first site on any of the TASEPs with equal probability. We define our MCS differently from the single TASEP case as well. Previously, one MCS consisted of $L+1$ updates [57]. Here, we define one MCS to be $\sum_i (L_i + 1)$, where L_i is the length of the ith TASEP. This definition allows for the possibility of a particle entering the lattice for each TASEP in a single MCS. Otherwise, the simulation processes is the same as for the single constrained TASEP.

In this model, we have chosen again to use the same form of α_{eff} as in [57], however we will modify the value of N^*. Previously, N^* was simply the average number of particles in the ordinary TASEP for a given α and β. This number depended upon the length of the TASEP. With multiple TASEPs connected to the same pool of particles, we choose N^* to

be:

$$N^* = M^{-1} \sum_{\ell=1}^{M} \bar{\rho}_\ell L_\ell \tag{4.1}$$

where M is the number of TASEPs connected to the pool and $\bar{\rho}_\ell$ is the average density of the ordinary TASEP of length L_ℓ with entry and exit rates α and β. Unless otherwise specified, this definition of N^* will be used throughout the rest of this discussion.

4.2 Simulation results

We present the Monte Carlo simulation results for two and three TASEPs in this section. We will study the average overall density, current, and density profile in the steady state as a function of N_{tot}. We begin with the simplest situation of having only two TASEPs connected to the pool. As in the constrained TASEP, four cases will be explored, corresponding to having α and β in the LD, HD, MC, and SP. In each case, we consider what happens when the lengths are equal and when they are unequal.

4.2.1 LD case

In the LD case, α and β are such that the ordinary TASEP would be in the LD phase. In Fig. 4.1(a), we see that both TASEPs are in the LD phase and have the same average overall density and current when the two lengths are equal. For unequal lengths, we observe that

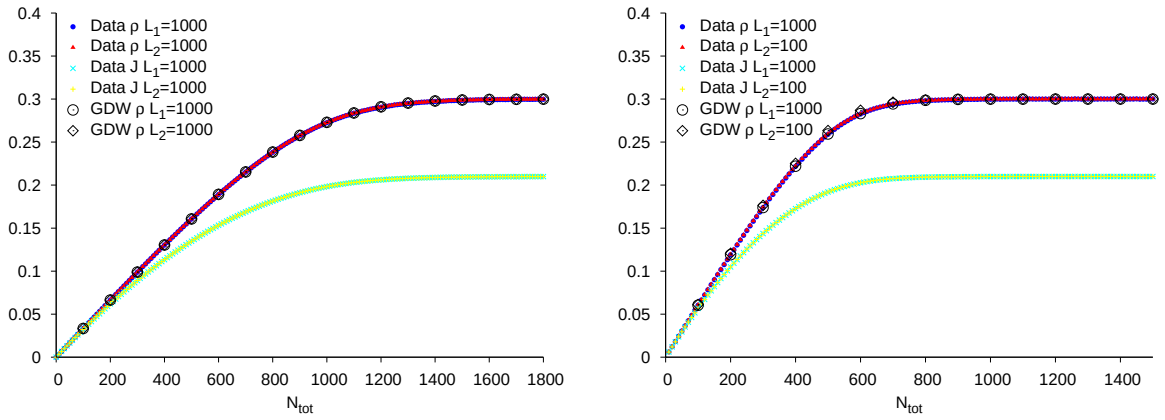

(a) (b)

Figure 4.1: Average overall density and current as a function of N_{tot} with $\alpha = 0.3$ and $\beta = 0.7$ for (a) $L_1 = L_2 = 1000$ and (b) $L_1 = 1000$ and $L_2 = 100$. Originally published in [63].

the current and overall density are again the same (Fig. 4.1(b)). The reason for the two

densities being equal is due to the TASEPs having the same α_{eff} and β. The overall density is equal to α in the ordinary TASEP, but here it is equal the average α_{eff}. The two TASEPs are connected to the same pool of particles and have the same α_{eff}. Thus, they will also have the same average overall density and current. The initial linear rise in ρ is due to the form of α_{eff} chosen. In this case, α_{eff} rises linearly with N_{tot} for small N_{tot}. Therefore, the overall density follows the same linear dependence on N_{tot}.

4.2.2 MC case

Next, we consider what happens when $\alpha > 1/2$ and $\beta > 1/2$ such that the TASEP would normally be in the MC phase. We will look at two TASEPs with equal and unequal lengths. When the lengths are equal, we again observe both TASEPs having the same average overall density and current (Fig. 4.2(a)). Finite size effects are observed when the lengths are

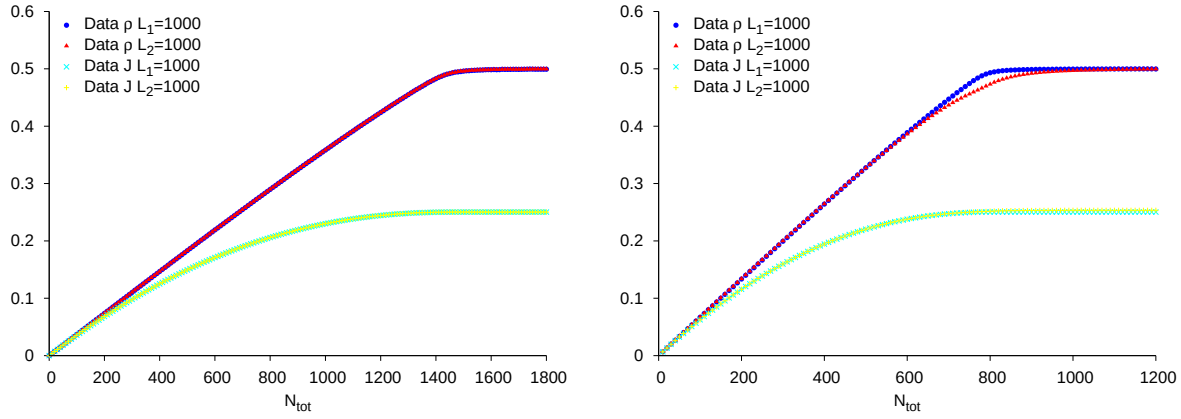

Figure 4.2: Average overall density and current as a function of N_{tot} with $\alpha = 0.7$ and $\beta = 0.7$ for (a) $L_1 = L_2 = 1000$ and (b) $L_1 = 1000$ and $L_2 = 100$. Originally published in [63].

unequal (Fig. 4.2(b)). The finite size effects are similar to those observed in [57].

To explain the linear rise in the overall density as N_{tot} is increased, we notice that the system is effectively in a LD state for small values of N_{tot}. There are not enough particles in the system for the TASEPs to reach the MC phase when N_{tot} is small, so the TASEPs will act as though they are in the LD phase. Eventually, the average α_{eff} will become greater than 1/2 and the overall density and current will reach a constant value of 1/2 and 1/4 respectively for each TASEP.

4.2.3 SP case

Now, we turn our attention to the case when $\alpha = \beta$. In the ordinary TASEP, the system would be in the SP along the coexistence line between the HD and LD phases. However for small N_{tot}, the two TASEPs are again effectively in a LD state. The crossover from the LD phase to the SP as N_{tot} is not as simple as going from the LD to MC phase. Fig. 4.3(a) shows how the overall density changes with N_{tot}. This curve is similar to the one found for a single

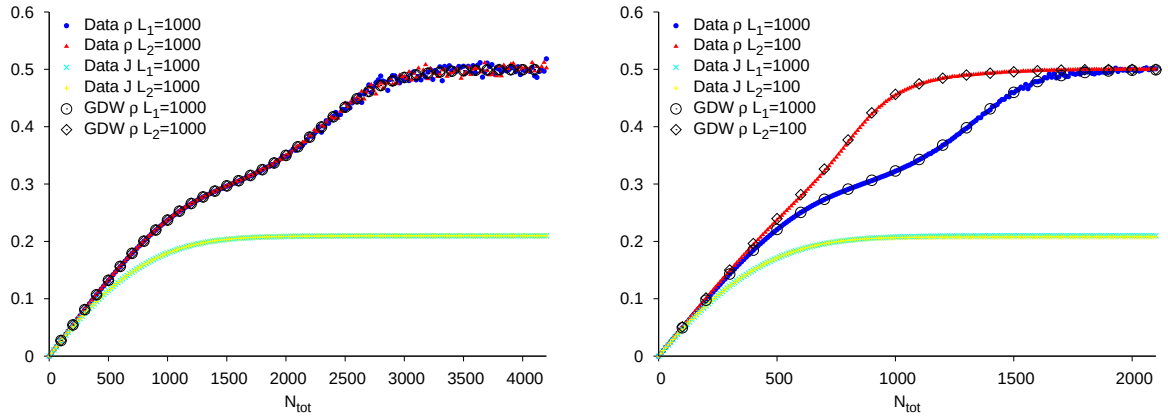

(a) (b)

Figure 4.3: Average overall density and current as a function of N_{tot} with $\alpha = \beta = 0.3$ for (a) $L_1 = L_2 = 1000$ and (b) $L_1 = 1000$ and $L_2 = 100$. Originally published in [63].

constrained TASEP in [57]. Again, the two overall densities and currents are equal due to α_{eff} and β being the same for both TASEPs. When the lengths are not equal, the overall densities are not always the same. As seen in Fig. 4.3(b), the $\rho(N_{tot})$ curves are different for different lengths. However, the overall density curve for each TASEP is similar to its single constrained TASEP counter part in [57]. In order to understand how the overall density depends on N_{tot} for each TASEP, we will need to use the generalized domain wall approach which will be covered later.

4.2.4 HD case

We see new phenomena occurring when α and β are set in the HD phase. When the TASEPs' lengths are equal, the overall densities and currents are equal and the $\rho(N_{tot})$ curve in Fig. 4.4 is similar to that of a single constrained TASEP in the HD case in [57]. However, the density profile in the crossover regime, as seen in Fig. 4.5, for each of the two TASEPs is different than the profile of a single constrained TASEP. The additional TASEP prevents the shock from becoming localized in either lattice. To understand how the second TASEP affects the system, let us recall the cause of the localization. The feedback effect of α_{eff} kept the number of particles in the pool close to its average value, which in turn kept the

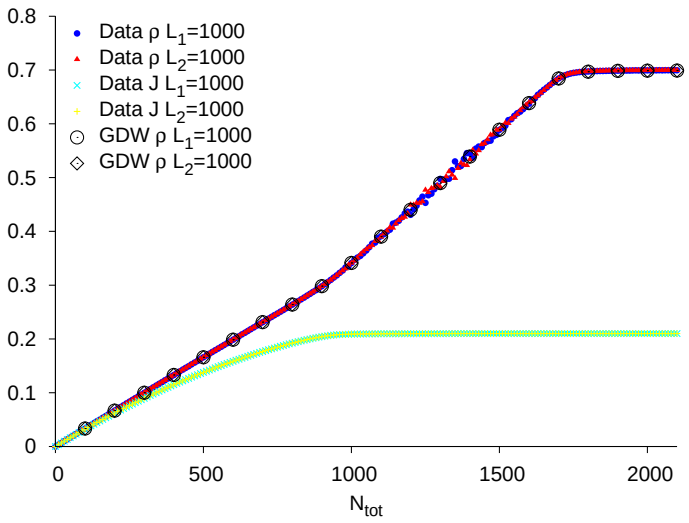

Figure 4.4: Average overall density and current as a function of N_{tot} with $\alpha = 0.7$ and $\beta = 0.3$ for $L_1 = L_2 = 1000$. Originally published in [63].

number of particles in the TASEP close to its average value [61]. This effect caused the shock between the LD and HD regions to be located about a certain site on the lattice. With two TASEPs, the feedback effect of α_{eff} still keeps N_p close to its average value, however, the two TASEPs can"trade" particles with one another via the pool. This transfer of particles allows the shocks in each lattice to wander over a larger region than the shock in the constrained TASEP case. The wandering of the shock gives rise to the linear part of the density profile in each TASEP, while the region of constant density (HD region in Fig. 4.5) shows where the shock is forbidden to wander.

When the lengths are unequal, a new feature arises in the overall density as a function of N_{tot}. A plateau forms in the overall density during the crossover regime for the smaller TASEP as seen in Fig. 4.6. The overall density of the smaller TASEP is constant in this region as well as N_p, so all of the extra particles coming from an increase in N_{tot} must go into the larger TASEP. The situation for the larger TASEP is similar to that of a single constrained TASEP. On the other hand, the overall density for the smaller TASEP is 1/2, which is the same as the ordinary TASEP in the SP. This view is confirmed when looking at the density profiles for each TASEP in Fig. 4.7. The smaller TASEP has a linear profile like the ordinary TASEP in the SP, while the larger TASEP has a localized shock as the constrained TASEP has in this regime. The explanation for the two different profiles can again be traced back to the particle exchange between the two TASEPs. The shock in each TASEP is allowed to wander as in the case when the lengths are equal. However, the wandering of the shock in the smaller TASEP is limited by its size. As N_{tot} is increased, the shock in the smaller TASEP is allowed to perform a random walk across its entire lattice. Yet, the two TASEPs can only exchange particles until the shock in the smaller TASEP is located at the entrance to the lattice. This limit puts a constraint on the wandering of the shock in the larger

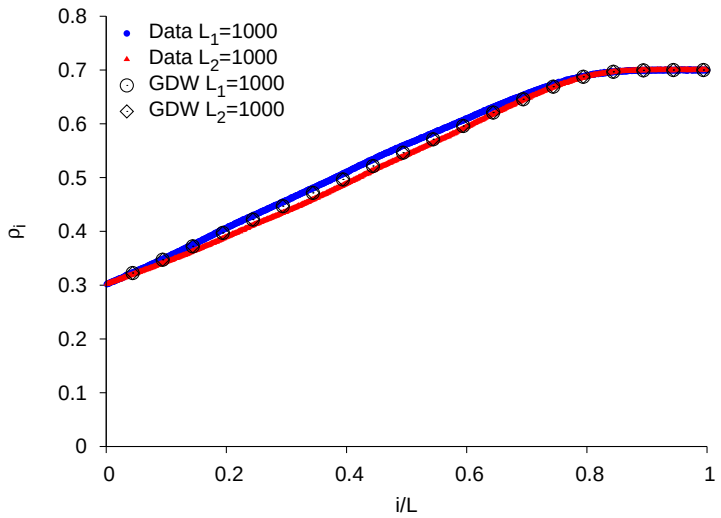

Figure 4.5: Average density profile with $\alpha = 0.7$, $\beta = 0.3$, and $N_{tot} = 1400$ for $L_1 = L_2 = 1000$. Originally published in [63].

TASEP, which localizes the shock. Also, the additional particles coming from the increase in N_{tot} must be absorbed into the larger TASEP. The extra particles change the location of the localization of the shock on the larger lattice, similar to what is seen in the constrained TASEP case [61].

On closer inspection, the width of the shock localization is larger than the width of the constrained TASEP [61]. The broadening of the localization is due to the additional TASEP. Thus, there are two effects contributing to this localization width. They are (i) the feedback from the fluctuating α_{eff} and (ii) the extra degree of freedom the smaller TASEP provides through particle exchange. We can eliminate the effects of (ii) to recover the "intrinsic" width due to (i). First, we calculate the location of the shock for each TASEP using the relation between the shock position k and the number of particles on the lattice N via $N = (1-\beta)(L-k) + \alpha_{eff}k$. We then shift the positions of the shocks in each lattice by δ given by:

$$\delta = \frac{N_1 - N_2 - (1-\beta)(L_1 - L_2)}{1 - 2\beta} \tag{4.2}$$

The $(1-\beta)(L_1 - L_2)$ term in the numerator accounts for the extra particles due to the difference in lengths and the $1 - 2\beta$ in the denominator is simply the shock height. The shock position on the larger lattice k_1 is decreased by δ, while the position on the shorter lattice k_2 is increase by δ. The two shocks positions are now at the same location. The occupations of each site on each TASEP are averaged together between sites 1 and L_1 in this new shifted coordinate. If the shifted site falls outside of the real lattice, then the extra sites are randomly filled with an average density of $1 - \beta$ if the location is greater than L or with an average density of β if the location is less than 1. With this procedure, we are able to reproduce the profile seen in a single constrained TASEP with length $L = L_1 + L_2$

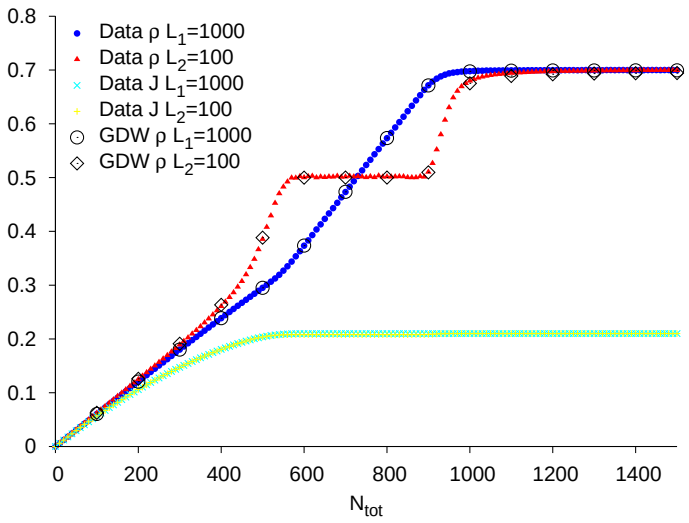

Figure 4.6: Average overall density and current as a function of N_{tot} with $\alpha = 0.7$ and $\beta = 0.3$ for $L_1 = 1000$ and $L_2 = 100$. Originally published in [63].

as shown in Fig. 4.8.

Another quantity of interest is the probability $P(N_1, N_2)$ of finding N_1 particles on the first TASEP and N_2 particles on the second one. This quantity is shown in Fig. 4.9(a) for equal length and Fig. 4.9(b) for when the length are not equal for the crossover regime in the HD case. The ridge in each figure confirms the particles exchange between the two TASEPs. Along the ridge, the probability of finding the pair (N_1, N_2) is approximately equal. However, the projection along each axis differs whether the lengths are equal or unequal. The projections are shown in Fig. 4.10(a) and Fig. 4.10(b) for the equal and unequal lengths, respectively. As one can see, the plots differ greatly. With the lengths equal, the distributions are the same, which should come as no surprise due to the symmetry between the two TASEPs. When the lengths are not equal, the smaller TASEP has a nearly flat distribution while the larger TASEP has a Gaussian distribution. The flat distribution comes from the random walk of the shock in the smaller TASEP and the Gaussian distribution comes from the localization of the shock. As the difference in the lengths decreases, the two projected distributions begin to approach the same distribution.

To understand the last statement better, we will schematically sketch in Fig. 4.11(a) and Fig. 4.11(b) how the probability distribution $P(N_1, N_2)$ changes as N_{tot} increases. For both equal and unequal TASEPs, the probability is concentrated about a single point for small N_{tot}. As the system enters the crossover regime, we see the distributions begin to form ellipses along a line of constant $N_1 + N_2$ and are bounded by the dotted box. The box represents the allowed region for the LD and HD to coexist. For the TASEPs with equal lengths, the size of the ellipse expands then contracts as the final HD state is reached. However when the lengths are unequal, the ellipse expands, then remains constant over a range of N_{tot}, and finally contracts to the HD state. The size of the smaller TASEP restricts the vertical length

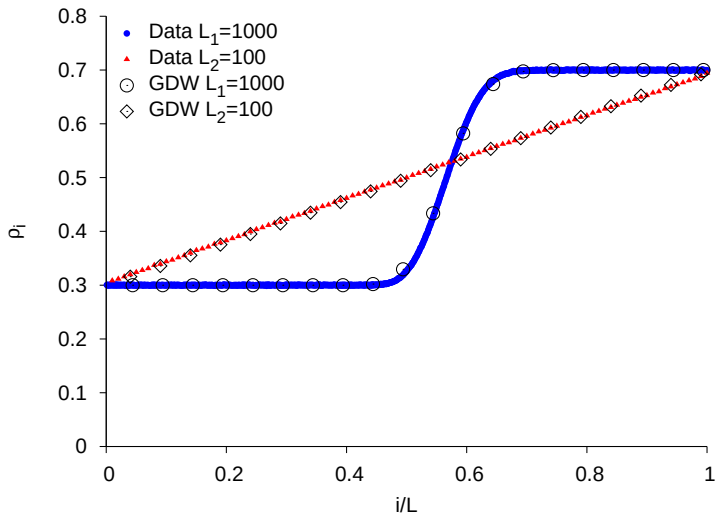

Figure 4.7: Average density profile with $\alpha = 0.7$, $\beta = 0.3$, and $N_{tot} = 700$ for $L_1 = 1000$ and $L_2 = 100$. Originally published in [63].

of the ellipse and forces the it to remain constant once the entire length has been filled.

The sketches give a qualitative explanation of the competition between the two TASEPs, but fail to capture the more subtle details. If we look at how the gradient of N changes with N_{tot} in Fig. 4.12 for both TASEPs and the pool, then we see five regimes during the HD/LD coexistence region instead of the three one would expect from Fig. 4.11(b). As the system approaches the crossover region, we see a rapid increase in the gradient for the smaller TASEP that precedes the increase in the larger one. After the rise in the smaller TASEP, the gradient decays to a value of zero. As the system leaves this coexistence region, the reverse process occurs for the smaller TASEP. For the larger one, an unexpected decrease in the gradient occurs before the system enters the crossover region. Also, the decrease in the gradient for the pool begins at the same N_{tot} value that the smaller TASEP's gradient begins to increase for both entering and leaving the crossover region. While the sketch in Fig. 4.11(b), does provide insight on how the system is changing with N_{tot}, it fails to explain the more subtle features seen in the gradients of N_1, N_2, and N_p. A more quantitative explanation is needed, mainly an appropriately generalized domain wall theory.

New features arise when two TASEPs have different lengths in the HD case, so what happens when additional TASEPs are added? To answer this question, we examine what happens when we have three TASEPs connected to a reservoir of particles. In the HD case with three different lengths, we again see a plateau in the crossover region (Fig. 4.13(a)). The smallest TASEP reaches the plateau first, then the second smallest. The largest TASEP follows a curve similar to a single constrained TASEP [57]. From the two TASEP case, we suspect that the smaller two TASEPs have delocalized shocks and are in a SP, while the largest TASEP has a localized shock in this regime. The suspicion is confirmed by the density profiles for each TASEP shown in Fig. 4.13(b). The smallest two TASEPs have linear profiles indicating

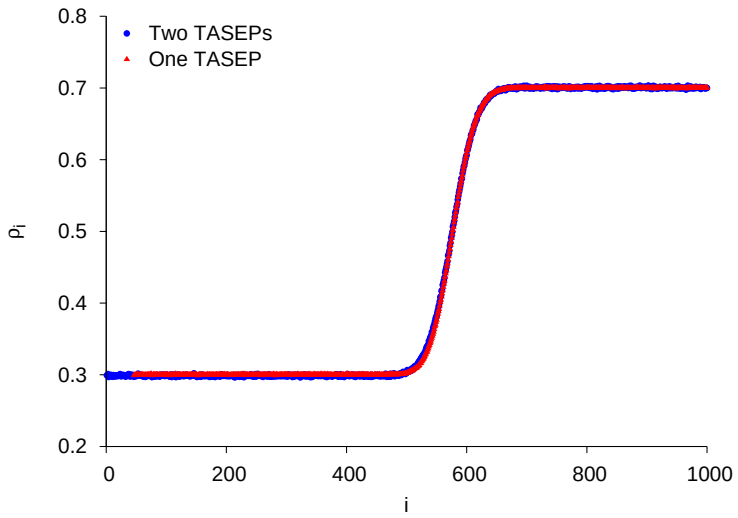

Figure 4.8: Comparison of the intrinsic shock localization for one and two TASEPs coupled to a finite reservoir. For two TASEPs, $L_1 = 1000$ and $L_2 = 700$ with $\alpha = 0.7$, $\beta = 0.3$, and $N_{tot} = 1000$. For the single TASEP, $L = 1700$ with $\alpha = 0.7$, $\beta = 0.3$, and $N_{tot} = 1250$. The data is shifted along the x-axis in order for the data to overlap.

a shock performing a random walk over each lattice. The largest TASEP contains a localized shock due to the effect of α_{eff} [61]. As we will see in the next section, these features can be explained by an appropriately generalized domain wall theory.

4.3 Generalized domain wall theory for multiple TASEPs

In this section, we will explain the above simulation results using the generalized domain wall (GDW) theory. The approach is similar to what is done in the previous chapter. We again incorporate α_{eff} into the hopping rates. Instead of one domain wall, multiple domain walls are found – one for each lattice. Since the positions of the walls do not have to be the same, we will label the positions by $\{k_m\}$ where k_m is the location of the DW on the mth lattice. Now, we define the effective entry rate α_{eff} given above in terms of $\{k_m\}$:

$$\alpha_{eff}(K) = \alpha \tanh\left(\frac{N_{tot} - (1-\beta)\sum_\ell L_\ell - (\alpha_{eff} + \beta - 1)K}{N^*}\right) \tag{4.3}$$

where

$$K = \sum_{\ell=1}^{M} k_\ell \tag{4.4}$$

and M is the number of TASEPs. Note that α_{eff} only depends on the sum of the $\{k_\ell\}$. α_{eff} can be solved for self-consistently in the above equation in terms of K. The calculation is

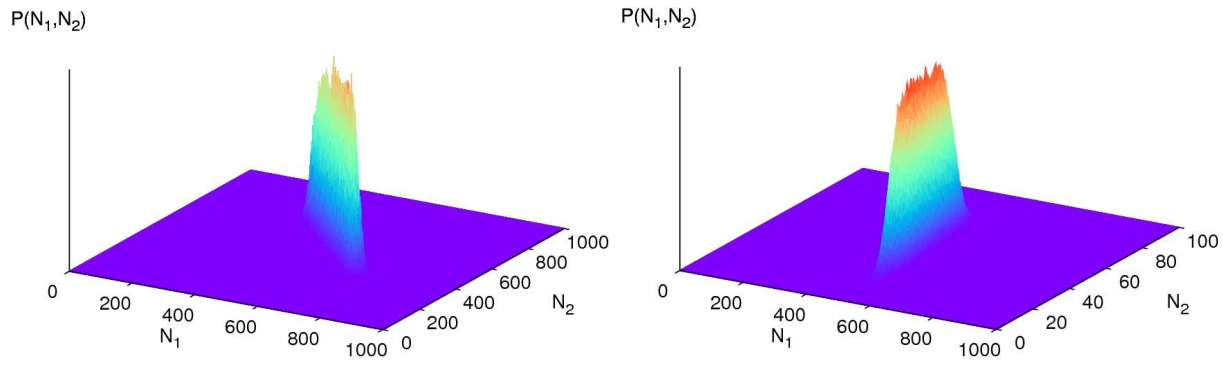

(a) (b)

Figure 4.9: Distribution of (N_1, N_2) with $\alpha = 0.7$ and $\beta = 0.3$ for (a) $L_1 = L_2 = 1000$ with $N_{tot} = 1400$ and (b) $L_1 = 1000$ and $L_2 = 100$ with $N_{tot} = 700$. Originally published in [63].

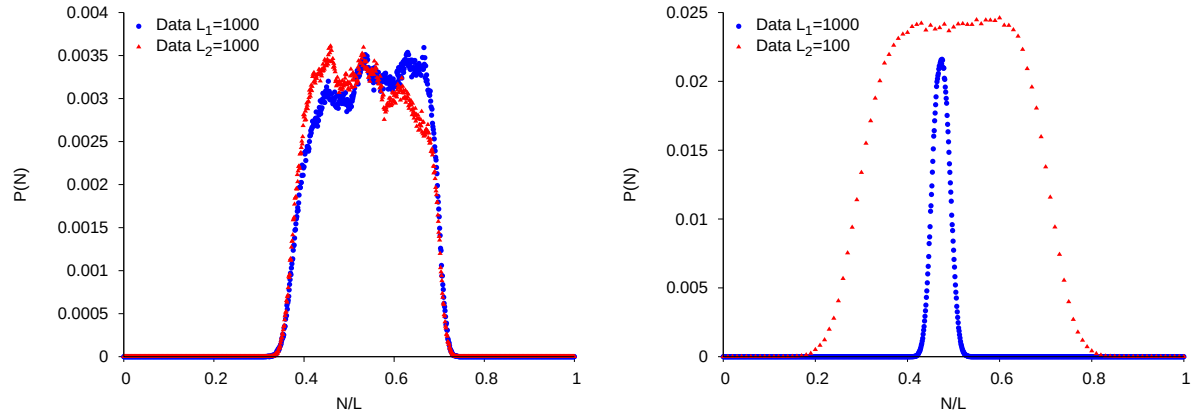

(a) (b)

Figure 4.10: Distribution of N_1 and N_2 with $\alpha = 0.7$ and $\beta = 0.3$ for (a) $L_1 = L_2 = 1000$ with $N_{tot} = 1400$ and (b) $L_1 = 1000$ and $L_2 = 100$ with $N_{tot} = 700$.

carried out numerically due to the non-linear nature of the tanh function. With $\alpha_{eff}(K)$ we can now define the hopping rate:

$$D_K^- = \frac{\alpha_{eff}(1-\alpha_{eff})}{1-\beta-\alpha_{eff}} \tag{4.5}$$

$$D_K^+ = \frac{\beta(1-\beta)}{1-\beta-\alpha_{eff}} \tag{4.6}$$

The hopping rates are the same for all TASEPs since they all have the same α_{eff} and same β.

In the single constrained TASEP, the value of N_{tot} restricted the DW's movements and created a minimum position k_{min} at which the DW could be located [61]. A similar situation occurs here for the multiple TASEPs. When all the particles are located on the TASEPs,

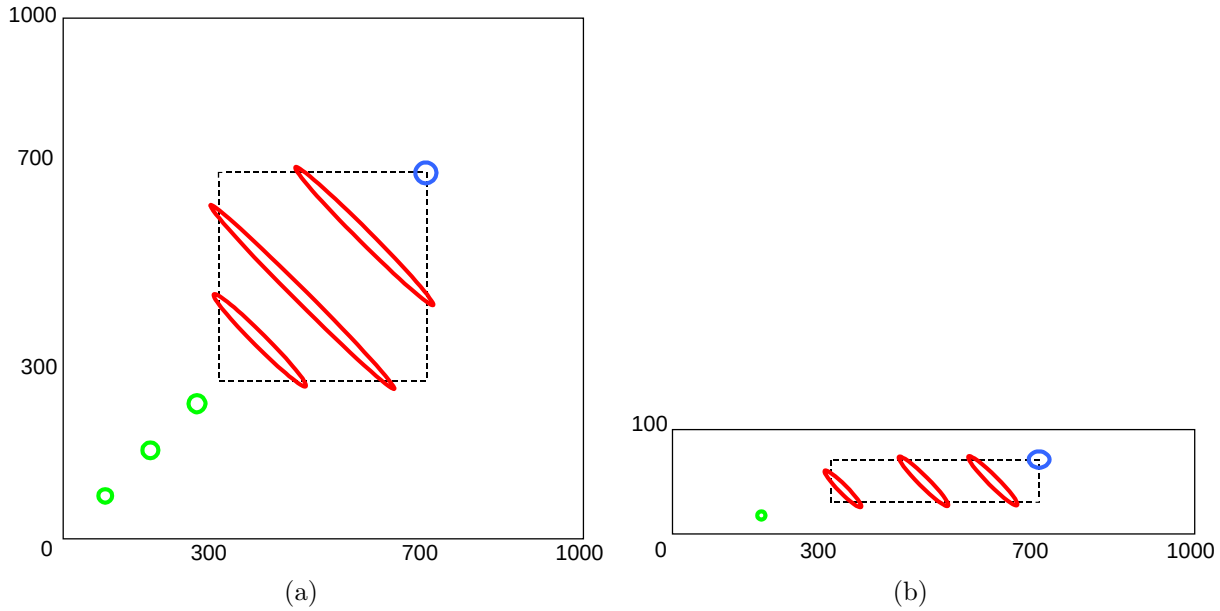

Figure 4.11: Sketch of distributions in the $N_1 - N_2$ plane with $\alpha = 0.7$ and $\beta = 0.3$ for (a) $L_1 = L_2 = 1000$ and (b) $L_1 = 1000$ and $L_2 = 100$. Originally published in [63].

no more particles can enter. So using the relation between the k and N for each TASEP, we have:

$$N_{tot} = (1-\beta)\sum_{\ell} L_\ell - (1-\beta)K \tag{4.7}$$

and we define K_{min} to be:

$$K_{min} = \sum_{\ell} L_\ell - \frac{N_{tot}}{1-\beta} \tag{4.8}$$

As opposed to the single constrained TASEP, the multiple TASEP situation allows for the TASEPs to trade particles between each other. The individual k's can be any value as long as their sums are greater than K_{min}. Thus, the sum of the DW positions is the important quantity in this case.

A master equation with reflecting boundary conditions is written for the probability $P(\{k_\ell\})$ of find the shocks in configuration $\{k_\ell\}$. We will begin with the simplest case of two TASEPs connected to the pool. From the insights gain from the two TASEP case, we will extend the results to an arbitrary number of TASEPs. We will then compare the results to the simulation data for two and three TASEPs.

4.3.1 Two TASEP Case

For the two TASEP case, the position of the domain wall performs a random walk in two dimensions with the hopping rates depending on the position of the walker. Each dimension

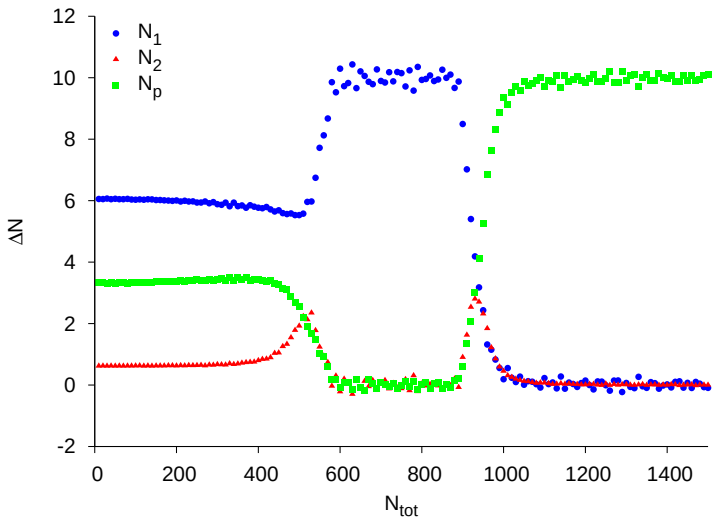

Figure 4.12: Gradients of the average occupation N_1, N_2, and N_p with respect to N_{tot} for $L_1 = 1000$ and $L_2 = 100$ with $\alpha = 0.7$ and $\beta = 0.3$.

represents the position of the shock in an individual TASEP. There is an average position in the two dimensional plane about which a random walk is performed. At steady-state, we must solve:

$$\begin{aligned} 0 &= D_{-(k_1+k_2+1)}[P(k_1+1,k_2)+P(k_1,k_2+1)] \\ &\quad +D_{+(k_1+k_2-1)}[P(k_1-1,k_2)+P(k_1,k_2-1)] \\ &\quad -2[D_{+(k_1+k_2)}+D_{-(k_1+k_2)}]P(k_1,k_2) \end{aligned} \tag{4.9}$$

along with the reflecting boundary conditions. The boundary is a rectangle in the $k_1 - k_2$ plane for large enough N_{tot}. The equations for the four corners are:

$$0 = D_1^-[P(0,1)+P(1,0)] - 2D_0^+P(0,0) \tag{4.10}$$

$$0 = D^+_{L_1+L_2-1}[P(L_1-1,L_2)+P(L_1,L_2-1)] - 2D^-_{L_1+L_2}P(L_1,L_2) \tag{4.11}$$

$$0 = D^+_{L_1-1}P(L_1-1,0) + D^-_{L_1+1}P(L_1,1) - [D^+_{L_1}+D^-_{L_1}]P(L_1,0) \tag{4.12}$$

$$0 = D^+_{L_2-1}P(0,L_2-1) + D^-_{L_2+1}P(1,L_2) - [D^+_{L_2}+D^-_{L_2}]P(0,L_2) \tag{4.13}$$

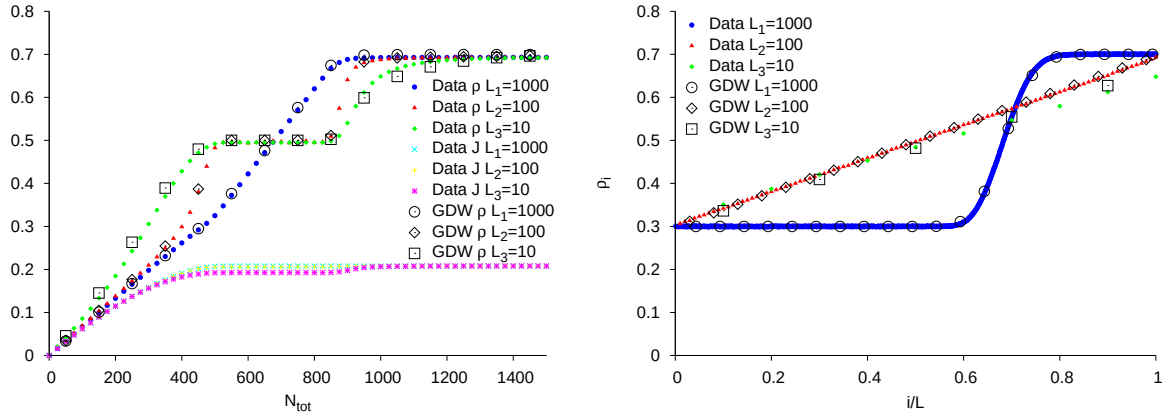

(a) (b)

Figure 4.13: (a) Average overall density and current as a function of N_{tot} with $\alpha = 0.7$ and $\beta = 0.3$ for $L_1 = 1000$, $L_2 = 100$, and $L_3 = 10$. (b) Average density profile with $\alpha = 0.7$, $\beta = 0.3$, and $N_{tot} = 600$ for $L_1 = 1000$, $L_2 = 100$, and $L_3 = 10$.

and the equations for the four sides are:

$$\begin{aligned} 0 &= D^-_{k_1+1}[P(k_1+1,0)+P(k_1,1)] \\ &\quad +D^+_{k_1-1}P(k_1-1,0) \\ &\quad -[D^-_{k_1}+2D^+_{k_1}]P(k_1,0) \end{aligned} \tag{4.14}$$

$$\begin{aligned} 0 &= D^-_{k_2+1}[P(0,k_2+1)+P(1,k_2)] \\ &\quad +D^+_{k_2-1}P(0,k_2-1) \\ &\quad -[D^-_{k_2}+2D^+_{k_2}]P(0,k_2) \end{aligned} \tag{4.15}$$

$$\begin{aligned} 0 &= D^+_{L_2+k_1-1}[P(k_1-1,L_2)+P(k_1,L_2-1)] \\ &\quad +D^-_{L_2+k_1+1}P(k_1+1,L_2) \\ &\quad -[D^+_{L_2+k_1}+2D^-_{L_2+k_1}]P(k_1,L_2) \end{aligned} \tag{4.16}$$

$$\begin{aligned} 0 &= D^+_{L_1+k_2-1}[P(L_1,k_2-1)+P(L_1-1,k_2)] \\ &\quad +D^-_{L_1+k_2+1}P(L_1,k_2+1) \\ &\quad -[D^+_{L_1+k_2}+2D^-_{L_1+k_2}]P(L_1,k_2) \end{aligned} \tag{4.17}$$

These equations can be solved analytically. We are basically looking for the zero eigenvalue of the transition matrix for $P(k_1, k_2)$. Since the hopping rates only depend on the sum of the shock positions, the product around a closed elementary loop is the same regardless of the direction taken. This observation means that the Kolmogorov criterion is satisfied and the process is reversible [64]. Therefore, we have detailed balance with

$$D^-_K P(k_1,k_2) = D^+_{K-1}P(k_1,k_2-1) = D^+_{K-1}P(k_1-1,k_2) \tag{4.18}$$

and the solution can be found using a recursion relation for $P(k_1, k_2)$. The solution is given by:

$$P(k_1,k_2) = \begin{cases} \frac{1}{Z}\prod_{j=K}^{L_1+L_2-1}\frac{D_{j+1}^-}{D_j^+} & \text{if } K \neq L_1+L_2, \\ \frac{1}{Z} & \text{if } K = L_1+L_2 \end{cases} \tag{4.19}$$

where Z is a normalization factor given by:

$$Z = 1 + \sum_{\{k_1,k_2\}} \prod_{j=K}^{L_1+L_2-1} \frac{D_{j+1}^-}{D_j^+} \tag{4.20}$$

Thus, the solution $P(k_1, k_2)$ only depends on the value of K. However, we have neglected K_{min} in the above equations. To incorporate this quantity, we define a region $\mathcal{R}$ to be bounded by:

$$\mathcal{R}: \quad 0 < k_1 < L_1, \quad 0 < k_2 < L_2, \quad K_{min} < k_1 + k_2 \tag{4.21}$$

Inside this region, $P(k_1, k_2)$ is given by Eqn. (4.19). Outside $\mathcal{R}$, the domain wall is not found in either lattice at position (k_1, k_2), so the probability is zero. The sum in the normalization Z is only summed over the (k_1, k_2) pairs in $\mathcal{R}$. By defining this region, we can successfully take into account the finite number of particles leading to K_{min}.

To see the dependence on K better, let us change the variables from $P(k_1, k_2)$ to $P(K, Q)$ where:

$$K = k_1 + k_2 \tag{4.22}$$
$$Q = k_1 - k_2 \tag{4.23}$$

Note, K and Q uniquely define the pair (k_1, k_2). We can rewrite the master equation in terms of the two new variables:

$$\begin{aligned} 0 = {} & D_{K+1}^-[P(K+1,Q+1) + P(K+1,Q-1)] \\ & + D_{K-1}^+[P(K-1,Q-1) + P(K-1,Q+1)] \\ & - 2[D_K^+ + D_K^-]P(K,Q) \end{aligned} \tag{4.24}$$

with the boundary conditions for the corners becoming:

$$0 = D_1^-[P(1,-1) + P(1,1)] - 2D_0^+P(0,0) \tag{4.25}$$

$$\begin{aligned} 0 = {} & D_{L_1+L_2-1}^+[P(L_1+L_2-1, L_1-L_2-1) + P(L_1+L_2-1, L_1-L_2+1)] \\ & - 2D_{L_1+L_2}^-P(L_1+L_2, L_1-L_2) \end{aligned} \tag{4.26}$$

$$\begin{aligned} 0 = {} & D_{L_1-1}^+P(L_1-1, L_1-1) + D_{L_1+1}^-P(L_1+1, L_1-1) \\ & - [D_{L_1}^+ + D_{L_1}^-]P(L_1, L_1) \end{aligned} \tag{4.27}$$

$$\begin{aligned} 0 = {} & D_{L_2-1}^+P(L_2-1, -L_2+1) + D_{L_2+1}^-P(L_2+1, -L_2-1) \\ & - [D_{L_2}^+ + D_{L_2}^-]P(L_2, -L_2) \end{aligned} \tag{4.28}$$

and the four edges:

$$\begin{aligned}
0 &= D_{-(k_1+1)}[P(k_1+1,k_1+1)+P(k_1+1,k_1-1)] \\
&\quad +D^+_{k_1-1}P(k_1-1,k_1-1) \\
&\quad -[D^-_{k_1}+2D^+_{k_1}]P(k_1,k_1) \qquad (4.29)\\
0 &= D_{-(k_2+1)}[P(k_2+1,-k_2-1)+P(k_2+1,-k_2+1)] \\
&\quad +D_{+(k_2-1)}P(k_2-1,-k_2+1) \\
&\quad -[D_{-(k_2)}+2D_{+(k_2)}]P(k_2,-k_2) \qquad (4.30)\\
0 &= D_{+(L_2+k_1-1)}[P(k_1+L_2-1,k_1-L_2-1)+P(k_1+L_2-1,k_1-L_2+1)] \\
&\quad +D_{-(L_2+k_1+1)}P(k_1+L_2+1,k_1-L_2+1) \\
&\quad -[D_{+(L_2+k_1)}+2D_{-(L_2+k_1)}]P(k_1+l_2,k_1-L_2) \qquad (4.31)\\
0 &= D_{+(L_1+k_2-1)}[P(L_1+k_2-1,L_1-k_2+1)+P(L_1+k_2-1,l_1-k_2-1)] \\
&\quad +D_{-(L_1+k_2+1)}P(L_1+k_2+1,L_1-k_2-1) \\
&\quad -[D_{+(L_1+k_2)}+2D_{-(L_1+k_2)}]P(L_1+k_2,L_1-k_2) \qquad (4.32)
\end{aligned}$$

We also have from detailed balance:

$$\begin{aligned}
D^-_K P(K,Q) &= D^+_{K-1}P(K-1,Q-1) \qquad (4.33)\\
&\quad D^+_{K-1}P(K-1,Q+1) \qquad (4.34)
\end{aligned}$$

which suggests that $P(K,Q)$ only depends on K. However, Q is needed to determine if the domain wall is located in $\mathcal{R}$. Therefore, the normalization Z takes into account the multiplicity of each K value through Q.

The result in Eqn. (4.19) is similar to the result for the constrained TASEP [61]. By simply replacing k with K, we get the same result. However, the normalization constant will be different in each case. The additional TASEP allows for multiple configurations of k_1+k_2 to equal the same K value. The difference in Z values for the constrained TASEP and the two TASEP cases is why the shock is less localized in the crossover regime for the HD case in the larger TASEP than in the single constrained TASEP.

Before continuing to the multiple TASEP case, we wish to compare the GDW theory results to the simulation results with two TASEPs. From the solution $P(k_1,k_2)$, the average density profiles are calculated for each TASEP. Using a similar approach as the constrained TASEP [61], we find the profiles to be:

$$\begin{aligned}
\rho_1(i) &= \sum_{k_2=0}^{L_2}\left[(1-\beta)\sum_{k_1=0}^{i}P(k_1,k_2)+\sum_{k_1=i+1}^{L_1}\alpha_{eff}(K)P(k_1,k_2)\right] \qquad (4.35)\\
\rho_2(i) &= \sum_{k_1=0}^{L_1}\left[(1-\beta)\sum_{k_2=0}^{i}P(k_1,k_2)+\sum_{k_2=i+1}^{L_2}\alpha_{eff}(K)P(k_1,k_2)\right] \qquad (4.36)
\end{aligned}$$

For $\rho_1(i)$, the quantity $\sum_{k_2} P(k_1, k_2)$ is simply the probability of finding the DW at k_1 for any position of the DW in the other TASEP. Similarly, $\sum_{k_1} P(k_1, k_2)$ is the probability of finding the DW at position k_2 regardless of the location of the DW in the first TASEP. The average overall density $\rho_\ell = \sum_i \rho_\ell(i)/L_\ell$ for each TASEP can be calculated from the density profile.

The GDW theory results agree well with simulation data for all regimes – even the complex crossover region in the HD case – with no fit parameters. The GDW density profile results for the HD case are shown in Figs. 4.5 and 4.7. For unequal lengths, the GDW theory correctly predicts the shock localization in the larger TASEP and the delocalized shock in the smaller one. For equal lengths, the particle exchange that results in the linear region of the profile is also correctly predicted by this theory. As for the average overall density, the comparisons are shown in Figs. 4.1(a), 4.1(b), 4.3(a), 4.3(b), 4.4, 4.6. The most remarkable agreement comes for the crossover region in the HD when the length are not equal. The GDW theory correctly predicts the rise to the plateau region from the LD state and the rise to the final HD state.

The previous discussion of the SP-like region in the HD case lacked a quantitative explanation, but it can now be explained from the DW point of view. First, let us look at the ordinary TASEP with no constraint. For a single TASEP with no constraint, the correlation length ξ increases as α increases with $\beta < 1/2$ fixed before crossing the first order phase transition. At $\alpha = \beta$, ξ diverges and the system is in the SP. Also, the overall average density ρ deviates from the $\rho = \alpha$ relation near the phase boundary. The deviation is a finite size effect which comes from the system size L being of the order of ξ or smaller. Simply, the exponential tail of the density profile decays further into the bulk. From a DW point of view, the shock is allowed to wander further and further into the bulk as ξ increases. The shock will eventually be found at the other side of the TASEP with some non-trivial probability. It is at this point that the overall average density rises faster than the usual linear relationship as α is increased.

For a single constrained TASEP, there is no "correlation length" as defined in the ordinary TASEP. Instead, the changing α_{eff} keeps the shock from wandering far from its average position. Therefore the DW cannot reach the other side before $\alpha_{eff} = \beta$. Even when $\alpha_{eff} = \beta$, the shock is still localized to a region on the lattice due to the feedback from α_{eff}. This feedback effect creates a range of N_{tot} over which $\alpha_{eff} = \beta$ while the average position of the shock moves from the left to the right on the lattice. Thus, the overall average density rises linearly with N_{tot} until $\alpha_{eff} = \beta$, where it then rises linearly (but with different slope) with N_{tot} while $\alpha_{eff} = \beta$.

For two TASEPs competing for resources, we again find a different physical explanation. The addition of a second TASEP allows the shock to move more freely than in the constrained TASEP case. This is due to the fact that the number of particles in the pool can remain constant and each TASEP can exchange (via the pool) particles with each other. The probability to find the DW wandering into the bulk is the same for each TASEP regardless

of their size difference due to this particle exchange. If the two TASEPs are of different lengths, then at some N_{tot} value the shock will reach the other side of the smaller lattice. At this point, the larger lattice will start to "see" the finite resource effects and behave like a single constrained TASEP. Also, the larger lattice will shield the small TASEP from these same effects and the smaller one will behave like a single unconstrained TASEP. This explains the sudden increase in the overall average density near $\alpha_{eff} = \beta$ for the smaller TASEP and the value of 1/2 when $\alpha_{eff} = \beta$. The sudden increase is due to the diverging "correlation length", which in turn lengthens the decay of the tail in the density profile, while the value of 1/2 is due to the shock performing a random walk about the entire lattice. This also creates a delocalizing effect on the larger TASEPs localized shock which is related to the size of the smaller TASEP.

Coming back to the gradients in Fig. 4.12, we can now explain the complex crossover region. The sudden increase in the gradient of the smaller TASEP is due to the DW being found with some non-trivial probability at the entrance. The subsequent decay to zero is due to the density profile changing from an exponential decay to a linear one as the DW becomes more likely to be found at the entrance. The reverse process occurs at the second peak in the gradient for the smaller TASEP. The TASEP goes from a SP to a HD phase with an exponential decay at the entrance. For the larger TASEP, the gradient simply increases from one value to another due to the effects of α_{eff} and shock localization. Once the final HD state is reached, the gradient of N_1 decays to zero.

As a final note in this section, the relationship between $P(k_1, k_2)$ and $P(N_1, N_2)$ have the same difficulties as in the constrained TASEP case. The lack of a one-to-one correspondence and the restriction of possible N values that the domain wall theory can produce prevents us from begin able to predict $P(N_1, N_2)$ from $P(k_1, k_2)$. However in the crossover regime in the HD case, the shape of the distributions are similar. Therefore, only qualitative results can be arrived at from the GDW theory for this quantity.

Multiple TASEP case

For a system with M TASEPs, we can extend the results from the two TASEP case. For two TASEPs, the allowed (k_1, k_2) pairs form a two-dimensional region $\mathcal{R}$. In the M TASEP case, $\mathcal{R}$ will be an M-dimensional region that defines the allowed set of $\{k_\ell\}$. Since each TASEP has the same entry and exit rate, the Kolmogorov criterion will again be satisfied and we will have detailed balance. The solution will again only depend on K, which makes this effectively a one-dimensional problem. Therefore, we have inside the region $\mathcal{R}$:

$$P(\{k_\ell\}) = \begin{cases} \frac{1}{Z} \prod_{j=K}^{\sum_{\ell=1}^{M} L_\ell - 1} \frac{D_{j+1}^-}{D_j^+} & \text{if } K \neq \sum_{\ell=1}^{M} L_\ell, \\ \frac{1}{Z} & \text{if } K = \sum_{\ell=1}^{M} L_\ell \end{cases} \tag{4.37}$$

where Z is a normalization factor. Outside of $\mathcal{R}$, $P(\{k_\ell\})$ is zero. The normalization is much more complicated than in the two TASEP case due to the shape of $\mathcal{R}$ in M-dimensions.

From this solution, we can calculate the average density profile and overall density. The results are shown in Figs. 4.13(a) and 4.13(b) for three TASEPs. The numerical results from the GDW theory agree well with the simulation data. The theory correctly predicts the "plateau" region for the overall density for both of the smaller TASEPs and the value of N_{tot} for which each one reaches a value of 1/2. In the density profile, the linear profiles are predicted, while the localized shock is captured in the largest TASEP.

The explanation of these results are similar to the two TASEP case. At small N_{tot}, the TASEPs are in a LD state and have the same density. The exponential decay near the exit begins to extend further into the bulk as the total number of particles is increased. In the domain wall picture, the shock becomes more likely to be found further in the bulk. Since the wandering of the DW into the bulk is the same for all TASEPs, the effect on the overall density is greater on the smaller TASEPs, which is indicated by the density rising faster in the smaller two TASEPs with the smallest one rising the fastest. As the crossover regime is approached, the rapid increase in the density is due to the DW being more likely to be found at the entrance until it is found equally at any point on the lattice, giving an average overall density of 1/2. The DW reaches the entrance of the smallest TASEP first, followed by the next smallest, which is the order at which they reach a density of 1/2. As in the two TASEP case, the smaller TASEPs act as a buffer against the effect of α_{eff}. Once in the crossover regime, the smaller two TASEPs are in a SP with linear profiles and the largest TASEP sees the effect of α_{eff}. The largest TASEP has a localized shock and behaves similar to the constrained TASEP. The reverse process occurs for the smaller two TASEPs as the system enter the final HD state. In this state, the TASEPs appear to act independently due to the large value of N_{tot}.

4.4 Power Spectrum

We now turn our attention to the power spectra for multiple TASEPs. In order to keep the analysis simple, only the two TASEP case will be discussed. We consider the cases when the lengths are equal and unequal. Unlike with a single TASEP, correlations between different TASEPs can occur. Also, the power spectrum of the pool is not necessarily the same as either of the TASEPs. Therefore, we will look at the power spectra of each TASEP and the pool separately. Finally, we will look at the power spectrum of the difference of the total occupancy for each TASEP.

4.4.1 Power Spectra of Individual TASEPs

We look at the power spectra for the two TASEPs and the pool individually. For equal lengths (Fig. 4.14) in the effectively LD state, we again see a suppression at low frequencies, similar to those seen in the constrained TASEP. The two TASEPs have the same power

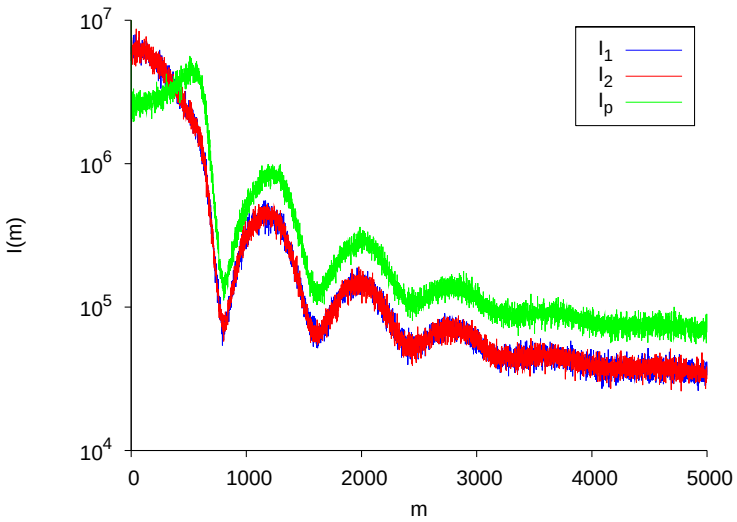

Figure 4.14: Power spectra for N_1, N_2, and N_p with $\alpha = 0.7$, $\beta = 0.3$, and $N_{tot} = 300$ for $L_1 = L_2 = 1000$.

spectra due to the symmetry of the system. The power spectrum associated with the pool occupation has a larger suppression than the power spectra of the TASEPs. This difference is due to the TASEPs exchanging particles which, as previously discussed, shields the TASEPs from seeing the effects of α_{eff}. The pool, however, has no such shielding and sees the effect of the fluctuating α_{eff}. To give another perspective, the power spectrum of the pool is effectively the power spectrum associated with $N_1 + N_2$. This quantity remains relatively constant, even if particle exchange occurs between the two TASEPs, leading to a smaller value of the power spectrum at low frequencies. α_{eff} keeps the sum constant on long time scales, but the sum's fluctuation on short time scales is unaffected by the changing entry rate. Thus, we only see the suppression at low ω and not at higher values.

On the other hand when compared to the power spectrum of the ordinary TASEP, the power spectra for the TASEPs are still suppressed at low ω. The constraint still affects each TASEP on long time scales, even though particle exchange can occur. If $N_1 + N_2$ is far from its average value, then the individual TASEPs will see the effects of α_{eff}. This effect will lead to a suppression similar to that of a single constrained TASEP, however, the particle exchange negates the full effects of the fluctuating α_{eff}. Thus, the suppression is not as great as that seen in the power spectrum of the pool occupation.

When the lengths are not equal, we see the suppression at low frequencies returning for the larger TASEP in Fig. 4.15. The suppression is much greater than in the equal lengths case and is nearly equal to that of the power spectrum of the pool for the larger TASEP. When looking at the smaller TASEP, we notice a "dip" at the same frequency as the first minimum of the larger TASEP. Since the minima are controlled by the lengths [55], we do not expect to see this feature in the smaller TASEP at such a low ω value. Also, the power spectrum is *enhanced* at small ω when compared to the power spectrum of the ordinary TASEP.

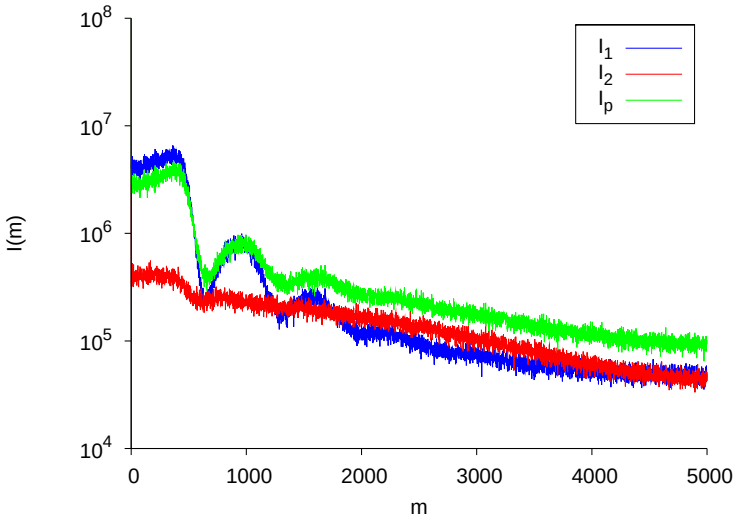

Figure 4.15: Power spectra for N_1, N_2, and N_p with $\alpha = 0.7$, $\beta = 0.3$, and $N_{tot} = 300$ for $L_1 = 1000$ and $L_2 = 100$.

Based on the arguments for the constrained TASEP power spectrum, the enhancement and additional minimum are not due to the effects of α_{eff} alone. Since the minimum is related to the length of the larger TASEP [55], the smaller TASEP clearly knows about the length of the larger one. One explanation for such an effect would be the particle exchange between the TASEPs. For example, a fluctuation could leave the smaller TASEP, enter and exit the larger TASEP, then re-renter the smaller one. This type of exchange would give a minimum in the smaller TASEP that is related to the length of the larger one.

For both equal and unequal lengths, one could write a linear theory for two TASEPs similar to that of the single constrained TASEP. Based on the previous results for a single constrained TASEP, a good agreement between the theory and the simulation data would be unlikely. Also, the two TASEPs would have different effective diffusion coefficients when the lengths are unequal that would be coupled to the power spectrum of the pool, making the theory difficult to fit to the simulation data. A more complete perturbative field theory approach should be used to incorporate the non-linear terms. This type of approach is beyond the scope of this dissertation. However, we will present the linear theory later to explain some of the features seen in the simulation data.

The crossover regime between the LD and HD states in the HD case also has interesting features. We will first discuss what is observed when the lengths are equal. The results are shown in Fig. 4.16 for $\alpha = 0.7$, $\beta = 0.3$, and $N_{tot} = 1400$ with $L_1 = L_2 = 1000$. Like in the constrained TASEP, we find the power spectrum of the pool to have a suppression at low ω. This finding agrees with what is observed in the LD case for the pool. The power spectra of the two TASEPs are equal, due to the symmetry in their sizes, and have a slight suppression at low frequencies when compared to the power spectrum of the ordinary TASEP, which is consistent with the results from the LD case. The difference in the suppressions follows the

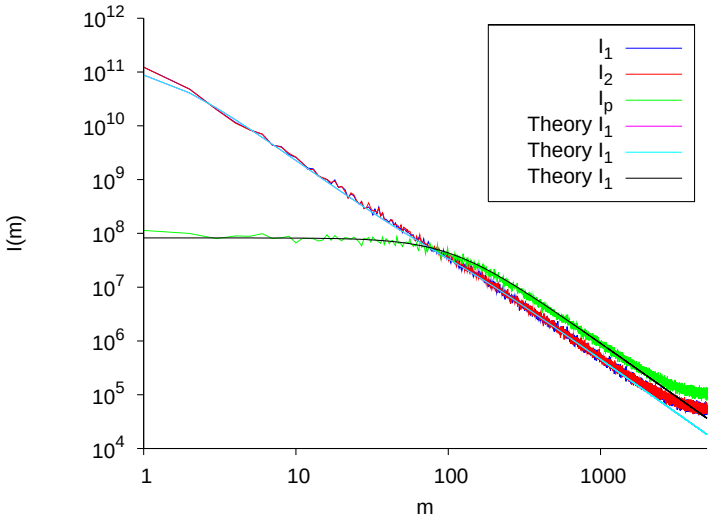

Figure 4.16: Power spectra for N_1, N_2, and N_p with $\alpha = 0.7$, $\beta = 0.3$, and $N_{tot} = 1400$ for $L_1 = L_2 = 1000$ and $L_2 = 100$.

same reasoning as the LD case. At large ω, all three power spectra decay as ω^{-2}, which is the same power law as the ordinary TASEP [55]. As we will see later, a simple mesoscopic theory can quantitatively explain the different suppression levels as well as the power law decay.

For unequal lengths in this crossover regime, we observe a suppression of the power spectra at low ω for both TASEPs and the pool in Fig. 4.17(a) for $\alpha = 0.7$, $\beta = 0.3$, and $N_{tot} = 700$ with $L_1 = 1000$ and $L_2 = 100$. Here the suppression is greatest with the pool, followed by the shorter TASEP, and finally the larger TASEP. However, the suppression at low ω for the smaller $L_2 = 100$ TASEP is due to finite size effects. When compared to the power spectrum of the ordinary TASEP I_0 with $L = 100$, we again see an enhancement at low ω as seen in Fig. 4.17(b). Unlike in the LD state, there is no indicator of the enhancement being linked to the particle exchange between the smaller and larger TASEP. Yet, particle exchange still occurs and should occur on long time scales, as evident in the LD state. Without a quantitative theory, the mechanism in the crossover regime for this enhancement is purely speculation. Such a theory will be discussed later.

4.4.2 Power Spectrum of the Difference

A more interesting quantity to study is the power spectrum of the difference. First, we define the difference of the total occupations of the TASEPs to be:

$$N_d(t) = N_1(t) - N_2(t) \tag{4.38}$$

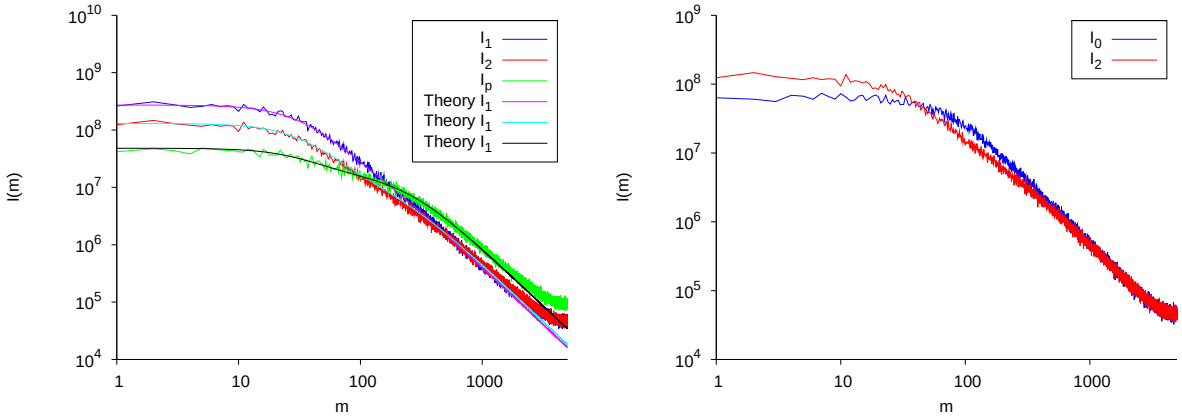

(a) (b)

Figure 4.17: (a) Power spectra for N_1, N_2, and N_p with $\alpha = 0.7$, $\beta = 0.3$, and $N_{tot} = 700$ for $L_1 = L_2 = 1000$ and $L_2 = 100$. (b) Comparison of the I_0 and I_2. For the ordinary TASEP, $\alpha = \beta = 0.3$ with $L = 100$. For the two TASEP case, $\alpha = 0.7$, $\beta = 0.3$, and $N_{tot} = 300$ with $L_1 = 1000$ and $L_2 = 100$.

We then define the power spectrum associated with this difference to be:

$$I_d(\omega) = \langle |\tilde{N}_d(\omega)|^2 \rangle \tag{4.39}$$

where $\tilde{N}_d(\omega)$ is the Fourier transform of $N_d(t)$. This quantity allows us to look at the correlation between the two TASEPs. It is closely related to the power spectrum of the pool, which corresponds to the power spectrum of the sum of N_1 and N_2. Yet as we will soon show, the power spectrum of the difference can be related to the power spectrum of the ordinary TASEP in a particular case, namely when the lengths of the two TASEPs are equal.

In the case that the two TASEPs have equal lengths, we find I_d does not show the suppression seen in the power spectra of the TASEPs and pool. This result is shown in Fig. 4.18(a) for $L_1 = L_2 = 1000$ with $\alpha = 0.7$, $\beta = 0.3$, and $N_{tot} = 300$. The average overall density is 0.1 for these parameters. When compared to the ordinary TASEP I_0, we see no suppression at low frequencies, instead, we find the overall amplitude is larger than the ordinary TASEP (Fig. 4.18(b)). In fact, the amplitude of I_d is twice the amplitude of I_0! One would expect a factor of two to naturally appear due to the symmetry of the model, but this argument neglects the effect of the finite resources. To understand the factor of two better, we expand I_d:

$$\begin{aligned} I_d &= \langle |\tilde{N}_1 - \tilde{N}_2|^2 \rangle \\ &= \langle |\tilde{N}_1|^2 + |\tilde{N}_2|^2 - 2Re(\tilde{N}_1 \tilde{N}_2^*) \rangle \\ &= I_1 + I_2 - 2Re\langle \tilde{N}_1 \tilde{N}_2^* \rangle \end{aligned} \tag{4.40}$$

where I_1 and I_2 are the power spectra for the two TASEPs connected to the pool. Note, the cross term $2Re\langle \tilde{N}_1 \tilde{N}_2^* \rangle$ has a negative sign in front of it. Since this term should remove the

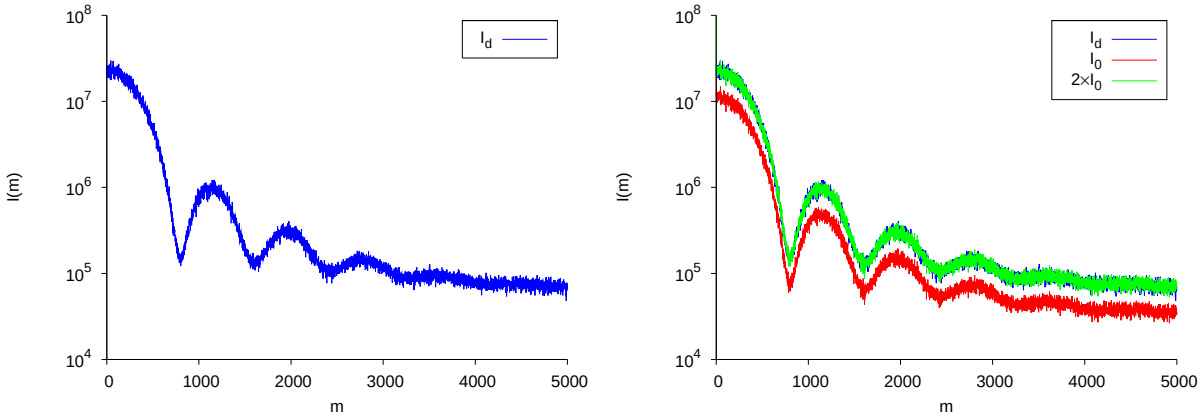

Figure 4.18: (a) Power spectrum associated with the difference of the total occupation of the TASEPs with $\alpha = 0.7$, $\beta = 0.3$, and $N_{tot} = 300$ for $L_1 = L_2 = 1000$. (b) Comparison of the I_0 and I_d. For the ordinary TASEP, $\alpha = 1 - \beta = 0.1$ with $L = 1000$. For the two TASEP case, $\alpha = 0.7$, $\beta = 0.3$, and $N_{tot} = 300$ with $L_1 = L_2 = 1000$.

suppression seen in I_1 and I_2 by increasing I_d, the sign of $2Re\langle\tilde{N}_1\tilde{N}_2^*\rangle$ should be negative, creating an overall positive quantity to add to $I_1 + I_2$. Also from the previous chapter, we related the constrained TASEP's power spectrum to that of the ordinary TASEP. Assuming a similar relation can be found here, the cross term exactly cancels the effects of α_{eff} in each TASEP. Therefore, we are left with twice I_0, since I_1 and I_2 are equal. This line of analysis requires a quantitative theory and will be discussed again later.

To understand the meaning of the cross term above, we first look at the ordinary TASEP. We consider taking the difference of the total occupancy of two different runs, N_1 and N_2. We isolate the cross term by subtracting out I_1 and I_2 and we also normalize it with respect to $I_1 + I_2$. We define:

$$C(\omega) = -\frac{2Re\langle\tilde{N}_1(\omega)\tilde{N}_2^*(\omega)\rangle}{I_1(\omega) + I_2(\omega)} \tag{4.41}$$

We find that $C(\omega) = 0$ from the simulation results. Since the two runs are independent of each other, we do not expect any correlation between $\tilde{N}_1$ and $\tilde{N}_2$. This correlation is what $C(\omega)$ is effectively measuring through $Re\langle\tilde{N}_1(\omega)\tilde{N}_2^*(\omega)\rangle$. Therefore, $C(\omega) = 0$ indicates no correlations exist between $\tilde{N}_1(\omega)$ and $\tilde{N}_2(\omega)$.

On the other hand, we consider the power spectrum associated with the difference between the pool occupation and the lattice occupation for the constrained TASEP. In this case, the two quantities are anti-correlated. Replacing N_2 with N_p, we find:

$$2Re\langle\tilde{N}_1\tilde{N}_p^*\rangle = -2\langle|\tilde{N}_1|^2\rangle = -2I_1 \tag{4.42}$$

If we normalize the cross term by $I_1 + I_p = 2I_1$ and take into account the negative sign in front of the term, then two anti-correlated occupations yield $C(\omega) = 1$. A similar argument

follows for two completely correlated occupations, leading to a value of -1 for $C(\omega)$. Thus, we can identify the behavior of the two TASEPs connected to the pool as independent, correlated, or anti-correlated based on the value of this cross term.

We study the cross term in the HD case for the two TASEPs. This case is chosen since it contains multiple regimes not found in the other cases. For small values of N_{tot} in a LD state, we find the renormalized cross term to be near zero for high frequencies and oscillating at low frequencies shown in Fig. 4.19(a). On short time scales, the two TASEPs should act

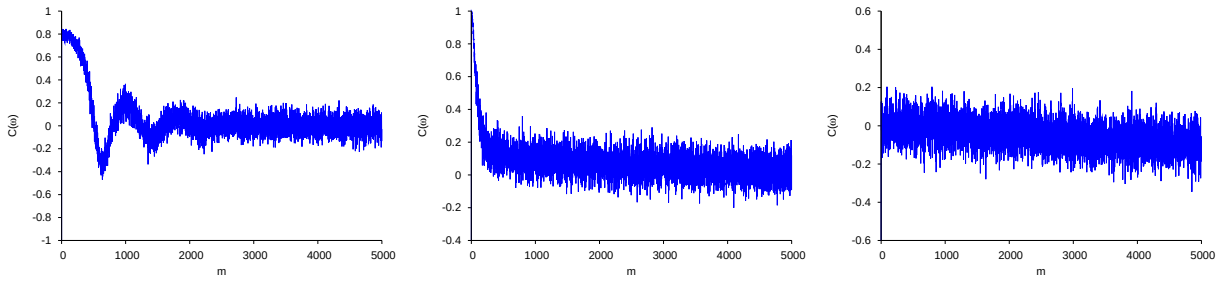

(a) (b) (c)

Figure 4.19: The quantity $C(\omega)$ as a function of $m = \omega T/2\pi$ with $L_1 = L_2 = 1000$ for $\alpha = 0.7$, $\beta = 0.3$, and (a) $N_{tot} = 300$, (c) $N_{tot} = 1400$, and (b) $N_{tot} = 2100$.

independently due to the effects of the finite resources not having enough time to propagate through the system and affect the total occupation. As discussed earlier in the chapter, the quantity $N_1 + N_2$ should remain relatively constant on long time scales. Thus, the occupations of N_1 and N_2 are nearly anti-correlated near $\omega = 0$ as evident in Fig. 4.19(a).

A surprising feature is the oscillations at low ω in Fig. 4.19(a). The correlation between the TASEPs has a frequency dependence that eventually damps out to zero. Oscillations are similar to those found in the ratio of the power spectrum of the constrained TASEP and that of the ordinary TASEP. Previously for the constrained TASEP, the ratio of the two power spectra depended on the rate of change of α_{eff} with respect to N_p. Here, the feedback effect of α_{eff} as well as the particle exchange via the pool between the TASEPs control the oscillations, which itself is effectively control by α_{eff}. To demonstrate this idea, we look at the HD case with a large N_{tot} value. Fig. 4.19(c) shows $C(\omega)$ for $\alpha = 07$, $\beta = 0.3$, and $N_{tot} = 2100$ with $L_1 = L_2 = 1000$. The figure shows that $C(\omega)$ is approximately zero with no oscillations and the two TASEPs are acting independently of each other. In this case, α_{eff} is nearly constant due to the large number of particles in the pool. The exchange of particles still occurs, but with so many particles in the pool, the effects of the exchange are minimal on the system. We conclude that the rate of change of α_{eff} with N_p is the major source of the oscillations for $C(\omega)$ at low frequencies.

Having explored the LD and HD states, we now turn our attention to the crossover regime between these two states. In this regime, I_d behaves like the power spectrum of the ordinary TASEP in the SP. Fig. 4.20 compares I_d for $\alpha = 0.7$, $\beta = 0.3$, and $N_{tot} = 1400$ with

$L_1 = L_2 = 1000$ with I_0 for $\alpha = \beta = 0.3$ with $L = 1000$. Once again, we find I_d being equal

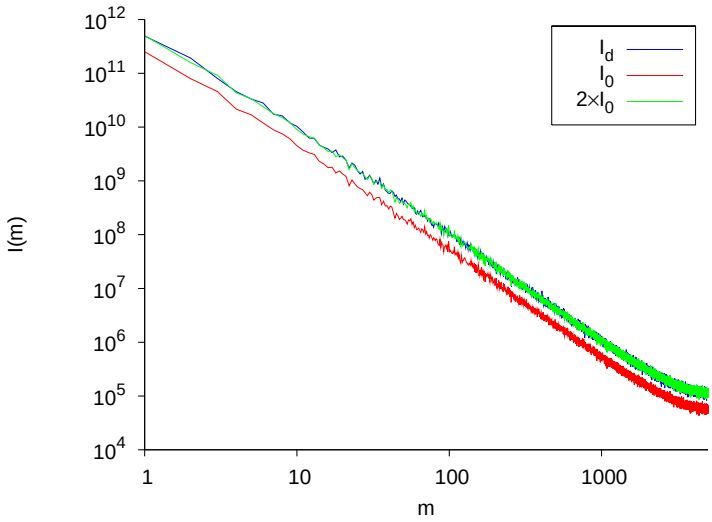

Figure 4.20: Comparison of the I_0 and I_d. For the ordinary TASEP, $\alpha = \beta = 0.3$ with $L = 1000$. For the two TASEP case, $\alpha = 0.7$, $\beta = 0.3$, and $N_{tot} = 1400$ with $L_1 = L_2 = 1000$.

to twice I_0 and decaying as ω^{-2}. Again, the symmetry of the lengths could account for the factor of two. Also, the effects of α_{eff} are absent as it is in the LD state. While I_p (which is effectively the power spectrum of the sum) is effected by the constrained, the difference between $N_1(t)$ and $N_2(t)$ has no constraint. Even for a fixed value of N_p, there are many combinations of N_1 and N_2 for that value, which allows the difference of the occupations to perform a random walk that leads to the ω^{-2} power spectrum. As for $C(\omega)$ shown in Fig. 4.19(b), the oscillations are no longer present that are found in the LD state. As $\omega \to 0$, $C(\omega)$ approaches a value of one. Thus on long time scales, the total occupation of the two TASEPs are anti-correlated. As ω increases,$C(\omega)$ decays eventually reaching zero indicating the two TASEPs are functioning independently of each other. A quantitative theory for the power spectrum of the difference in this regime will be presented later to explore the relationship with the ordinary TASEP.

4.4.3 Theoretical considerations for the power spectra of two TASEPs

The power spectra for the two TASEP case in both the LD and SP-like regimes show interesting new features not seen in either the constrained TASEP or ordinary TASEP, such as different levels of suppression at low frequencies for the individual TASEPs and pool and the enhancement at low frequencies for the smaller TASEP when the lengths are not equal. To understand these features better, we explore the solution to the linearized Langevin equations in the case of two TASEPs in the LD state. The feedback effect due to α_{eff} depends on both N_1 and N_2. Then $N_1(t)$ will depend on $N_2(t)$ through the pool, and vice versa. Despite

this seemingly complicated dependence, a solution for the power spectra of the individual TASEPs is still found analytically.

We begin from the Langevin equations for the density for the first TASEP:

$$\begin{aligned}
\partial_t\rho_1(1,t) &= \alpha_{eff}[1-\rho_1(1,t)] - \rho_1(1,t)[1-\rho_1(2,t)] + \xi_1(0,t) - \xi_1(1,t) && (4.43)\\
\partial_t\rho_1(x_1,t) &= \rho_1(x_1-1,t)[1-\rho_1(x_1,t)] - \rho_1(x_1,t)[1-\rho_1(x_1+1,t)] && (4.44)\\
&\quad +\xi_1(x_1-1,t) - \xi_1(x_1,t) \quad x_1 \in [2, L_1-1]\\
\partial_t\rho_1(L_1,t) &= \rho_1(L_1-1,t)[1-\rho_1(L_1,t)] - \beta\rho_1(L_1,t) + \xi_1(L_1-1,t) - \xi_1(L_1,t) && (4.45)
\end{aligned}$$

and for the second TASEP:

$$\begin{aligned}
\partial_t\rho_2(1,t) &= \alpha_{eff}[1-\rho_2(1,t)] - \rho_2(1,t)[1-\rho_2(2,t)] + \xi_2(0,t) - \xi_2(1,t) && (4.46)\\
\partial_t\rho_2(x_2,t) &= \rho_2(x_2-1,t)[1-\rho_2(x_2,t)] - \rho_2(x_2,t)[1-\rho_2(x_2+1,t)] && (4.47)\\
&\quad +\xi_2(x_2-1,t) - \xi_2(x_2,t) \quad x_2 \in [2, L_2-1]\\
\partial_t\rho_2(L_2,t) &= \rho_2(L_2-1,t)[1-\rho_2(L_2,t)] - \beta\rho_2(L_2,t) + \xi_2(L_2-1,t) - \xi_2(L_2,t) && (4.48)
\end{aligned}$$

where $x_1 \in [1, L_1]$, $x_2 \in [1, L_2]$, and ξ is assumed to be Gaussian noise with zero mean and variance A. The noise for each TASEP is uncorrelated which the noise from the other TASEP. In other words,

$$\begin{aligned}
\langle \xi_1(x_1,t)\xi_2(x_2^{'},t^{'})\rangle &= 0 && (4.49)\\
\langle \xi_1(x_1,t)\xi_1(x_1^{'},t^{'})\rangle &= A_1\delta_{x_1,x_1^{'}}\delta_{t,t'} && (4.50)\\
\langle \xi_2(x_2,t)\xi_2(x_2^{'},t^{'})\rangle &= A_2\delta_{x_2,x_2^{'}}\delta_{t,t'} && (4.51)
\end{aligned}$$

For simplicity, we choose α and β such that the profile is flat in both TASEPs. This choice of parameters also ensures that the average density in both TASEPs are equal. Thus, we have:

$$\begin{aligned}
\bar{\rho}_1(x_1) &= \bar{\rho}_2(x_2) = \bar{\rho} && (4.52)\\
1-\beta &= \bar{\rho} && (4.53)\\
\bar{N}_p &= N_{tot} - \bar{\rho}(L_1+L_2) && (4.54)\\
\alpha f(\bar{N}_p) &= \bar{\rho} && (4.55)
\end{aligned}$$

We now define:

$$\begin{aligned}
\varphi_1(x_1,t) &= \rho_1(x_1,t) - \bar{\rho} && (4.56)\\
\varphi_2(x_2,t) &= \rho_2(x_2,t) - \bar{\rho} && (4.57)
\end{aligned}$$

and their Fourier transforms:

$$\begin{aligned}
\varphi_1(x_1,t) &= \sum_{k,\omega} e^{i(kx_1+\omega t)}\tilde{\varphi}_1(k,\omega) && (4.58)\\
\varphi_2(x_2,t) &= \sum_{p,\omega} e^{i(px_2+\omega t)}\tilde{\varphi}_2(p,\omega) && (4.59)
\end{aligned}$$

with

$$k = \frac{2\pi j}{L_1+1} \quad j \in [0, L_1] \tag{4.60}$$

$$p = \frac{2\pi i}{L_2+1} \quad i \in [0, L_2] \tag{4.61}$$

For the pool, the total occupation of both TASEPs are taken into account. We define the fluctuations about the average pool occupation, $\bar{N}_p$, to be:

$$\varphi(0,t) = N_p(t) - \bar{N}_p \tag{4.62}$$

$$= -N_1(t) + \bar{N}_1 - N_2(t) + \bar{N}_2 \tag{4.63}$$

$$= \varphi_1(0,t) + \varphi_2(0,t) \tag{4.64}$$

where $\varphi_1(0,t)$ and $\varphi_2(0,t)$ are the fluctuations in the pool due to the change in the corresponding TASEP's occupation. As in the constrained TASEP case, we expand α_{eff} about $\bar{N}_p$ to first order in $\varphi(0,t)$:

$$\alpha_{eff} = \alpha f(\bar{N}_p) + [N_p - \bar{N}_p]\partial_{N_p}\alpha_{eff}|_{N_p=\bar{N}_p} + \dots \tag{4.65}$$

$$= \bar{\rho} + [\varphi_1(0,t) + \varphi_2(0,t)]\alpha f^{'} \tag{4.66}$$

where

$$f^{'} = \partial_{N_p} f(N_p)|_{N_p=\bar{N}_p} \tag{4.67}$$

For each TASEP, we can separate out the parts that violate translational invariance. The part that obeys translational invariance in the first TASEP is:

$$\partial_t\varphi(x_1,t) = (1-\bar{\rho})\varphi_1(x_1-1,t) - \varphi_1(x_1,t) + \bar{\rho}\varphi_1(x_1+1,t) + \xi_1(x_1-1,t) - \xi_1(x_1,t) + \dots \tag{4.68}$$

where the $\dots$ represent the parts that violate translational invariance. Writing φ in terms of $\tilde{\varphi}$ and inverse Fourier transforming the equation, we get:

$$e^{i\omega} - 1\tilde{\varphi}_1(k,\omega) = \left[(1-\bar{\rho})e^{-ik} - 1 + \bar{\rho}e^{ik}\right]\tilde{\varphi}_1(k,\omega) + \left(e^{-ik}-1\right)\tilde{\xi}_1(k,\omega) + \frac{1}{(L_1+1)T}\sum_{x_1,t} e^{-i(kx_1+\omega t)}\dots \tag{4.69}$$

$$\tilde{\varphi}_1(k,\omega) = \frac{e^{-ik}-1}{P_1(k,\omega)}\tilde{\xi}_1(k,\omega) + \frac{1}{P_1(k,\omega)(L_1+1)T}\sum_{x_1,t} e^{-i(kx_1+\omega t)}\dots \tag{4.70}$$

where

$$P_1(k) = e^{i\omega} - 1 + (1-\cos k) + iv\sin k \tag{4.71}$$

and $v = 1 - 2\bar{\rho}$. The part that contains the inhomogeneity is given by:

$$\dots = \delta_{x,0}\left\{\varphi_1(0,t) - (1-\bar{\rho})\alpha f^{'}[\varphi_1(0,t) + \varphi_2(0,t)]\right\} \tag{4.72}$$

$$+\delta_{1,x}\left\{(1-\bar{\rho})\alpha f^{'}[\varphi_1(0,t) + \varphi_2(0,t)] - (1-\bar{\rho})\varphi_1(0,t)\right\} \tag{4.73}$$

$$+\delta_{L,x}\left\{-\bar{\rho}\varphi_1(0,t)\right\} \tag{4.74}$$

Before performing the inverse Fourier transform, we note that

$$\varphi_1(0,t) = \sum_{k,\omega} e^{i(k\cdot 0+\omega t)}\tilde{\varphi}_1(k,\omega) \tag{4.75}$$

which leads to

$$\frac{1}{T}\sum_t e^{-i\omega t}\varphi_1(0,t) = \sum_k \tilde{\varphi}_1(k,\omega) \tag{4.76}$$

A similar relation is found for the second TASEP. Now, we perform the inverse Fourier transform for the inhomogeneous part to arrive at:

$$\begin{aligned}\frac{1}{(L_1+1)T}\sum_{x_1,t} e^{-i(kx_1+\omega t)}\ldots &= \frac{1}{(L_1+1)T}\sum_t e^{-i\omega t} \\ &\times\big\{\varphi_1(0,t) - (1-\bar{\rho})\alpha f'[\varphi_1(0,t)+\varphi_2(0,t)] \\ &+[(1-\bar{\rho})\alpha f'[\varphi_1(0,t)+\varphi_2(0,t)] - (1-\bar{\rho})\varphi_1(0,t)]e^{-ik} \\ &+[-\bar{\rho}\varphi_1(0,t)]e^{ik}\big\}\end{aligned} \tag{4.77}$$

We exchange the sum over t for the one over k and combine with the translationally invariant part. So, we have

$$\tilde{\varphi}_1(k,\omega) = \frac{e^{-ik}-1}{P_1(k,\omega)}\tilde{\xi}_1(k,\omega) + \frac{b_k}{(L_1+1)P_1(k,\omega)}\sum_k \tilde{\varphi}_1(k,\omega) + \frac{c_k}{(L_1+1)P_1(k,\omega)}\sum_p \tilde{\varphi}_2(p,\omega) \tag{4.78}$$

where

$$b_k = 1-(1-\bar{\rho})\alpha f' + [(1-\bar{\rho})\alpha f' - (1-\bar{\rho})]e^{-ik} - \bar{\rho}e^{ik} \tag{4.79}$$

$$c_k = -(1-\bar{\rho})\alpha f' + (1-\bar{\rho})\alpha f' e^{-ik} \tag{4.80}$$

We are interested in finding $\tilde{N}_1(\omega)$ in order to calculate the power spectrum for the first TASEP. From the definition of $\varphi_1(0,t)$, we find

$$\tilde{N}_1(\omega) = -\frac{1}{T}\sum_t e^{-i\omega t}\varphi_1(0,t) = -\sum_k \tilde{\varphi}_1(k,\omega) \tag{4.81}$$

and similarly for the second TASEP

$$\tilde{N}_2(\omega) = -\sum_p \tilde{\varphi}_2(p,\omega) \tag{4.82}$$

Therefore, we only need to find a solution for the sum over the φ's. Returning to Eqn. (4.78), we sum over k to get:

$$\begin{aligned}\sum_k \tilde{\varphi}_1(k,\omega) &= \sum_k \frac{e^{-ik}-1}{P_1(k,\omega)}\tilde{\xi}_1(k,\omega) + \left[\sum_k \frac{b_k}{(L_1+1)P_1(k,\omega)}\right]\left[\sum_k \tilde{\varphi}_1(k,\omega)\right] \\ &+ \left[\sum_k \frac{c_k}{(L_1+1)P_1(k,\omega)}\right]\left[\sum_p \tilde{\varphi}_2(p,\omega)\right]\end{aligned} \tag{4.83}$$

By collecting terms and replacing $\sum \tilde{\varphi}$ with $\tilde{N}$, we arrive at:

$$-\tilde{N}_1(\omega) = \sum_k \frac{e^{-ik}-1}{P_1(k,\omega)B_1(\omega)}\tilde{\xi}_1(k,\omega) - \frac{C_1(\omega)}{B_1(\omega)}\tilde{N}_2(\omega) \tag{4.84}$$

where

$$B_1(\omega) = 1 - \frac{1}{L_1+1}\sum_k \frac{b_k}{P_1(k,\omega)} \tag{4.85}$$

$$C_1(\omega) = \frac{1}{L_1+1}\sum_k \frac{c_k}{P_1(k,\omega)} \tag{4.86}$$

Similarly for the second TASEP,

$$-\tilde{N}_2(\omega) = \sum_p \frac{e^{-ip}-1}{P_2(p,\omega)B_2(\omega)}\tilde{\xi}_2(p,\omega) - \frac{C_2(\omega)}{B_2(\omega)}\tilde{N}_1(\omega) \tag{4.87}$$

where

$$B_2(\omega) = 1 - \frac{1}{L_2+1}\sum_p \frac{b_p}{P_2(p,\omega)} \tag{4.88}$$

$$C_2(\omega) = \frac{1}{L_2+1}\sum_p \frac{c_p}{P_2(p,\omega)} \tag{4.89}$$

We have two equations and two unknowns. The solution to the set of equations is easily found. It is:

$$\begin{aligned}\tilde{N}_1(\omega) = {} & \frac{B_1(\omega)B_2(\omega)}{C_1(\omega)C_2(\omega)-B_1(\omega)B_2(\omega)}\left[\sum_k \frac{e^{-ik}-1}{P_1(k,\omega)B_1(\omega)}\tilde{\xi}_1(k,\omega)\right. \\ & \left. + \frac{C_1(\omega)}{B_1(\omega)}\sum_p \frac{e^{-ip}-1}{P_2(p,\omega)B_2(\omega)}\tilde{\xi}_2(p,\omega)\right]\end{aligned} \tag{4.90}$$

$$\begin{aligned}\tilde{N}_2(\omega) = {} & \frac{B_1(\omega)B_2(\omega)}{C_1(\omega)C_2(\omega)-B_1(\omega)B_2(\omega)}\left[\sum_p \frac{e^{-ip}-1}{P_2(p,\omega)B_2(\omega)}\tilde{\xi}_2(p,\omega)\right. \\ & \left. + \frac{C_2(\omega)}{B_2(\omega)}\sum_k \frac{e^{-ik}-1}{P_1(k,\omega)B_1(\omega)}\tilde{\xi}_1(k,\omega)\right]\end{aligned} \tag{4.91}$$

From this solution, the power spectra of each individual TASEP, the pool, and the difference

are calculated. The power spectra of the individual TASEPs are given by

$$\begin{aligned} I_1(\omega) &= \langle|\tilde{N}_1(\omega)|^2\rangle \qquad (4.92)\\ &= \frac{|B_1(\omega)B_2(\omega)|^2}{|C_1(\omega)C_2(\omega)-B_1(\omega)B_2(\omega)|^2}\left[\sum_k \frac{A_1(2-2\cos k)}{|P_1(k,\omega)B_1(\omega)|^2}\right.\\ &\quad \left.+\frac{|C_1(\omega)|^2}{|B_1(\omega)|^2}\sum_p \frac{A_2(2-2\cos p)}{|P_2(p,\omega)B_2(\omega)|^2}\right]\\ I_2(\omega) &= \langle|\tilde{N}_2(\omega)|^2\rangle \qquad (4.93)\\ &= \frac{|B_1(\omega)B_2(\omega)|^2}{|C_1(\omega)C_2(\omega)-B_1(\omega)B_2(\omega)|^2}\left[\sum_p \frac{A_2(2-2\cos p)}{|P_2(p,\omega)B_2(\omega)|^2}\right.\\ &\quad \left.+\frac{|C_2(\omega)|^2}{|B_2(\omega)|^2}\sum_k \frac{A_1(2-2\cos k)}{|P_1(k,\omega)B_1(\omega)|^2}\right] \end{aligned}$$

We see that the first term in the square brackets resembles the power spectrum of the constrained TASEP, however, the factor in front of the bracket will alter the dependence on $f^{'}$ that is carried in the B's and C's. The lengths of the TASEPs are taken into account explicitly in the B's and C's and implicitly in the definitions of k and p. The complicated expression allows for the many different features seen in the power spectra, especially when the lengths are not equal.

To simplify the power spectra, we consider what happens when the lengths are equal. In this situation, $A_1 = A_2 = A$, $B_1 = B_2 = B$, and $C_1 = C_2 = C$. Then the power spectra becomes:

$$I_1(\omega) = I_2(\omega) = \sum_k \frac{A(2-2\cos k)(|B(\omega)|^2+|C(\omega)|^2)}{|P(k,\omega)([C(\omega)]^2-[B(\omega))]^2|^2} \qquad (4.94)$$

The expression is exactly the expression we found for the constrained TASEP with $|Q(\omega)|^2 = |[C(\omega)]^2-[B(\omega)]^2|^2/(|B(\omega)|^2+|C(\omega)|^2)$. While this expression is still complicated, it indicates that the effects of $f^{'}$ are reduced by having the function on both the numerator and denominator of the fraction. Therefore, the suppression will not be as great as having a single constrained TASEP.

For the pool's power spectrum, we have

$$\begin{aligned} I_p(\omega) &= \langle|\tilde{N}_1(\omega)+\tilde{N}_2(\omega)|^2\rangle \qquad (4.95)\\ &= \frac{|B_1(\omega)B_2(\omega)|^2}{|C_1(\omega)C_2(\omega)-B_1(\omega)B_2(\omega)|^2}\left[\left|1+\frac{C_2(\omega)}{B_2(\omega)}\right|^2\sum_k \frac{A-1(2-2\cos k)}{|P_1(k,\omega)B_1(\omega)|^2}\right.\\ &\quad \left.+\left|\frac{C_1(\omega)}{B_1(\omega)}+1\right|^2\sum_p \frac{A_2(2-2\cos p)}{|P_2(p,\omega)B_2(\omega)|^2}\right] \end{aligned}$$

Again, we simplify the expression by setting the two lengths equal. The power spectrum for the pool in this case is:

$$I_p(\omega) = \sum_k \frac{2A(2-2\cos k)}{|P(k,\omega)[B(\omega)-C(\omega)]|^2} \tag{4.96}$$

This equation is the same as the constrained TASEP with $Q(\omega) = B(\omega) - C(\omega)$ and $A \to 2A$. If we look at $B(\omega) - C(\omega)$, we find

$$C(\omega) - B(\omega) = \frac{1}{L+1} \sum_k \frac{e^{i\omega} - 1 + 2(1-\bar{\rho})\alpha f^{'} - 2(1-\bar{\rho})\alpha f^{'} e^{-ik}}{P(k,\omega)} \tag{4.97}$$

which is $Q(\omega)$ from the constrained TASEP with $f^{'} \to 2f^{'}$. The strength of the suppression due to $f^{'}$ is effectively doubled. Thus, we find that the power spectrum of the pool has a simple relationship to the power spectrum of the constrained TASEP when the lengths of the two TASEPs are equal.

Finally, the power spectrum of the difference is

$$\begin{aligned} I_d(\omega) &= \langle |\tilde{N}_1(\omega) - \tilde{N}_2(\omega)|^2 \rangle \qquad (4.98) \\ &= \frac{|B_1(\omega)B_2(\omega)|^2}{|C_1(\omega)C_2(\omega) - B_1(\omega)B_2(\omega)|^2} \left[\left| 1 - \frac{C_2(\omega)}{B_2(\omega)} \right|^2 \sum_k \frac{A - 1(2-2\cos k)}{|P_1(k,\omega)B_1(\omega)|^2} \right. \\ &\quad \left. + \left| \frac{C_1(\omega)}{B_1(\omega)} - 1 \right|^2 \sum_p \frac{A_2(2-2\cos p)}{|P_2(p,\omega)B_2(\omega)|^2} \right] \end{aligned}$$

When the lengths are equal, this equation simplifies to

$$I_d(\omega) = \sum_k \frac{2A(2-2\cos k)}{|P(k,\omega)[B(\omega)+C(\omega)]|^2} \tag{4.99}$$

If we look more closely at $B(\omega) + C(\omega)$, then we see that

$$B(\omega) + C(\omega) = \frac{1}{L+1} \sum_k \frac{e^{i\omega} - 1}{P(k,\omega)} \tag{4.100}$$

The $f^{'}$ terms cancel out leaving the same expression for $Q(\omega)$ found in the power spectrum of the ordinary TASEP ($f^{'} = 0$). Therefore, we can write $I_d = 2I_0$, which is exactly what we found in the simulation results. However, this result is only true when the lengths are equal. If the symmetry is broken between the lengths, then the cancellations of terms that make use of the symmetry does not happen. In the case of unequal lengths, we do not expect such a simple relationship between I_d and I_0.

Moving to the crossover regime with α and β such that the ordinary TASEP would be in the HD phase, we begin with a continuity equation for both TASEPs.

$$\partial_t \rho_1(x_1,t) = \partial_{x_1} J_1(x_1) + \partial_{x_1}\xi_1(x_1,t) \quad (4.101)$$
$$\partial_t \rho_2(x_2,t) = \partial_{x_2} J_2(x_2) + \partial_{x_2}\xi_2(x_2,t) \quad (4.102)$$

where $J(x)$ is the time independent part of the current and $\xi(x,t)$ contains the time dependent parts. Integrating over x_1 and x_2, we have

$$\partial_t N_1(t) = J_1(L_1) - J_1(1) + \xi_1(L_1,t) - \xi_1(1,t) \quad (4.103)$$
$$\partial_t N_2(t) = J_2(L_2) - J_2(1) + \xi_2(L_2,t) - \xi_2(1,t) \quad (4.104)$$

where

$$J_1(L_1) = J_2(L_2) = \beta(1-\beta) \quad (4.105)$$
$$J_1(1) = J_2(1) = \alpha_{eff}(1-\alpha_{eff}) \quad (4.106)$$

We expand α_{eff} about the average occupation of the pool to first order in N_p. Then to first order in N_p, the currents $J_1(1)$ and $J_2(1)$ become:

$$J_1(1) = J_2(1) = \bar{\alpha}_{eff}(1-\bar{\alpha}_{eff}) + (N_p - \bar{N}_p)(1-2\bar{\alpha}_{eff})\left.\frac{\partial \alpha_{eff}}{\partial N_p}\right|_{N_p=\bar{N}_p} + (O)(N_p-\bar{N}_p)^2 \quad (4.107)$$

Since $\bar{\alpha}_{eff} = \beta$, the first term in $J(1)$ cancels with $J(L)$ in both TASEPs. Upon performing the Fourier transform, we have for $\omega > 0$:

$$-i\omega\tilde{N}_1(\omega) = \gamma[\tilde{N}_1(\omega) + \tilde{N}_2(\omega)] + \tilde{\eta}_1(\omega) \quad (4.108)$$
$$-i\omega\tilde{N}_2(\omega) = \gamma[\tilde{N}_1(\omega) + \tilde{N}_2(\omega)] + \tilde{\eta}_2(\omega) \quad (4.109)$$

where

$$\gamma = (1-2\bar{\alpha}_{eff})\left.\frac{\partial \alpha_{eff}}{\partial N_p}\right|_{N_p=\bar{N}_p} \quad (4.110)$$
$$\tilde{\eta}_1(\omega) = \tilde{\xi}_1(L_1,t) - \tilde{\xi}_1(1,t) \quad (4.111)$$
$$\tilde{\eta}_2(\omega) = \tilde{\xi}_2(L_2,t) - \tilde{\xi}_2(1,t) \quad (4.112)$$

At this point, we wish to include finite size effects for both TASEPs. How the length of the TASEP affects the power spectrum in this regime is given in Appendix B. We add the terms $\delta_1\tilde{N}_1(\omega)$ and $\delta_2\tilde{N}_2(\omega)$ to Eqns. (4.108) and (4.109), respectively. The solution to these two equations is:

$$\tilde{N}_1(\omega) = \frac{\gamma\tilde{\eta}_2(\omega) + [-i\omega - \gamma - \delta_2]\tilde{\eta}_1(\omega)}{[\delta_1\delta_2 + \gamma(\delta_1+\delta_2) - \omega^2] + i\omega[2\gamma + \delta_1 + \delta_2]} \quad (4.113)$$
$$\tilde{N}_2(\omega) = \frac{\gamma\tilde{\eta}_1(\omega) + [-i\omega - \gamma - \delta_1]\tilde{\eta}_2(\omega)}{[\delta_1\delta_2 + \gamma(\delta_1+\delta_2) - \omega^2] + i\omega[2\gamma + \delta_1 + \delta_2]} \quad (4.114)$$

From the above solution, we calculate the power spectra for each TASEP and the pool:

$$I_1(\omega) = \langle|\tilde{N}_1(\omega)|^2\rangle = \frac{\gamma^2 A_2 + [\omega^2 + (\gamma+\delta_2)^2]A_1}{[\delta_1\delta_2 + \gamma(\delta_1+\delta_2) - \omega^2]^2 + \omega^2[2\gamma+\delta_1+\delta_2]^2} \tag{4.115}$$

$$I_2(\omega) = \langle|\tilde{N}_2(\omega)|^2\rangle = \frac{\gamma A_1 + [\omega^2 + (\gamma+\delta_1)^2]A_2}{[\delta_1\delta_2 + \gamma(\delta_1+\delta_2) - \omega^2]^2 + \omega^2[2\gamma+\delta_1+\delta_2]^2} \tag{4.116}$$

$$I_p(\omega) = \langle|\tilde{N}_p(\omega)|^2\rangle = \frac{(\omega^2+\delta_2^2)A_1 + (\omega^2+\delta_1^2)A_2}{[\delta_1\delta_2 + \gamma(\delta_1+\delta_2) - \omega^2]^2 + \omega^2[2\gamma+\delta_1+\delta_2]^2} \tag{4.117}$$

using

$$\langle\tilde{\eta}_1(\omega)\tilde{\eta}_1^*(\omega)\rangle = A_1 \tag{4.118}$$

$$\langle\tilde{\eta}_2(\omega)\tilde{\eta}_2^*(\omega)\rangle = A_2 \tag{4.119}$$

$$\langle\tilde{\eta}_1(\omega)\tilde{\eta}_2^*(\omega)\rangle = \langle\tilde{\eta}_2(\omega)\tilde{\eta}_1^*(\omega)\rangle = 0 \tag{4.120}$$

The power spectrum of the difference between N_1 and N_2 is:

$$I_d(\omega) = \langle|\tilde{N}_1(\omega) - \tilde{N}_2(\omega)|^2\rangle = \frac{[\omega^2 + (2\gamma+\delta_2)^2]A_1 + [\omega^2 + (2\gamma+\delta_1)^2]A_2}{[\delta_1\delta_2 + \gamma(\delta_1+\delta_2) - \omega^2]^2 + \omega^2[2\gamma+\delta_1+\delta_2]^2} \tag{4.121}$$

When we compare the theory to the simulations data, the agreement is remarkable as seen in Figs. 4.16 and 4.17(a). The fit parameters, A and δ, have the same values that were used to fit the power spectrum of the ordinary TASEP.

To understand the theory better, we consider the case with large ($\delta_1 = \delta_2 = 0$) and equal lengths ($A_1 = A_2 = A$) for each TASEP. In this limit, the power spectrum of the pool becomes:

$$I_p(\omega) = \frac{2A}{\omega^2 + (2\gamma)^2} \tag{4.122}$$

This equation has the same form as the power spectrum of the constrained TASEP with $\gamma \to 2\gamma$. The doubling of γ is similar to what is seen for the pool with two TASEPs of equal lengths in the LD state, f' is doubled. Recall for the LD state with equal lengths, the power spectrum of the difference was equal to twice the power spectrum of the ordinary TASEP. We find the same result here. Looking at $I_d(\omega)$ in the crossover regime, we find:

$$I_d(\omega) = \frac{2A}{\omega^2} \tag{4.123}$$

The γ completely cancels out of Eqn. (4.121), as well as the ω in the numerator. In fact, Eqn. (4.123) is simply twice the power spectrum of the ordinary TASEP, which is what we find from the simulation data and in the LD state. Both theoretical results for the power spectra of the pool and difference support the findings in the Monte Carlo simulations and compliment the relationships found in the LD state between the various power spectra.

4.5 Summary

In this chapter, we studied how competition between multiple TASEPs affects the system. We first looked at how competition affected the average overall density, density profile, and current as a function of the number of particle in the system N_{tot}. While the overall density curve for each TASEP was similar to a single constrained TASEP when the lengths where equal, the density profiles were completely different in the crossover regime in the HD case from the constrained TASEP. For two TASEPs, both profiles were found to have linear profiles near the exit that extended deeper into the bulk as N_{tot} increased. Neither shock in the TASEPs were localized, instead, the TASEPs "exchanged" particles via the pool. This exchange kept the number of particles in the pool relatively constant while allowing the number of particle in each TASEP to fluctuate. A similar exchange occurred when the lengths of the two TASEPs were not equal in the crossover regime. In this case, the length of the smaller TASEP put a limit on the fluctuations in the number of particles on each TASEP. The size difference led to the smaller TASEP having a linear profile along its entire lattice, indicating a delocalized shock, while the larger one had a localized shock. The width of the localization was larger than that found in the constrained TASEP due to additional degree of freedom the second TASEP granted. When three TASEPs were allowed to compete, all with different lengths, only the largest TASEP contained the localized shock and the smaller two had delocalized shocks.

A generalized domain wall theory was presented to explain the different phenomena seen in the overall densities and density profiles. A master equation for the probability to find the shocks of each TASEP in configuration $\{k_\ell\}$ was solved in the steady state. In the master equation, the hopping rates depended on the configuration of the k's. Fortunately, these hopping rates satisfied the Kolmogorov criterion [64] which allowed the system to be solved using a recursion relation. The results from the GDW theory agreed remarkably well with the simulation data for both the average overall densities and density profiles for the two and three TASEP cases.

The dynamics of the two TASEP case was studied through the power spectrum of the total occupancy of the individual TASEP as well as the pool. Simulation results were shown for two TASEPs with equal and unequal lengths. These results were compared to the power spectra of the ordinary TASEP and the constrained TASEP. For equal lengths, the power spectra of the two TASEPs showed a suppression at low frequencies when compared to the ordinary TASEP. However, the suppression was not as great as what was seen in the constrained TASEP. Since the suppression was connected to $\partial_{N_p}\alpha_{eff}$, the addition of a second TASEP reduced the feedback effect due to the extra degree of freedom it offered. For unequal lengths, we found the larger TASEP had a suppression at low frequencies while the smaller one had an enhancement when compared to the ordinary TASEP. We concluded the enhancement was due to the particle exchange between the larger and smaller TASEP through the pool.

The power spectrum of the difference of the occupancies of the two TASEPs was also ex-

plored. From the simulations, we found for two TASEPs with equal lengths that the power spectrum of the difference was twice the power spectrum of the ordinary TASEP. Since the difference in occupancies had no constraint imposed on it by the system, its power spectrum should be the same as that of the unconstrained ordinary TASEP. For unequal lengths, the amplitude of the power spectrum of the difference is greater than either of the individual TASEPs or the pool. No simple relation exists between the power spectrum of the difference and the ordinary TASEP's power spectrum as it did in the equal case.

Theoretical approaches were presented for two TASEPs when the system was in either the LD state or in the crossover regime in the HD case. For the LD state, a set of discrete, coupled Langevin equations for the densities were written for each TASEP. The solution to these equations was found in Fourier space and the power spectra for each TASEP and the pool were calculated. By exploring particular limits, we found the analytical solutions had the same features (such as the different levels of suppression for the different power spectra) as the simulations did. For the crossover regime, a set of coupled continuity equations were solved in Fourier space to arrive at the power spectra for the TASEPs. Using only one fit parameter, the theoretical results were in good agreement with the simulation results, except when one of the TASEP had a small length. Here, finite size corrections were needed to produce the correct fit to the data. As in the LD state, the different levels of suppression and enhancement are accounted for by this simple theory.

Chapter 5

Applications to protein synthesis in a cell

In a cell, proteins are created from the genetic information stored in the DNA molecules in a process called protein synthesis [25]. This process is carried out the same way in all organisms. During protein synthesis, the information stored in a portion of the nucleotide sequence, a gene, on the DNA is copied onto a messenger RNA (mRNA) in a process called transcription [25]. The information is stored in the combination of three nucleotides called a codon. The protein is then created from the mRNA codon sequence during the translation process [25]. Once the protein is completed, or expressed, it detaches from the mRNA and move into the rest of the cell. The translation process during protein synthesis is what we will focus on during the rest of this chapter.

Translation is a multi-step process. First, a ribosome will attach itself at the 5' (initiation) end. The ribosome itself is made of two subunits, a large subunit and a small one, which combine on the mRNA near the 5' end. The smaller subunit ensures the correct transfer RNA (tRNA) with an amino acid matches the mRNA codon sequence, while the large subunit catalyzes the peptide bonds of the amino acids [25]. The size of the ribosome covers approximately 12 codon sites. When the ribosome reaches a start codon for a gene, it then begins to create the protein and moves along the mRNA from the 5' end to the 3' (terminal) end. As the ribosome moves (elongation), the polypeptide chain is constructed using the amino acids delivered by the tRNA that compliments the mRNA codon. The are 64 possible codons for the mRNA, but only 60 anti-codons for the tRNA [25]. Finally at 3' end, a stop codon is reached and the protein is complete. The ribosome detaches from the mRNA and the subunits separate to be used again to express another gene [25].

Certain factors affect the rate at which the protein is produced. The initiation rate, the rate at which ribosomes attach themselves to the mRNA, is controlled by multiple factors [25]. During elongation, the concentration of the tRNA corresponding to a given codon on the mRNA is proportional to the rate at which the amino acid is added to the chain [26, 27].

Thus, each codon site will have a different rate based on what codon is at the site [27]. Other factors exist, such as ribosome recycling [28], however in the model to be presented next, we will focus on including only the two factors discussed above in addition to competition between genes.

5.1 Model

In order to create a more realistic model of translation, we will modify the TASEP model to include elongated particles, site dependent hopping rates, and finite resources. The extended particles and site dependent hopping rates have been studied previously [32, 33, 34, 35], but not with finite resources. The particles cover 12 sites on the TASEP in order to model the large size of the ribosomes. The sites on the TASEP are given different hopping rates γ_i in order to model the different codons of a gene. These rates are not chosen at random, but they are taken from 10 genes found in E. coli, each gene having a different length L_m. In [27], the concentrations of each tRNA are given, which in turn are used to create the hopping rates, while the gene sequences are retrieved from GenBank [65]. This procedure has already been carried out in [66] for the 2.5 doubling rate. The names of the specific genes and the associated site hopping rates are found in Appendix C.

We will also connect 10 different genes to a finite reservoir of particles. This modification will model competition for ribosomes among the 10 genes. For a large concentration of ribosomes, the initiation rate should reach some intrinsic value, which we will take to be one. At low concentrations, the rate should be limited by the concentration of ribosomes. Therefore, we choose to model the effective entry rate α_{eff} with:

$$\alpha_{eff} = \tanh\left(\frac{N_p}{N^*}\right) \tag{5.1}$$

where N_p is the number of ribosomes remaining in the pool and N^* is a normalization factor which is (arbitrarily) set to 500. By changing the number of particles initially in the pool, we can study the effects of the competition between the genes using Monte Carlo simulations.

The Monte Carlo simulations are performed using a similar method as the multiple TASEP simulations. The site on the elongated particles furthest from the TASEP's exit is chosen to be the reader site. This site is used to determine the hopping rate of the particle. A particle can enter the TASEP if the first 12 sites are empty with a probability α_{eff}. In the interior of the TASEP, a particle can move to the next site with a probability γ_i provided the site which is 12 sites ahead is empty. When the reader reaches the last site, the particle can exit the TASEP with probability $\beta = 1$ and the particle is immediately recycled back into the pool. The system is updated $\sum_m L_m + 10$ times in one Monte Carlo step. The system is allowed to reach steady state by discarding the first 100k MCS. Data is then taken every 100 MCS for a total of 1M MCS, which constitutes a single run. The data is averaged over

100 runs. In this study, we are interested in the average overall particle density, coverage density, and particle current.

5.2 Simulation results

We now present our results from the Monte Carlo simulations. We begin by exploring the average particle density ρ. This quantity measures the average number of particles on each TASEP, normalized by the length of the lattice. The results for the particle density as a function of N_{tot} are shown in Fig. 5.1 for each of the 10 genes. The particle densities

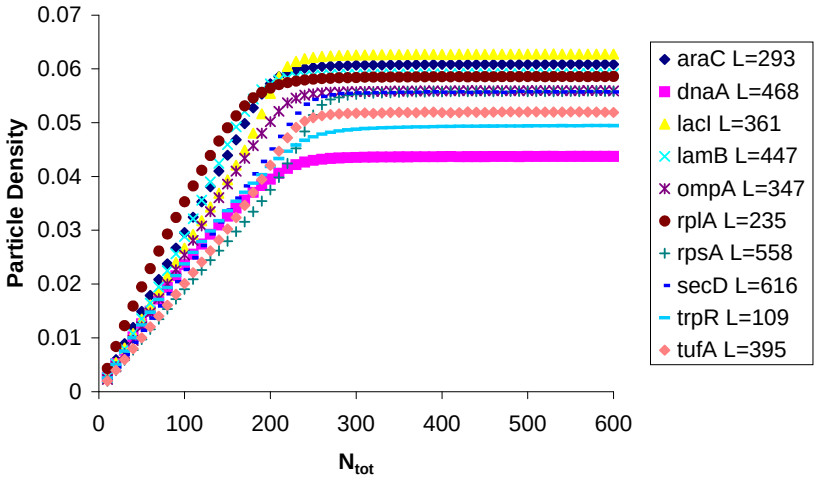

Figure 5.1: Average particle density of 10 different genes as a function of N_{tot} with $\beta = 1$.

are approximately equal at small N_{tot} values. At such low densities, the densities of the genes are limited by the initiation rate. As the number of particles increases, each TASEP reaches a different constant particle density. This is a deviation from what was seen in the multiple TASEP study [63]. The different densities come about from the site dependent hopping rates. Some of these rates are below the average value of α_{eff} and cause a buildup of particles preceding the slow site. Even without the feedback effect, the different genes have different particle densities for the same entry rate [66]. However, the TASEPs do not reach their final density at the same N_{tot}. Again looking back to the multiple TASEPs in the HD case with unequal lengths, we find the largest TASEP reaching its final density value followed by the shorter TASEPs in the order of their lengths with the largest one first. Yet, no length dependence exists for the 10 genes studied here. Due to the complexity of the system, it is difficult to isolate the exact cause of why each TASEP reaches its final particle density at different N_{tot} values.

The average coverage density ρ_c is also studied. This quantity measures how often a site is covered by some part of the particle. It is approximately the average particle density multiplied by the length of the particle, in this case 12. The results for the average coverage

density are shown in Fig. 5.2 for the 10 genes as a function of N_{tot}. We find the same

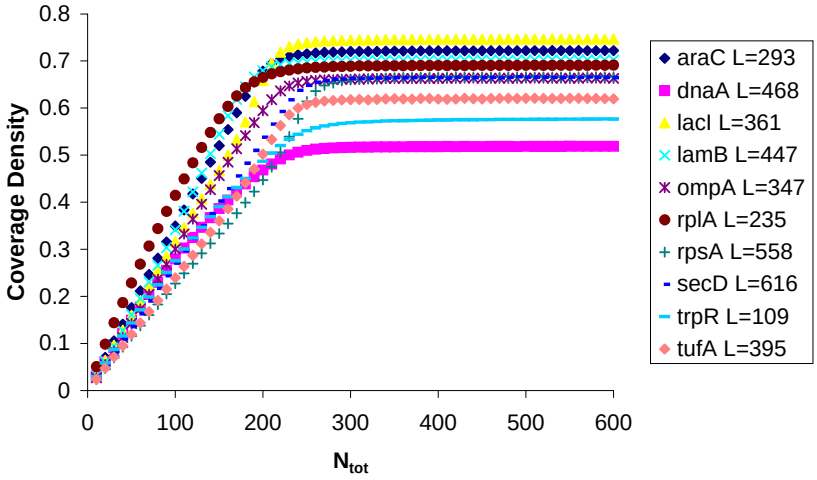

Figure 5.2: Average coverage density of 10 different genes as a function of N_{tot} with $\beta = 1$.

behavior as the particle density due to the particle covering 12 sites. The coverage density rises as N_{tot} increases until a final value is reached. Some work has been done to predict the coverage density profile with random hopping rates [58]. The authors in [58] extend the method used by [29] and [30] to include the inhomogeneous internal hopping rates in a mean field approach. The theoretical results did not have a high degree of agreement, but they did provide insight on how the two-point correlation affected the profile [58]. Furthermore, the authors suggest that higher order correlations could be added at the expense of increased complexity.

Upon closer inspection of the two densities, we find the increase from zero to their final values is not linear for all of the genes. The gradient of the coverage density with respect to N_{tot} is shown in Fig. 5.3. We see some genes whose gradient are monotonically decreasing until reaching a final value of zero. Other genes' gradients rise to a peak value then decrease to a value of zero. We are reminded of the two TASEP results in the HD case, where the average density gradient for the smaller TASEP has a peak value as it enter and leaves the crossover regime between the LD and HD states. Unlike the two TASEP case, no correlation between the system size and the existence of the peaks is found. Here again, the complexity of the system makes understanding the physics behind the different properties of the gradients difficult.

We also compare the densities with those of a single gene connected to a pool. We find no noticeable difference between the two situations, but this result should not come as a surprise. Recall when α and β are chosen to be in the MC phase for the multiple TASEPs, we saw no new features in density as a function of N_{tot} [63]. Here, we have a similar situation for the single and 10 genes densities. The nonlinear rise in the densities is not due to the competition between the genes. Instead, it could possibly be due to the inhomogeneous hopping rates and the feedback of α_{eff}. Based on what is presented here, no definitive

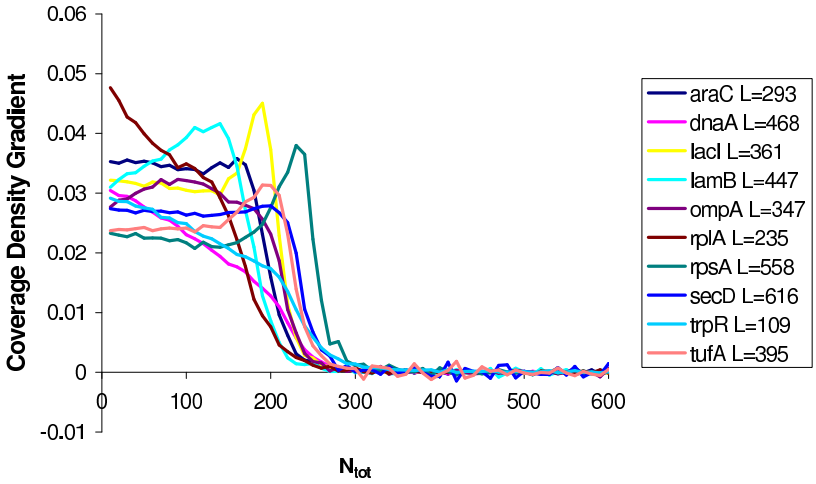

Figure 5.3: Gradient of the average particle density with respect to N_{tot} of 10 different genes as a function of N_{tot} with $\beta = 1$.

conclusion can be drawn.

The last quantity we will look at is the particle current J through each TASEP as a function of N_{tot}. In the multiple TASEP study, all TASEPs had the same current (ignoring finite size effects) regardless of the different lengths. The currents were equal due to the TASEPs having the same entry and exit rates and homogeneous internal hopping rates. The currents through the TASEPs are not equal for the different genes as shown in Fig. 5.4. Unlike the

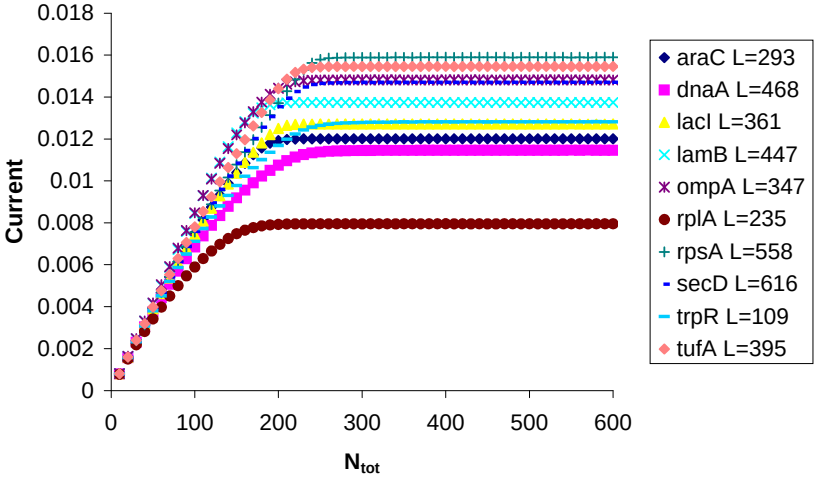

Figure 5.4: Average particle current of 10 different genes as a function of N_{tot} with $\beta = 1$.

multiple TASEP study, the bulk hopping rates are not equal. Indeed, the location of the slow sites affect the value of the current [34]. However, the currents are equal at extremely small N_{tot} values. At these values, α_{eff} is smaller than the slowest internal hopping rate. Thus, the current is controlled by the value of α_{eff} for all 10 genes until $\sim N_{tot} = 30$. As the

total number of particles is increased further, the different internal γ_i's of the different gene sequences gives rise to different current values, but the currents are still lower than their final values. Clearly, the effect of having finite resources limits the currents by limiting the number of particles entering each TASEP. Once N_{tot} is large enough, enough particles exists for all of the TASEPs to reach their final current values.

A mean-field approach to finding the currents has previously been developed [58]. In fact, the authors in [58] successfully predict the currents seen in the Monte Carlo simulations with a mean-field theory to within a few percent for actual genes of E. coli. However, the genes in [58] are not the same ones studied here. The difference between the theoretical currents and simulations currents decreases when the two point correlation is included [58]. Since this mean-field theory has both large particles and inhomogeneous internal hopping rates, it could possibly be extended to include competition and finite resources.

In the ordinary TASEP, a simple relationship between the density and current exists, namely $J = \rho(1-\rho)$. We explore this relation for the 10 genes presented here. The results of the simulations are shown in Fig. 5.5. At low N_{tot} and ρ_c, all the genes haves the same current, but

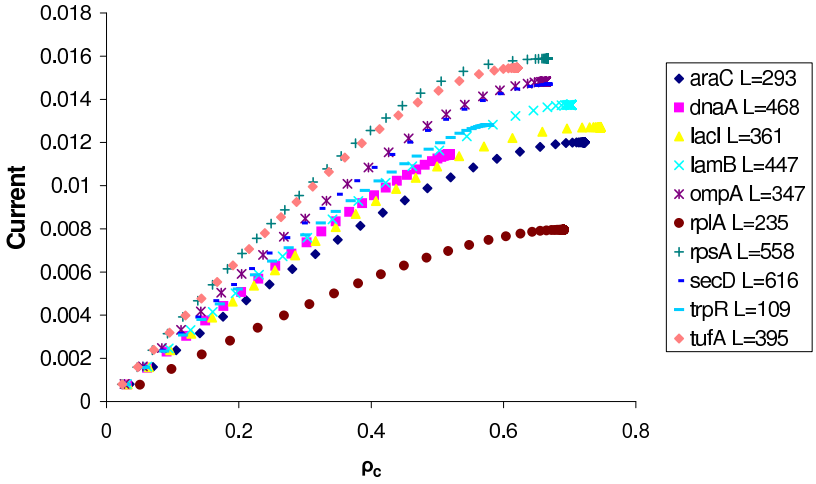

Figure 5.5: Average particle current of 10 different genes as a function of ρ_c with $\beta = 1$.

they each have a different density. This observation suggests that the current is independent of the density. However for larger ρ_c, we have a variety of densities and currents with no clear relationship between the two quantities. The result should come as no surprise as the current and density of the ordinary TASEP is controlled by the boundary parameters, α and β. In the genes, the inhomogeneity of the bulk also effects the current [34]. Since the different internal hopping rates create different densities and currents, we should not expect such a simple relationship to hold.

We also study how the derivatives of the currents with respect to ρ_c differ for each gene. By looking at the derivatives, we can gain insight on the exact relationship between J and ρ_c for each gene. We begin with the first derivative of the current. The ordinary TASEP has

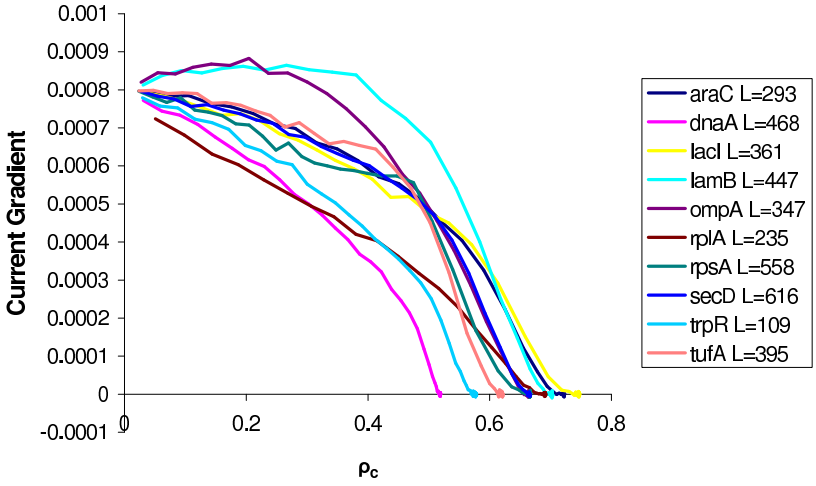

Figure 5.6: Gradient of the particle current of 10 different genes as a function of ρ_c with $\beta = 1$.

a linear relation ship between $\partial_\rho J$ and ρ given by $\partial_\rho J = 1 - 2\rho$. As seen in Fig. 5.6, none of the curves are exactly linear. The gene that codes for rplA has a nearly linear curve, and it is the closest to mimicking what is seen for the ordinary TASEP. Yet, the other genes clearly have higher order terms in ρ_c due to their nonlinear nature. Some of the genes have current gradients that are not monotonically decreasing, which is what occurs in the ordinary TASEP. We speculate the inhomogeneous hopping rates, in particular the location of the slowest sites, cause the differences in the curves for the different genes. However, the system is too complex to isolate the actual cause for the different gradients from the data shown.

To explore the relationship further between the particle current and the coverage density, we turn to the curvature of $J(\rho_c)$. For the ordinary TASEP, the curvature is $\partial_\rho^2 J = -2$. For the 10 genes, Fig. 5.7 shows that the curvature is not a constant. Most of the genes' currents have a large change in the curvature of their current right before they reach their highest density values. While both the ordinary TASEP and the genes have the negative curvatures for their currents, the curvatures for the genes are much more complex. Here again, we speculate that the cause for the dips in the curvature at higher densities is due to the different spacings of the slower sites. But as before, we cannot isolate the cause for the dips from this data alone.

While the current-density relation $J(\rho_c)$ for the completing genes seems to have no connection with the ordinary TASEP, we now turn our attention to understanding the relation in the context of certain modified versions of the TASEP. First, we consider the ordinary TASEP with particles covering more than one site. This model has been previously studied in [32, 33]. The consequence of having large particles is a shift of the maximum current to a higher coverage density as the particle size increases [33]. A different approach using an extremal principle based on the domain wall theory is used in [31], but it has the same

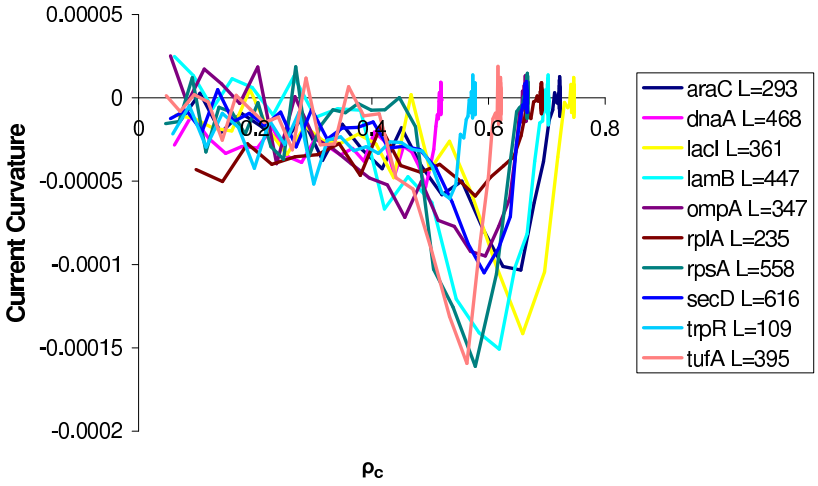

Figure 5.7: Curvature of the particle current of 10 different genes as a function of ρ_c with $\beta = 1$.

conclusion. From the results in [31], we can show that

$$J = \frac{\rho(1-\rho)}{(1-\rho)\ell + \rho} \tag{5.2}$$

where ℓ is the size of the particle. From this equation, the gradient of J would not be linear, which is what we see in Fig. 5.6. However, all of the genes have the same particle size, so the expected shift would be the same for all 10 genes. We do not see the same shift in Fig. 5.5 for all the genes. Furthermore, the curvature of J should not be zero according to Eqn. (5.2), but constantly decreasing. Therefore, the size of the particle alone is not responsible for the changes in the current-density relation from what is seen in the ordinary TASEP.

Next, we consider the effects of disorder on $J(\rho_c)$. TASEP with quenched random disorder has been studied in [59] with a particle size of one. The authors found that a plateau region forms in the current-density plot about the maximum value of the ordinary TASEP. The size of the plateau is related to how the random hopping rates change the current throughout the TASEP [59]. In the case of the genes, the hopping rates are not "random" in the sense that they are not explicitly obtained from a distribution. Yet, the flattening seen in the quenched random disorder TASEP would explain the curvature of J becoming zero for all the genes in Fig. 5.7. The inhomogeneous hopping rates would also shift the density at which the maximum current is reached [59]. The shift would be different for each gene since the size of the shift depends on the distribution of the hopping rates. This shift would be in addition to the shift from the large particles. However, the results from the quenched random disorder TASEP does give us insight into how the inhomogeneous hopping rates affect the current-density relation.

A final note on the range of ρ_c in Fig. 5.5 before concluding. Here, the maximum ρ_c value is determined by the density in the maximal current phase because of the α_{eff} and β chosen.

In order to get a larger ρ_c, the value of β would need to be decreased so that the genes would be in a HD phase. While termination is not the limiting factor in protein production [26], a slow site near the exit would produce the same effect [34, 35]. We expect $J(\rho_c)$ to return to zero as $\rho_c \to 1$. However, the extension of $J(\rho_c)$ to higher densities would not change any of the arguments presented above and would not give any new insights into the effects of competition in a real cell.

5.3 Summary

To summarize, we explored how competition affects the production rate of proteins using a simplified model in which 10 genes from E. coli compete for a finite number of ribosomes. We studied the average particle density, coverage density, and current for each gene, which is modeled using an inhomogeneous TASEP, as a function of the total number of particles in the system. In all three quantities, severely limiting the number of particles in the system caused their values to be decreased from their unlimited resource value, regardless of the size and internal hopping rates of a TASEP. In this limit, the system lacks enough particles to supply all of the TASEPs with their desired number of particles. As the number of particles in the system increased, the inhomogeneous internal hopping rates caused each TASEP to reach a different final density and current, which was found in previous studies [66, 58]. Also, the crossover to these final values occurred at different N_{tot} values. By looking at the gradient of the coverage density with respect to N_{tot}, we saw additional features that were similar to what was seen for multiple TASEPs with homogeneous internal hopping rate competing for particles. However, the large particles and inhomogeneous internal hopping rates modifications made a direct connection to the multiple TASEP study difficult.

Unlike the ordinary TASEP, simple relationships between the density and the current were found to not exist. To understand how the current depends on the density, we looked at previous studies with quench random disorder [59] and large particles [31]. In both cases, the results from the previous studies alluded to what we see for the competing genes. Yet due to the complexity of the model, separating out the effect of competition from the large particle effects and the effects of the inhomogeneous internal hopping rates is nearly impossible. One would need to understand how all these effects are coupled to each other in order to truly understand the translation process in protein synthesis.

Chapter 6

Summary and Outlook

Throughout this dissertation, we have looked at the effects of finite resources on totally asymmetric simple exclusion processes. The motivation for the study came from attempting to understand the effects of competition for resources between genes during the translation process in protein synthesis. We started by studying a simple model – a single TASEP connected to a reservoir with a finite number of particles where the entry rate of particles into the TASEP depended on the number of particles in this reservoir. Additional TASEPs were connected to the pool of particles to study the effects of competition between the TASEPs. Since the motivation for studying the effects of finite resources was to understand how competition for resources in cells affect the process of translation during protein synthesis, we made the leap forward to model competition between real genes of Escherichia coli using a set of modified TASEPs connected to a reservoir of particles. In all the situations that we studied, finite resources had an effect on the system.

6.1 Summary

For the constrained TASEP, the average overall density and current were previously studied as a function of the total number of particles in the TASEP and pool, N_{tot}, and a simple domain wall theory (SDW) was presented to explain the results of the Monte Carlo simulations [57]. Upon looking at the average density profile as N_{tot} is varied, we found a new phenomenon, shock localization, that is not seen in the ordinary TASEP. This localization occurred during the crossover regime when α and β where such that the ordinary TASEP would be in the HD phase. In this regime, the number of particles in the pool remained constant as N_{tot} is increased [57]. The SDW theory presented in [57] could not reproduce the localization. Instead, we generalized the domain wall theory to include how the effective entry rate, α_{eff}, changed with the shock position k [61]. The dependence on k led to site dependent hopping rates for the motion of the shock. The site dependence acted like a

restoring force, thereby keeping the shock localized about a certain position. A solution was found for the master equation of $P(k)$, the probability to find the domain wall at position k, and the density profile was calculated from this solution. By adding in the site dependence to the hopping rates, the localized shock was correctly predicted and had good agreement with the data from the Monte Carlo simulations.

In addition to the density profile, the average overall density was calculated from the generalized domain wall (GDW) solution. The only noticeable improvement over the SDW theory came in the case when $\alpha = \beta$ (SP). The SDW theory had a slight disagreement with the simulation data as the system crossed over from an effective LD state to the SP [57]. On the other hand, the GDW theory had better agreement with the simulation data. While the improvement was minimal, it showed the importance of the feedback effect from the finite resources for the average overall density.

Another quantity studied for the constrained TASEP was the power spectrum of the total occupancy. The power spectrum contained information about the time evolution of the number of particles in the TASEP. We found the power spectrum was suppressed at low ω when compared to the power spectrum of the ordinary TASEP. Through Monte Carlo simulations, the level of suppression was related to the rate of change of α_{eff} with respect to the pool. Two simple theories were presented to explain how feedback effect caused the suppressions. In the LD phase, a set of Langevin equations were solved with the feedback effect incorporated into them. The solution predicted the suppression as well as the oscillations previously seen in the ordinary TASEP [55]. However, the theoretical result did not agree with the simulation results. Yet, the ratio of the power spectra for the constrained TASEP and the ordinary TASEP from the theory did agree with the ratios from the simulations. A second approach for solving the set of Langevin equations was presented and yielded the same results. In the crossover regime in the HD case, we started from a continuity equation to find the power spectrum. Again, the dependence of α_{eff} on the occupation of the TASEP was incorporated into the theory. The results agreed well when the TASEP had a large length. At smaller lengths, a finite size correction had to be inserted by hand. In both cases, the suppression was controlled by how α_{eff} changed as the number of particles in the pool changed in time.

We then moved to competition between multiple TASEPs in our study. We first considered competition between only two TASEPs as the simplest case of competition. Each TASEP had the same entry and exit rates, and the entry rate depended on the number of particles left in the pool as it did with the constrained TASEP. We explored how the average overall density, density profile, and current changed as a function of N_{tot}. When the two lengths of the TASEPs were equal, we discovered that the average overall density and current had a similar behavior as a single constrained TASEP in all cases. However, the average density profile differed in the crossover regime in the HD case. Here, shock localization did not occur as it did for the constrained TASEP. Instead, a portion of the profile was linear near the exit and the rest contained a flat profile. The linear portion increased as N_{tot} increased. The linear part of the profile indicated a shock performing an unbiased random walk between two points

on the lattice. The addition of the second TASEP allowed for particles to be exchanged via the pool between the two TASEPs, effectively keeping the number of particles in the pool constant. This view was reinforced by the distribution of $P(N_1, N_2)$, the probability of finding N_1 particles in the first TASEP and N_2 particles in the second one.

When the lengths were not equal, the overall density as well as the profiles differed from the equal case. For the LD case, no new phenomena were seen. In the MC case, finite size effects due to the lengths of each TASEP arose in looking at the overall density as a function of N_{tot}, which was already seen for the constrained TASEP [57]. In the SP case, the overall density for each TASEP followed a curve similar to what was seen for the constrained TASEP with their given lengths. The HD case had more interesting phenomena. First, a plateau region formed during the crossover regime in the overall density for the smaller TASEP, while the larger TASEP behaved in a manner similar to a constrained TASEP. Second, shock localization reappeared in the density profile of the larger TASEP. The width of this localization was broader than just having a single constrained TASEP and it depended on the length of the second TASEP. The reason for the broadening was the smaller TASEP acted as a buffer of particles for the larger TASEP, thereby decreasing the localization effect of having a changing entry rate. The third new phenomenon seen was the complete delocalization of the shock in the smaller TASEP in the crossover regime. The smaller TASEP behaved like an ordinary TASEP in the SP. Particle exchange via the pool allowed the shock in the smaller TASEP to become delocalized over a range of N_{tot} values. Again, the exchange of particles was evident in the $P(N_1, N_2)$ distribution.

For both the equal and unequal lengths, we used a GDW theory to predict the profiles and overall densities for each TASEP. Since the entry and exits rates were the same for both TASEPs, the Kolmogorov criterion was satisfied [64] and we used detailed balance to find the solution to the master equation for $P(k_1, k_2)$. The theoretical results for the average density profile were in agreement with the simulation results for all cases, as well as the average overall densities. The theory was extended to include arbitrarily many TASEPs, which agreed with the simulation results presented for three TASEPs of different lengths. No new features were seen in the results for more than two TASEPs for the cases studied.

The power spectra of the TASEPs and reservoir were also studied with two TASEPs through Monte Carlo simulations. Two situations were considered – one where the lengths of the TASEPs were the same and the other with different lengths. For equal lengths, we saw a suppression at low ω for the power spectra of the two TASEPs and the power spectrum of the pool. As in the single constrained TASEP, the rate of change of α_{eff} with respect to the pool controlled the level of suppression. However, the suppression for the pool was greater than the suppression for the TASEPs. The difference was due to the particle exchange between the TASEPs through the pool. Thus, the pool saw the full effects of the constraint, while the particle exchange shielded the TASEPs from the effects. For unequal lengths, we found a suppression for the power spectra of the larger TASEP and the pool, but the power spectrum of the smaller TASEP was enhanced when compared to the ordinary TASEP's power spectrum. The enhancement was concluded to be caused by the exchange of particles

between the larger and smaller TASEP via the pool. One piece of evidence supporting this claim came from the LD state. Here, oscillations in the power spectrum of the smaller TASEP corresponded to the oscillations in power spectrum of the larger one, which did not exist in the power spectrum of the ordinary TASEP. A similar enhancement was seen in the crossover regime in the HD case, however, no oscillations were present for either TASEP in this regime to indicate the effects of one on the other.

The power spectrum of the difference of the two occupations of the TASEPs was explored as well. Again we considered having equal and unequal lengths. For the equal lengths, the power spectrum of the difference behaved like the power spectrum of the ordinary TASEP. In fact, the Monte Carlo simulations showed that the difference had twice the amplitude of the ordinary TASEP. For the unequal lengths case, we again saw the suppression at low frequencies, but the amplitude of the power spectrum was larger than that of either TASEP or the pool. Thus, the relationship between the power spectra of the difference and ordinary TASEP came from the symmetry of the two TASEPs. Without this symmetry, no simple relationship between the two was found.

For the power spectra of the TASEPs, pool, and difference, a theoretical approach was developed to better understand quantitatively the results from the simulations. For the LD state, we again solve a set of Langevin equations where the two TASEPs were coupled together through the pool. We showed how the different levels of suppression came about for the case of equal lengths. We also showed in this case that the power spectrum of the difference was twice the power spectrum of the ordinary TASEP. For the crossover regime in the HD case, we solved a set of coupled continuity equations to find the power spectrum of each TASEP. The finite size effects had to be incorporated by inserting a term that accounted for the size of the system. This term was taken from a fit parameter to the power spectrum of the ordinary TASEP at small lengths. By including the size dependence in this way, we were able to predict the various levels of suppression for the larger TASEP and pool and the enhancement seen for the smaller TASEP in the unequal lengths case. For the equal lengths case, we showed how the power spectrum of the pool was related to the power spectrum of the constrained TASEP and that the power spectrum of the difference was equal to twice the power spectrum of the ordinary TASEP.

Finally, we increased the complexity of our model in order to attempt to model ten real genes of Escherichia coli (E. coli). In addition to competition, we incorporated particles covering more than one site and inhomogeneous internal hopping rates. The internal hopping rates were chosen to model a specific sequence of codons. We studied the particle density, coverage density, and current as a function of N_{tot}. While the densities and current seemed to rise linearly before leveling off to a final value, the exploration of the derivatives of these quantities with respect to N_{tot} showed otherwise. Some of the features seen in the derivatives of the density were similar to those seen with homogeneous TASEPs competing, but the complexity of the model for the genes prevented any concrete conclusions from being made. However, the effects of severely limiting the resources were seen in the lower steady state values of the densities and current at small N_{tot} values when compare to their values without any

constraint on the resources.

6.2 Outlook on Future Research

While our study of competition between TASEPs has given us an insight into the effects of competition for resources, many questions remain unexplored and unanswered. One such area of exploration is the effect of having different entry and exit rates for each TASEP. The difference could be used to model the difference between highly and rarely expressed genes during protein synthesis. From a physical standpoint, detailed balance will be broken even in the domain wall picture, which will make a theoretical approach more difficult to develop. Also, the parameter space for this system would be much larger than keeping all the rates the same for each TASEP. Many Monte Carlo simulations would be needed to explore the entire parameter space, even for just two TASEPs. Simulations could possibly be the only means of gaining an understanding of the physics if a theoretical approach could not be developed.

Another open question is related to disagreement between the theory and simulation results for the power spectrum of the TASEP. The theoretical result did not agree with the simulation data for any combination of fitting parameters. Is there any way to improve the agreement? One way to improve this theoretical result would be to include the nonlinear terms that were dropped from the Langevin equations. To solve such a problem, a perturbative field theoretical approach would need to be used to correctly account for the nonlinear terms. The correct renormalization of the diffusion coefficient would be calculated from this theory and may renormalize different powers of k differently. This renormalization would be different than multiplying all even powers of k by a single constant. Therefore, the field theoretic approach would fit the simulation data better than the linear theory.

The complexity of the real gene model we studied could be simplified to having only one or two slow sites on each TASEP. Since the effects of slow sites has already been studied [32, 33], the effect of coupling the two modifications could be studied. The insights gained from studying the coupling in this simple system would assist in our attempt to understand the results of simulating real genes with inhomogeneous hopping rates. Along the same lines, incorporation of particles covering more than one site [34, 35] with finite resources could also be explored to see if there is any coupling between the two modifications. Again, the results of studying the effect of large particles and finite resources would aid in understanding competition between real genes.

In addition to competition between genes for ribosomes, we should include competition for tRNA since it also appears in the cell in a finite amount for a more realistic model. A pool for each type of tRNA would be used to determine the site hopping rate for a given codon. A "usage time" would also need to be associated with the tRNA to determine how long a gene uses it. Experimental data would need to be reviewed to determine a realistic timescale

of a tRNA being used by one gene and then another. The study of such a system would give us insight into how the levels of tRNA affect protein production rates.

In the context of both biology and physics, much more work needs to be done in order to understand the translation process during protein synthesis. By studying simple models, we can build an understanding of how different aspects of a more complex system are coupled together. While we have concentrated on the effects of finite resources here, it is only but one piece of a larger puzzle. In the context of biology, other factors besides the concentration of ribosomes affect the protein production rate. In the context of physics, the TASEP model and its modifications are a small subset of systems that fall into being non-equilibrium systems. By exploring simple models, we hope to someday be able to have a comprehensive theory for non-equilibrium statistical mechanics. Until that day, we have much work remaining.

Bibliography

[1] *Condensed-Matter and Materials Physics: The Science of the World Around Us*, 2007, Committee on CMMP 2010, Solid State Sciences Committee, National Research Council (National Academies Press)

[2] Zia R K P and Schmittmann B, 2007 *J. Stat. Mech.* P07012

[3] Ising E, 1925 *Z. Physik* **31** 253

[4] Onsager L, 1944 *Phys. Rev.* **65** 117

[5] Yang C N and Lee T D, 1952 *Phys. Rev.* **87** 410

[6] Wilson K G and Fisher M E, 1972 *Phys. Rev. Lett.* **28** 240

[7] Schmittmann B and Zia R K P, 1995 *Statistical Mechanics of Driven Diffusive Systems* (*Phase Transition and Critical Phenomena* Vol. 17), ed C Domb and J L Lebowitz (London: Academic)

[8] Spitzer F, 1970 *Adv. Math.* **5** 246

[9] Derrida B, Domany E, and Mukamel D, 1992 *J. Stat. Phys.* **69** 667

[10] Derrida B, Evans M R, and Pasquier V, 1993 *J. Phys. A: Math. Gen.* **26** 4911

[11] Schütz G M and Domany E, 1993 *J. Stat. Phys.* **72** 277

[12] Kolomeisky A B, Schütz G M, Kolomeisky E B and Straley J P, 1998 *J. Phys. A: Math. Gen.* **31** 6911

[13] Santen L and Appert C, 2002 *J. Stat. Phys.* **106** 187

[14] De Masi A and Ferrari P A, 1985 *J. Stat. Phys.* **38** 603

[15] Kutner R and van Beijeren H, 1985 *J. Stat. Phys.* **39** 317

[16] Dhar D, 1987 *Phase Transit.* **9** 51

[17] Majumdar S N and Barma M, 1991 *Phys. Rev. B* **44** 5306

[18] Gwa L-H and Spohn H, 1992 *Phys. Rev. A* **46** 844

[19] Kim D, 1995 *Phys. Rev. E* **52** 3512

[20] Golinelli O and Mallick K, 2004 *J. Phys. A: Math. Gen.* **37** 3321

[21] Golinelli O and Mallick K, 2005 *J. Phys. A: Math. Gen.* **38** 1419

[22] Gupta S, Majumdar S N, Godrèche C and Barma M, 2007 *Phys. Rev. E* **76**, 021112

[23] Krug J, 1991 *Phys. Rev. Lett.* **67** 1882

[24] Crick F, 1970 *Nature* **227** 561

[25] Alberts B, Johnson A, Lewis J, Raffs M, Roberts K, and Walter P, 2002, *The Molecular Biology of the Cell* 4th edition (Garland: New York)

[26] Gilchrist M A and Wagner A, 2006 *J. Theor. Biol.* **239** 417

[27] Dong H, Nilsson L, and Kurland C G, 1996 *J. Mol. Biol.* **260** 649

[28] Chou T, 2003 *Biophys. J.* **85** 755

[29] MacDonald C, Gibbs J, and Pipken A, 1968 *Biopolymers* **6** 1

[30] MacDonald C and Gibbs J, 1969 *Biopolymers* **7** 707

[31] Shaw L B, Zia R K P, and Lee K H, 2003 *Phys. Rev. E* **68** 021910

[32] Dong J J, Schmittmann B, and Zia R K P, 2007 *J. Stat. Phys.* **128** 21

[33] Chou T and Lakatos G, 2004 *Phys. Rev. Lett.* **93** 198101

[34] Dong J J, Schmittmann B, and Zia R K P, 2007 *Phys. Rev. E* **76** 051113

[35] Chou T and Lakatos G, 2003 *J. Phys. A: Math. Gen.* **36** 2027

[36] Popkov V, Santen L, Schadschneider A, and Schütz G M, 2001 *J. Phys. A: Math. Gen.* **34** L45

[37] Chowdhury D, Santen L, and Schadschneider A, 1999 *Curr. Sci.* **77** 411

[38] Kardar M, Parisi G, and Zhang Y-C, 1986 *Phys. Rev. Lett.* **56** 889

[39] Wolf D and Tang L-H, 1990 *Phys. Rev. Lett.* **65** 1591

[40] Popkov V, Rákos A, Willmann R D, Kolomeisky A B, and Schütz G M, 2003 *Phys. Rev. E* **67** 066117

[41] Evans M R, Juhász R, and Santen L, 2003 *Phys. Rev. E* **68** 026117

[42] Juhász R and Santen L, 2004 *J. Phys. A: Math. Gen.* **37** 3933

[43] Lipowsky R, Klumpp S, and Nieuwenhuizen T M, 2001 *Phys. Rev. Lett.* **87** 108101

[44] Parmeggiani A, Franosch T, and Frey E, 2003 *Phys. Rev. Lett.* **90** 086601

[45] Klumpp S and Lipowsky R, 2003 *J. Stat. Phys.* **113** 233

[46] Ha M and den Nijs M, 2002 *Phys. Rev. E* **66** 036118

[47] Dudzinski M and Schütz G M, 2000 *J. Phys. A: Math. Gen.* **33** 8351

[48] Belitzky V and Schütz G M, 2002 *El. J. Prob.* **7** Paper no. 11

[49] Schütz G M 2001, *Exactly solvable models in many-body systems* (*Phase Transitions and Critical Phenomena* Vol. 19) ed C Domb and J L Lebowitz (London: Academic)

[50] Derrida B, 1998 *Phys. Rep.* **301** 65

[51] Nagy Z, Appert C and Santen L, 2002 *J. Stat. Phys.* **109** 623

[52] de Gier J and Essler F H L, 2006 *J. Stat. Mech.* P12011

[53] Takesue S, Mitsudo T and Hayakawa H, 2003 *Phys. Rev. E* **68** 015103

[54] Pierobon P, Parmeggiani A, von Oppen F and Frey E, 2005 *Phys. Rev. E* **72** 036123

[55] Adams D A, Schmittmann B, and Zia R K P, 2007 *Phys. Rev. Lett.* **99** 020601

[56] Mukherjee S, 2009 *Applications of Field Theory to Reaction Diffusion Models and Driven Diffusive Systems*, PhD thesis, Virginia Tech.
<http://scholar.lib.vt.edu/theses/available/etd-08292009-150038/restricted/thesis_new_2.pdf>

[57] Adams D A, Schmittmann B, and Zia R K P, 2008 *J. Stat. Mech.* P06009

[58] Shaw L B, Sethna J P, Lee K H, 2004 *Phys. Rev. E* **70** 021901

[59] Harris R J, Stinchcombe R B, 2004 *Phys. Rev. E* **70** 016108

[60] Foulaadvand M E, Chaaboki S, and Saalehi M, 2007 *Phys. Rev. E* **75** 011127

[61] Cook L J and Zia R K P, 2009 *J. Stat. Mech.* P02012

[62] Angel A G and Zia R K P, 2009 *J. Stat. Mech.* P03009

[63] Cook L J, Zia R K P, and Schmittmann B, 2009 *Phys. Rev. E* **80** 031142

[64] Kolmogorov A N, 1936 *Math. Ann.* **112** 155

[65] *GenBank Overview*, http://www.ncbi.nlm.nih.gov/Genbank/

[66] Dong J J, 2008 *Inhomogeneous Totally Asymmetric Simple Exclusion Processes: Simulations, Theory and Application to Protein Synthesis*, PhD thesis, Virginia Tech. <http://scholar.lib.vt.edu/theses/available/etd-04092008-113617/restricted/thesis_V200803_rev4.pdf>

Appendix A

Relation Between Fourier Transforms with Different Sampling Rates

Given a function $f(t)$, we define its discrete Fourier transform on the interval $t \in [0, T-1]$ to be:

$$\tilde{f}(\omega) = \sum_{t=0}^{T-1} e^{-i\omega t} f(t) \tag{A.1}$$

where

$$\omega = \frac{2\pi k}{T} \quad k \in [0, T-1] \tag{A.2}$$

Instead, let us choose a subset of the t's such that:

$$t = n\ell \tag{A.3}$$

In other words, we take only every ℓ t up to $T-1$. If we now define:

$$g(n) = f(n\ell) \quad n \in [0, N-1] \tag{A.4}$$

with

$$N = \frac{T}{\ell} \tag{A.5}$$

then the Fourier transform of this new function is:

$$\tilde{g}(\nu) = \sum_{n=0}^{N-1} e^{-i\nu n} g(n) \tag{A.6}$$

where

$$\nu = \frac{2\pi m}{N} \tag{A.7}$$

We wish to relate $\tilde{g}(\nu)$ to $\tilde{f}(\omega)$. To do this, we note:

$$\begin{aligned}
\tilde{g}(\nu) &= \sum_{n=0}^{N-1} e^{-i\nu n} g(n) \\
&= \sum_{n=0}^{N-1} e^{-i\nu n} f(n\ell) \\
&= \frac{1}{T} \sum_{n=0}^{N-1} e^{-i\nu n} \sum_{k=0}^{T-1} e^{i\omega n\ell} \tilde{f}(\omega) \\
&= \frac{1}{T} \sum_{k=0}^{T-1} \tilde{f}(\omega) \sum_{n=0}^{N-1} e^{i\frac{2\pi}{N}(k-m)n} \\
&= \frac{1}{T} \sum_{k=0}^{T-1} \tilde{f}(\omega) \frac{1 - e^{i2\pi(k-m)}}{1 - e^{i\frac{2\pi}{N}(k-m)}}
\end{aligned} \tag{A.8}$$

Since k, m, and N are all integers, the fraction on the right becomes N times a Kronecker delta when $k = m + jN$ with $j \in [0, \ell]$. Thus, we have:

$$\begin{aligned}
\tilde{g}(\nu) &= \frac{1}{\ell} \sum_{k=0}^{T-1} \tilde{f}(\omega) \delta_{k,m+jN} \\
&= \frac{1}{\ell} \sum_{j=0}^{\ell-1} \tilde{f}\left(\frac{2\pi}{T}[m + jN]\right)
\end{aligned} \tag{A.9}$$

This result amounts to summing over the first ℓ Nth harmonics.

Appendix B

Finite Size Effects of the Power Spectrum of the TASEP on the Coexistence Line

For the TASEP with $\alpha = \beta$, a coexistence between a LD region and a HD region form on the lattice. This coexistence is sometimes referred to as the "shock" phase (SP) because a shock forms between these two regions. The shock's position performs a random walk about the entire lattice. The random walk of the shock leads to a ω^{-2} power law for the power spectrum of the total occupancy [55]. However, a deviation from ω^{-2} is seen for small lattice lengths as shown in Fig. B.1.

The power spectrum is suppressed at low ω values from the ω^{-2} curve. The suppression effect is also seen in the constrained TASEP when the average $\alpha_{eff} = \beta$ and the shock is localized to a small region on the TASEP. For the ordinary TASEP, the shock is "localized" to the lattice, so the length of the TASEP should have the same effect as the localization mechanism in the constrained TASEP. Therefore, we assume the power spectrum to have the form:

$$I(\omega) = \frac{A}{\omega^2 + \delta^2} \tag{B.1}$$

where A and δ are fit parameters. The δ parameter controls the L-dependent suppression of the power spectrum.

By fitting A and δ to the simulation data, we find the L dependence of δ. We expect a power law of the form:

$$\delta = \frac{a}{L^b} \tag{B.2}$$

From Fig. B.2, we indeed get a power law with $a = 2$ and $b = 1.81$ with $\alpha = \beta = 0.3$ over the range of L shown. The values of α and β also effect the values of a and b. For $\alpha = \beta = 0.2$, $a = 0.9$ and $b = 1.79$. The difference is due to the change in the shock height δ accounts for the finite size effects in the power spectrum of the total occupancy.

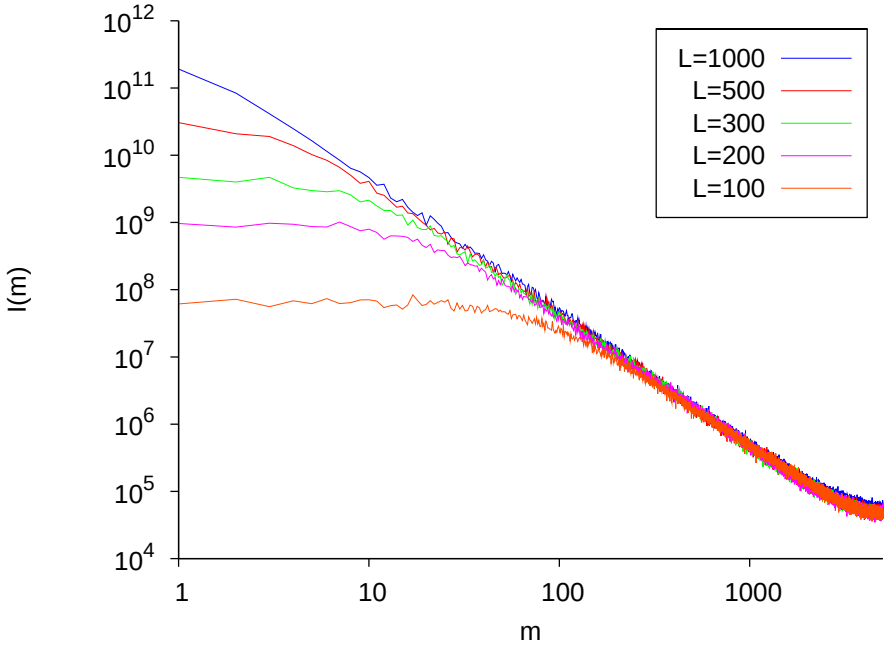

Figure B.1: Power spectrum of the total occupancy with $\alpha = \beta = 0.3$ for various lengths.

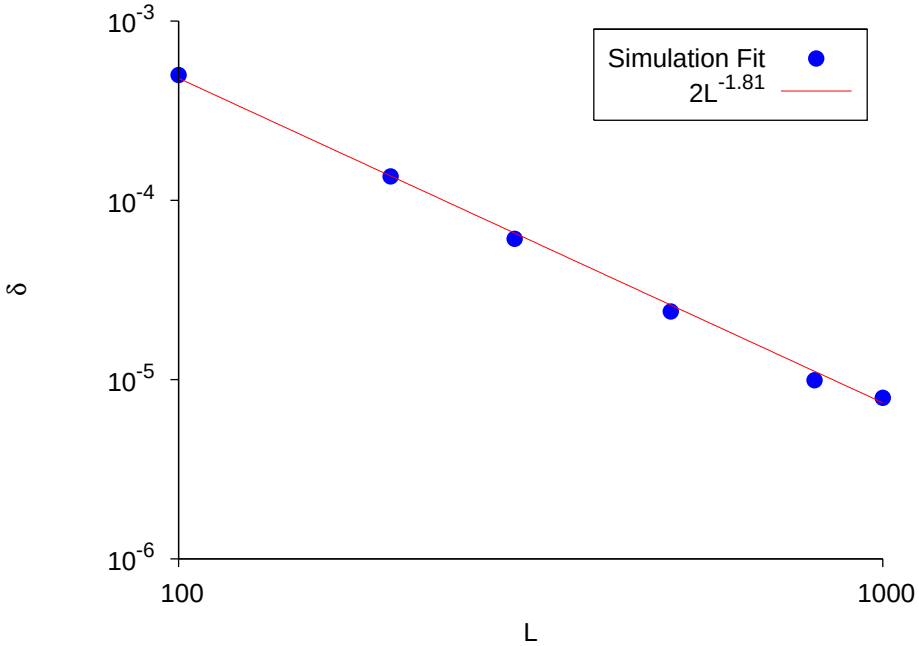

Figure B.2: δ as a function of L with $\alpha = \beta = 0.3$.

Appendix C

Table of Internal Hopping Rates For Escherichia Coli Genes

Site	secD	rpsA	dnaA	lamB	tufA	lacI	ompA	araC	rplA	trpR
1	0.6947	0.4767	0.6947	0.4767	0.6947	0.6947	0.4767	0.4767	0.4767	0.4767
2	0.1288	0.4463	0.2508	0.4767	0.3881	0.3554	0.3554	0.7145	0.7145	0.1216
3	0.2484	1.0000	0.2020	0.4215	0.3554	0.0872	0.3554	1.0000	0.3554	0.1492
4	0.8712	0.3881	0.3002	0.4463	1.0000	0.6947	0.2348	0.7145	0.8644	0.1492
5	0.3145	0.1741	0.2020	0.8644	0.3554	0.3411	0.7145	0.1492	0.2116	0.2508
6	0.2150	0.7145	0.1710	0.8712	0.1741	0.1288	0.4215	0.2484	0.3554	0.1278
7	0.4457	0.1492	0.2136	0.3554	1.0000	0.3145	0.7145	0.5267	0.8712	0.3145
8	0.1710	0.2020	0.2136	0.2020	0.8712	0.5267	0.4215	0.1278	0.4767	0.2508
9	0.3554	0.1741	0.2409	0.2150	0.2348	0.2457	0.7145	0.8644	0.8712	0.7145
10	0.3145	1.0000	0.2020	0.8644	0.3554	0.7145	0.6947	0.8644	0.9404	0.7145
11	0.2457	1.0000	0.1216	0.7145	0.1782	1.0000	0.7145	0.1782	0.4215	0.4767
12	0.4767	0.1373	0.8712	0.9404	0.1492	0.3145	0.8644	0.1888	0.8712	0.7145
13	0.8644	0.1288	0.4457	0.1216	0.9404	0.1216	0.7145	0.3145	1.0000	1.0000
14	0.4215	0.3554	0.2136	0.2457	0.2484	0.8504	0.8504	0.3002	0.3554	0.2136
15	0.6947	1.0000	0.5267	0.7145	0.9404	0.2457	0.1741	0.1741	0.9404	0.8712
16	0.6947	0.4215	1.0000	0.7145	0.8504	0.3881	0.7145	0.2484	0.5267	0.1492
17	0.4215	1.0000	0.1288	0.8504	0.4463	0.3145	0.2116	0.1216	0.7145	0.2136
18	0.2457	0.2116	0.0872	0.6947	0.4215	0.2136	0.6947	0.1492	0.2116	1.0000
19	0.4215	0.8712	0.1216	0.4767	0.8504	0.2116	0.7145	0.8644	0.3554	0.1710
20	0.8504	0.1782	0.2348	0.3881	0.1492	0.9404	0.2136	0.6947	0.2136	0.1288
21	0.8644	0.8504	1.0000	0.7145	0.9404	0.1373	0.1216	0.7145	0.3145	0.8712
22	0.8644	0.3881	0.1741	0.2136	0.5267	0.8712	0.7145	0.8504	0.5267	0.1741
23	0.3145	0.4215	0.1932	0.7145	0.1492	0.6947	0.1782	0.1288	0.4215	0.2457
24	0.7145	0.9404	0.4767	0.4767	0.8504	0.6947	0.3554	0.3411	0.2484	0.5267
25	0.2020	0.8712	0.1710	0.7145	0.3554	0.2484	0.5267	0.1782	1.0000	0.8644
26	0.1278	0.8504	0.4215	0.9404	0.4463	0.2136	0.2484	0.4215	0.7145	0.2020
27	0.2484	0.9404	0.8712	0.5267	0.4463	0.1216	0.2116	1.0000	0.4215	0.3554
28	0.8644	0.9404	0.0872	0.1741	0.8644	0.1932	0.1710	0.1216	0.7145	0.2484
29	0.1741	0.9404	0.4457	0.1492	0.2116	0.1492	0.3145	0.2484	0.8644	0.1216
30	0.8504	0.7145	0.2136	0.8504	0.7145	0.9404	0.4463	0.8504	0.8644	0.3145
31	1.0000	0.4215	0.7145	0.3145	0.7145	0.3881	0.8504	0.3145	0.3554	0.1492
32	0.5267	0.5267	1.0000	0.7145	0.4215	0.7145	0.7145	0.2020	1.0000	0.2484
33	0.1782	0.3554	0.8644	0.8712	0.2116	0.3554	0.3554	0.5267	0.8644	0.5267
34	0.7145	0.5267	0.1932	0.1373	0.2116	0.3411	0.8644	0.1741	0.7145	0.2020
35	0.9404	0.6947	0.5267	0.8504	0.6947	0.0784	0.8504	0.1741	0.4463	0.1492
36	0.2136	0.6947	0.2484	0.4215	0.8644	1.0000	0.1710	0.4215	0.7145	0.1288
37	0.4215	0.8644	0.3411	0.8504	0.7145	0.3554	0.1373	0.5267	0.3554	0.1782
38	0.4463	0.9404	0.8644	0.1710	0.3554	0.6947	0.2136	0.8712	0.1741	0.4457
39	0.8504	0.5267	0.1216	0.2348	0.2116	1.0000	0.3145	0.1782	0.6947	0.1288
40	0.7145	0.7145	0.8644	0.8504	0.3145	0.7145	0.1492	0.8644	1.0000	0.2484

Site	secD	rpsA	dnaA	lamB	tufA	lacI	ompA	araC	rplA	trpR
41	0.8712	0.8504	0.3145	0.1932	0.8504	0.7145	0.5267	0.1888	0.1932	0.8644
42	0.1888	0.8644	0.7145	0.8504	0.8504	0.4767	0.4463	0.4767	0.6947	0.4767
43	0.2457	0.3554	0.0872	0.8504	0.7145	0.7145	0.8504	0.3554	0.5267	0.8644
44	0.1216	0.3881	0.2484	1.0000	0.7145	1.0000	0.1741	0.8504	0.6947	0.3411
45	0.1216	1.0000	0.8712	0.1492	0.8712	0.8644	0.4215	0.3145	0.7145	0.0872
46	0.1932	0.1373	0.1741	0.2136	0.7145	0.2484	0.2484	0.4215	0.9404	0.5267
47	1.0000	0.1216	0.2457	0.2409	0.1741	0.3145	0.2484	0.2020	0.2484	1.0000
48	0.1492	0.4215	0.2020	0.1741	0.5267	0.4215	0.2484	0.2484	0.2020	0.8712
49	0.3411	0.1782	0.5267	0.2136	0.2136	0.1278	0.8504	0.2020	0.8504	1.0000
50	0.8644	0.7145	0.1710	0.4463	0.4215	0.2484	0.1782	0.2116	0.4215	0.7145
51	0.4215	1.0000	0.6947	0.2116	0.5267	0.8712	0.2116	0.4215	0.5267	0.4457
52	0.2136	0.2136	0.0784	0.8504	0.2484	0.6947	0.1492	0.8712	0.7145	0.3775
53	0.2457	0.1741	0.5267	0.7145	0.7145	0.7145	1.0000	0.8504	0.8712	0.4463
54	0.2136	0.3554	0.3554	0.1492	0.1782	0.1492	0.2484	0.2136	0.3554	0.8712
55	0.3554	0.2484	0.3145	0.1932	1.0000	0.1492	0.1492	0.3775	0.3881	0.6947
56	0.3411	0.1216	0.2020	0.3554	1.0000	0.8644	0.8644	0.6947	0.5267	0.8712
57	0.1288	0.2136	0.2484	0.3145	0.3554	0.7145	0.8504	0.6947	0.2136	0.4215
58	0.1492	0.8504	0.2484	0.8712	0.7145	0.8504	0.7145	0.3554	0.2484	0.2457
59	1.0000	1.0000	0.4215	0.2020	0.8712	0.3554	0.8504	0.2484	0.6947	1.0000
60	1.0000	0.8644	0.2484	0.8504	0.8504	0.2136	0.7145	0.2136	0.8712	1.0000
61	0.3554	1.0000	0.1888	0.2484	0.4215	0.3002	0.1741	0.1888	0.8504	0.8644
62	0.4215	0.4215	0.8644	1.0000	0.2116	0.4457	0.8504	0.8712	0.7145	0.4457
63	0.4463	0.2136	0.1080	0.2409	0.4215	0.8644	0.8504	1.0000	0.4463	0.8712
64	0.7145	0.6947	0.2116	1.0000	0.2484	0.4215	0.3145	0.1741	0.6947	0.8504
65	0.3554	0.8504	0.1932	0.4463	0.4463	0.8504	0.2136	0.2457	0.8644	1.0000
66	0.3881	0.5267	0.1741	0.3145	0.3881	0.9404	0.9404	0.2409	0.1782	0.4767
67	0.6947	1.0000	0.2409	0.7145	0.1492	0.1216	0.2484	0.8712	0.1492	0.1932
68	0.7145	0.9404	0.1888	1.0000	0.9404	0.2116	0.1782	0.1782	0.8504	0.2136
69	0.8644	0.5267	0.7145	0.1288	1.0000	0.1373	0.3145	0.8504	0.4463	0.8712
70	1.0000	0.9404	0.5267	0.3554	0.3145	0.1932	0.9404	0.5267	0.8504	1.0000
71	1.0000	0.7145	0.1216	0.4457	0.5267	0.8644	0.8504	0.4215	0.8712	0.1288
72	0.8504	0.8644	0.0872	0.8504	0.2116	0.1216	0.1741	0.4457	0.1373	0.3554
73	0.7145	0.5267	0.2136	0.2136	0.1782	0.8644	1.0000	0.8644	0.9404	0.2484
74	0.4215	0.7145	0.8644	1.0000	0.2116	0.1492	0.4767	0.1741	0.8712	1.0000
75	0.2020	0.6947	0.8712	0.6947	0.8712	0.7145	0.8504	0.1782	0.6947	0.2020
76	0.7145	1.0000	0.1741	0.1710	0.1492	0.1782	0.3145	0.0872	0.1216	0.8504
77	0.8712	0.5267	1.0000	0.3554	0.3145	0.3002	0.5267	0.1888	0.6947	0.7145
78	0.1741	0.8504	0.2457	1.0000	0.7145	0.1492	0.1710	1.0000	0.1741	0.8504
79	0.5267	0.1741	0.8504	0.8504	0.1492	0.4215	0.1288	0.4215	0.2116	0.4215
80	0.1373	0.8504	0.2116	0.5267	0.6947	0.2457	0.8504	0.1492	0.1492	0.7145
81	0.4463	1.0000	0.3554	0.3554	0.5267	0.7145	0.8712	0.1492	0.8504	0.3411
82	0.5267	0.4463	0.1782	0.1932	0.2409	0.7145	0.4767	0.3145	0.7145	0.4215
83	0.2116	0.8644	0.6947	0.1741	0.1782	0.4215	0.1782	0.8504	0.2484	0.3411
84	0.2136	0.8644	0.3411	0.3145	0.3775	0.3554	0.3145	0.8712	0.7145	0.8712
85	0.4457	0.1373	0.1492	0.1741	0.1492	0.3881	0.3554	0.1492	1.0000	0.1888
86	0.8712	0.8712	0.3411	0.5267	0.1216	0.8712	0.8504	0.1782	0.7145	0.3881
87	0.7145	1.0000	0.0872	0.4463	0.5267	0.1216	0.1932	1.0000	0.7145	0.2484
88	0.8712	0.3554	0.1492	0.2484	0.3145	0.5267	0.9404	0.7145	0.3554	0.1932
89	1.0000	0.7145	0.7145	0.6947	0.9404	0.1492	1.0000	0.8712	0.7145	0.8644
90	0.7145	0.3554	0.7145	0.1216	0.3554	0.8644	0.2484	1.0000	0.7145	0.3554
91	0.1288	0.8712	0.6947	0.3145	0.2484	0.8504	0.8504	0.1710	0.8504	0.1216
92	0.4767	0.1492	0.3411	0.1373	0.4767	0.1216	0.7145	0.3145	0.7145	0.7145
93	0.8504	1.0000	0.1932	0.2457	0.4215	0.1932	0.3145	0.1492	1.0000	0.1278
94	0.9404	0.1216	0.2484	0.7145	0.2116	0.6947	0.3554	0.2136	0.8644	0.2457
95	0.4767	0.1710	0.2457	0.1492	0.8504	0.6947	0.7145	0.1710	0.6947	1.0000
96	0.8504	0.4215	0.7145	0.2136	0.7145	0.6947	0.2136	0.9404	0.8504	0.8644
97	0.5267	0.3411	0.1216	0.2484	0.7145	0.3002	0.8504	0.3145	0.4767	0.8712
98	0.3554	0.8644	0.2150	0.5267	0.2136	0.4767	0.9404	0.1741	1.0000	0.2136
99	0.3145	1.0000	0.7145	0.1710	0.4767	0.6947	0.1492	0.8712	0.5267	0.1710
100	0.2457	0.3554	0.2136	1.0000	0.5267	1.0000	0.8644	0.1782	0.8644	0.8644
101	0.6947	0.7145	0.6947	0.7145	0.8504	0.8712	0.2116	0.8712	0.7145	1.0000
102	0.7145	0.3145	0.7145	0.2116	0.7145	0.1932	0.7145	0.1216	0.5267	1.0000
103	0.2020	1.0000	0.1492	0.5267	0.4215	0.8504	0.3554	0.3145	0.2136	0.6947
104	0.2484	0.5267	0.3411	0.1782	0.8644	0.2457	0.8644	0.1710	0.4215	0.4457
105	0.2020	0.7145	0.2136	0.1216	0.6947	1.0000	0.8504	0.1492	0.3554	0.8644
106	0.1216	1.0000	0.1782	0.1741	0.9404	0.1216	0.3145	1.0000	0.3554	0.3554
107	0.1782	0.4463	0.1492	0.8712	0.7145	0.2409	0.0872	0.1710	0.8504	0.1932
108	0.7145	0.9404	0.8712	1.0000	0.7145	0.3554	0.4215	0.2020	1.0000	0.5267
109	0.3411	0.2116	0.7145	0.7145	0.4463	0.7145	0.4463	0.2484	0.4767	
110	0.1782	0.8504	0.7145	0.2484	0.5267	0.7145	0.5267	0.1710	0.2484	
111	0.8712	0.9404	0.2150	0.6947	0.8504	0.6947	0.5267	0.1782	0.1741	
112	0.1710	0.4215	0.3881	0.2136	0.1782	0.1492	0.8644	0.2508	0.5267	
113	0.8644	0.2484	0.3411	0.8504	0.4767	0.2484	0.5267	0.4215	0.9404	
114	0.7145	0.8504	0.8712	0.3554	0.1782	0.2020	0.4215	0.1741	0.9404	
115	0.7145	0.3554	0.2508	0.2484	0.2136	0.2020	0.3145	0.1216	0.4215	

Site	secD	rpsA	dnaA	lamB	tufA	lacI	ompA	araC	rplA	trpR
116	0.4215	0.9404	0.8504	0.8644	0.4463	0.7145	0.4463	0.2484	0.7145	
117	0.1492	0.3554	0.1710	0.4215	0.8712	0.1492	0.8712	0.3411	0.3881	
118	0.7145	0.8504	0.5267	1.0000	1.0000	0.8712	0.8644	0.8504	0.1782	
119	1.0000	0.8504	0.2484	0.1710	0.1492	0.2457	0.8504	0.1741	0.5267	
120	0.1782	0.1741	0.2457	0.8644	0.4215	0.1932	0.8504	0.1741	0.7145	
121	0.4767	0.4463	0.1782	0.0872	0.8644	0.3775	0.4767	0.8712	0.4767	
122	0.3554	0.9404	0.1216	0.8504	0.8644	0.8644	0.6947	0.1782	0.8712	
123	0.2020	1.0000	0.1782	0.1373	0.8504	0.4215	0.1710	0.5267	0.9404	
124	0.8504	0.8644	0.7145	0.2116	0.8712	0.4215	0.8712	1.0000	0.9404	
125	0.2020	0.2484	1.0000	0.4215	0.2136	0.2484	0.7145	0.7145	0.8504	
126	0.5267	0.8504	0.1782	0.1710	0.6947	0.3145	0.5267	0.1492	0.2136	
127	0.8644	0.4215	0.2116	0.7145	0.8504	0.1782	0.4463	0.2136	0.8644	
128	0.8712	0.8712	0.3145	0.8504	0.9404	0.8644	0.3554	0.1782	0.8504	
129	0.8504	0.7145	0.8712	0.3554	0.1782	0.5267	0.1373	0.1492	0.2136	
130	0.8504	0.1741	0.3881	0.8712	0.3145	0.5267	0.2484	0.1741	0.9404	
131	0.9404	0.8644	0.2484	0.1741	0.4215	0.2136	0.9404	0.1932	0.8644	
132	0.1492	0.0872	0.6947	0.3145	0.4215	0.5267	0.3145	0.5267	0.8504	
133	0.1741	0.8504	0.2484	0.1492	0.6947	0.1216	0.8504	0.8644	0.1782	
134	0.8644	0.3881	0.2457	0.8712	0.1741	0.4215	0.3554	0.1741	0.8712	
135	0.4767	0.8644	0.3554	0.1492	0.8644	0.7145	0.2484	0.3775	0.8504	
136	1.0000	0.6947	0.1492	0.5267	0.2484	0.6947	0.1492	0.1492	0.8644	
137	0.6947	0.5267	0.3411	0.9404	0.3554	1.0000	0.5267	0.4215	0.4767	
138	0.5267	0.9404	0.1741	0.1492	0.2409	0.7145	0.2116	0.4215	0.0872	
139	0.4767	0.8712	0.5267	0.4767	0.5267	0.1216	0.8504	0.2484	0.2484	
140	0.5267	0.1782	0.2484	0.4215	0.4767	0.2409	0.9404	0.1216	0.1782	
141	0.2116	0.6947	0.1741	0.5267	0.9404	0.4463	0.3881	0.3775	0.3554	
142	0.7145	0.8712	0.9404	0.1741	0.5267	0.2484	0.1782	0.1492	0.6947	
143	0.2020	0.5267	1.0000	0.3145	0.5267	0.9404	0.2457	0.3775	0.8504	
144	0.8504	0.4463	0.8504	0.3145	1.0000	0.1782	0.1741	1.0000	0.4463	
145	0.3554	0.8644	0.3554	0.1710	1.0000	0.7145	0.7145	0.3775	0.6947	
146	0.2020	0.1492	0.3881	0.5267	0.8644	0.1288	0.8504	0.8712	0.2348	
147	0.2136	0.8644	0.2484	0.4215	0.8644	0.1741	0.8504	0.3145	0.1782	
148	1.0000	1.0000	0.1492	0.3881	1.0000	0.2020	0.9404	0.3002	0.2484	
149	0.1492	0.8504	0.8644	0.8504	0.8644	0.5267	1.0000	1.0000	0.9404	
150	0.2484	0.3554	0.7145	0.2150	0.9404	0.2457	0.3145	0.8644	0.7145	
151	0.4215	1.0000	0.8712	0.8504	1.0000	0.3881	0.7145	0.8644	1.0000	
152	0.5267	0.2020	0.7145	0.1216	0.4767	0.5267	0.4215	0.7145	0.7145	
153	0.1932	1.0000	0.7145	0.8504	1.0000	0.2136	0.4463	0.4215	0.9404	
154	0.1080	0.1741	0.7145	0.8644	0.9404	0.2348	0.2150	0.2484	0.3554	
155	0.8712	0.3554	0.8712	1.0000	0.8712	0.1278	1.0000	0.8644	0.2484	
156	0.1932	0.6947	0.2136	0.2484	1.0000	0.4215	0.4215	0.2020	0.7145	
157	0.5267	0.4215	0.6947	0.4215	0.2020	0.2484	0.7145	1.0000	0.3554	
158	0.8644	0.3554	0.7145	0.5267	0.8644	0.1932	0.2116	0.1492	0.7145	
159	0.8712	0.8644	0.5267	0.9404	0.3881	0.4215	0.8712	0.4457	0.8504	
160	1.0000	0.5267	0.2484	0.8504	0.2136	0.4215	0.8644	0.1288	0.2136	
161	0.3554	0.2136	0.2150	0.1741	0.3145	0.1741	1.0000	0.8644	0.9404	
162	0.8504	0.3554	0.8504	0.8504	0.5267	0.1373	0.3145	0.0784	0.8712	
163	0.4215	0.8712	0.8504	0.3554	0.1741	0.1492	0.2136	0.8712	0.3145	
164	0.1782	0.2484	0.1216	0.2020	0.1782	1.0000	0.1710	0.4767	0.8712	
165	0.3145	0.2484	0.3145	0.3881	0.8504	0.5267	0.2116	1.0000	0.2484	
166	0.2116	0.9404	0.2484	0.8644	0.5267	0.8504	0.2484	0.7145	0.5267	
167	0.4463	0.9404	0.1782	0.7145	0.5267	0.3411	0.2484	0.4215	0.3554	
168	0.9404	0.9404	0.4457	0.7145	0.4463	0.8712	0.4215	0.2484	0.2484	
169	0.8712	0.3881	0.1741	0.2116	0.1782	0.8644	0.8504	1.0000	0.8504	
170	0.3554	0.8712	0.2020	0.8712	0.4215	0.8504	0.5267	0.3002	0.4215	
171	1.0000	0.8712	0.3145	0.1373	0.9404	0.6947	0.7145	0.2020	0.4215	
172	0.2484	0.1216	0.8504	0.3881	0.8712	1.0000	0.1492	0.1492	0.1492	
173	0.2484	0.9404	0.8504	1.0000	0.8504	0.1492	0.2116	0.0872	0.2116	
174	0.3145	0.4215	0.3411	0.7145	0.3881	0.8644	0.4215	0.1782	0.2116	
175	0.8504	1.0000	0.8504	0.8504	0.7145	0.2457	0.8504	0.4767	0.4215	
176	0.8644	0.1373	0.8644	0.8504	0.8644	0.7145	0.4463	0.5267	0.8504	
177	0.1932	1.0000	0.8504	0.3881	0.3554	0.4457	0.8712	0.2484	0.3554	
178	0.4215	0.2484	0.3554	0.1373	0.7145	0.8504	0.1782	0.0784	0.6947	
179	0.4463	0.1932	0.4463	0.3881	0.8644	0.1492	0.5267	0.6947	0.5267	
180	0.1741	0.7145	0.1492	0.1741	1.0000	0.2136	0.2484	0.8712	0.1741	
181	0.8712	1.0000	0.8644	0.1216	0.8504	0.1492	0.8504	1.0000	0.5267	
182	0.5267	0.8712	0.8644	0.1932	0.5267	0.4215	0.4767	0.7145	0.7145	
183	0.7145	0.5267	0.1492	0.2484	0.7145	0.7145	0.8644	0.2409	0.5267	
184	0.3554	0.2136	0.7145	0.2484	1.0000	0.8644	0.1932	0.2136	0.3554	
185	0.7145	0.8644	0.6947	0.4215	0.1710	0.1288	0.8644	0.3145	0.8644	
186	0.8712	0.8644	0.8504	0.3145	1.0000	0.7145	0.8504	0.4215	0.3554	
187	0.5267	1.0000	0.2484	0.5267	0.7145	0.8504	0.9404	0.1932	1.0000	
188	1.0000	0.2484	0.8504	0.3145	0.3554	0.0872	0.1373	0.5267	0.2484	
189	0.1216	0.8644	0.4215	0.2116	0.4215	0.1288	0.3145	0.1492	0.8644	
190	0.4215	0.2136	0.4767	0.2484	0.8644	0.1932	0.8712	0.8644	1.0000	

Site	secD	rpsA	dnaA	lamB	tufA	lacI	ompA	araC	rplA	trpR
191	0.7145	1.0000	0.7145	1.0000	1.0000	0.3881	0.1741	0.7145	0.7145	
192	0.3145	0.8504	0.8712	0.2116	0.8644	0.2457	0.8504	0.5267	0.8644	
193	0.8644	0.4767	0.3554	0.7145	0.7145	0.3002	0.2136	0.1932	0.8644	
194	0.1932	1.0000	0.1782	0.2484	0.8504	0.7145	0.8504	0.2484	0.9404	
195	0.3554	0.9404	0.2484	0.5267	0.1741	0.8712	1.0000	0.1741	0.7145	
196	0.8712	0.3554	0.1216	0.9404	0.8644	0.8644	0.7145	0.5267	0.8644	
197	0.1492	0.8504	0.3554	0.1741	0.5267	0.8712	0.7145	0.4215	0.3554	
198	0.1782	0.4215	0.6947	0.5267	0.3881	0.8644	0.0872	0.1216	0.3554	
199	0.5267	0.9404	0.9404	0.6947	0.3145	0.7145	0.6947	0.1932	0.7145	
200	0.8644	0.3554	0.3145	0.8712	0.4215	0.8504	0.9404	0.2457	0.3554	
201	0.6947	0.2484	0.4767	0.1288	0.1782	0.1710	0.7145	0.7145	0.1782	
202	0.4215	0.2020	0.1492	0.7145	1.0000	0.1492	0.1782	0.2136	0.4463	
203	0.1932	0.4463	0.1373	0.2136	0.0872	0.3554	0.7145	0.1492	0.2136	
204	0.1932	0.5267	1.0000	0.4767	1.0000	0.3145	0.0872	0.9404	0.7145	
205	0.2136	0.3145	0.8712	1.0000	0.8712	0.2020	0.7145	0.2409	0.3554	
206	0.8504	0.8504	0.1741	0.4215	0.7145	0.4463	0.1782	0.4457	0.8504	
207	0.1932	0.7145	0.9404	0.2484	0.4215	0.8712	0.7145	0.3002	0.6947	
208	0.2484	0.1741	0.2136	0.1782	0.5267	0.2484	0.1782	0.1782	0.3145	
209	0.2136	0.9404	0.5267	0.8504	0.3554	0.1492	1.0000	0.3002	0.4215	
210	0.8644	0.5267	0.4767	0.8504	0.1782	0.4215	0.6947	0.8712	0.3554	
211	0.8712	0.8644	0.9404	0.2348	0.1741	0.2136	0.2136	0.8644	0.3554	
212	0.7145	0.8504	0.3554	0.1288	0.8644	0.1782	0.2116	0.2508	0.9404	
213	0.6947	0.8504	0.1216	1.0000	0.8644	0.4215	0.3554	0.1492	0.1932	
214	0.4767	0.9404	0.8644	0.8644	0.1782	0.7145	0.1492	0.2020	0.4215	
215	0.1932	0.5267	0.1492	0.8504	0.4215	1.0000	0.1741	0.1741	0.1373	
216	0.5267	0.8504	0.2484	0.2457	1.0000	0.0784	0.4463	0.8712	0.2116	
217	0.7145	0.8644	0.2484	0.5267	0.5267	1.0000	0.8644	0.2136	0.2116	
218	0.8712	0.8644	0.7145	0.3145	0.6947	0.8504	0.3554	0.2136	0.4767	
219	0.8644	0.1492	0.4215	0.8504	0.1741	0.5267	0.3881	0.1288	0.8504	
220	0.1932	0.4215	1.0000	0.8712	0.1373	0.1710	0.5267	0.3775	0.7145	
221	1.0000	0.4463	1.0000	0.1216	0.4215	0.1932	0.9404	0.4215	0.8504	
222	0.7145	0.5267	0.1741	0.2484	0.1373	0.1216	0.8644	0.1932	0.9404	
223	0.8712	0.4767	0.3554	0.4457	0.8504	0.4767	0.1741	0.2457	0.7145	
224	1.0000	0.1216	0.8712	0.8712	0.8712	0.1373	0.2484	0.1288	0.9404	
225	0.3145	0.1710	0.3145	0.5267	0.8504	0.8504	0.1741	0.1932	0.5267	
226	0.7145	0.3554	0.3145	0.2484	0.2116	0.1741	0.2484	0.1710	0.2136	
227	0.6947	0.8712	0.8712	0.3145	0.9404	0.1492	0.3554	0.8712	0.7145	
228	0.2136	0.9404	0.1373	0.8712	0.9404	0.1492	0.7145	1.0000	0.8504	
229	0.2136	0.3554	0.6947	0.8644	0.2116	0.2116	0.2116	0.5267	0.8644	
230	0.2484	0.1492	0.5267	0.9404	0.8504	0.4767	0.8644	0.1492	0.1932	
231	0.4215	0.1782	0.7145	0.5267	0.8712	0.1492	0.3554	0.8712	0.7145	
232	0.2484	0.1932	0.8644	0.8504	0.6947	0.4767	0.1782	0.4215	0.3881	
233	0.4215	1.0000	0.8644	0.7145	1.0000	0.8644	1.0000	0.1932	0.6947	
234	0.8644	0.4215	0.4215	0.3002	0.8712	0.2484	0.8504	0.2136	0.2484	
235	0.8712	0.2457	0.5267	0.3554	0.8504	1.0000	0.2136	0.7145	0.0000	
236	0.2484	0.2484	0.5267	0.5267	0.4215	0.8504	0.7145	0.3554		
237	0.8712	0.6947	0.4215	0.8504	0.4215	0.4215	0.7145	0.8644		
238	0.6947	0.8504	0.2136	0.1710	0.3554	0.9404	0.8644	0.2020		
239	0.2484	0.5267	0.1741	0.1288	0.9404	0.1278	0.5267	0.4457		
240	0.1492	1.0000	0.1741	0.1741	0.8504	0.4463	0.2136	0.1932		
241	0.2020	0.4215	0.7145	0.4463	1.0000	0.7145	0.8644	0.4463		
242	0.8504	0.4463	0.2484	0.7145	1.0000	0.4767	0.3145	0.2116		
243	0.6947	0.9404	0.3554	1.0000	0.9404	0.8644	0.1932	0.0784		
244	0.7145	0.3554	1.0000	0.1492	1.0000	0.9404	0.2136	0.4767		
245	1.0000	0.6947	0.8712	0.4463	0.4215	0.1216	0.8644	0.2150		
246	0.1782	0.8644	0.3881	0.2136	0.9404	0.2484	0.1932	0.4215		
247	0.6947	0.3554	0.2136	0.1932	0.8504	0.5267	0.2484	0.1216		
248	0.9404	0.1741	1.0000	0.2457	0.4215	0.2136	0.8644	0.2116		
249	0.2136	0.5267	1.0000	0.8644	0.3554	0.4767	0.5267	0.2457		
250	0.8712	0.8712	0.1741	0.3554	1.0000	0.7145	0.1782	0.8504		
251	0.2136	1.0000	0.1741	0.8504	0.4463	0.8644	0.3554	0.8712		
252	0.8504	0.8712	0.1492	0.1741	0.2136	0.8504	0.5267	0.2484		
253	0.7145	0.2116	0.2116	0.2484	0.3554	0.7145	0.8504	0.9404		
254	0.5267	0.8712	0.1741	0.3554	0.3881	0.4767	0.1373	0.8504		
255	0.8712	0.6947	0.2484	0.1741	0.2116	0.8712	0.6947	0.1741		
256	0.4215	0.1373	0.1216	0.9404	0.2409	0.1216	0.9404	0.5267		
257	0.9404	0.8644	0.8644	0.9404	0.4463	0.4215	0.9404	0.5267		
258	0.9404	0.8504	0.8644	0.2136	0.8504	0.2116	0.8644	0.1492		
259	1.0000	0.8644	1.0000	0.3145	0.9404	1.0000	0.8504	0.2020		
260	0.8644	0.3554	0.8504	0.7145	1.0000	0.1373	0.3145	0.3145		
261	0.0872	0.2136	0.2484	0.4463	0.4767	0.3775	0.2116	0.1741		
262	0.8504	0.8644	0.1492	0.5267	0.1741	0.8644	0.5267	0.3002		
263	0.4215	0.8504	0.2136	0.3002	0.8712	0.8712	0.8712	0.8712		
264	0.2136	1.0000	0.4215	0.4767	0.3554	0.9404	0.4215	0.6947		
265	0.5267	0.5267	0.4215	0.2116	0.8644	0.8504	0.8504	0.1741		

Site	secD	rpsA	dnaA	lamB	tufA	lacI	ompA	araC	rplA	trpR
266	0.4463	0.1782	0.2020	0.3002	0.8644	0.7145	0.3881	0.3554		
267	0.7145	0.1710	0.2116	0.2136	0.5267	0.5267	0.5267	0.3554		
268	0.8712	0.6947	0.3002	0.8504	1.0000	0.4215	0.7145	0.2409		
269	0.7145	0.7145	0.5267	0.3554	0.8504	0.3002	0.3145	0.2116		
270	0.3554	0.4215	0.8712	0.3775	0.8712	0.6947	0.2484	0.3775		
271	1.0000	0.7145	0.3145	0.8644	0.7145	0.6947	0.2136	0.1216		
272	0.4215	0.3554	0.1782	0.3002	0.8504	0.1888	0.8504	0.1932		
273	0.8644	0.8712	0.3554	0.2136	1.0000	0.3145	0.8644	0.1782		
274	0.8504	0.3145	1.0000	0.8504	0.2484	0.5267	0.1373	0.1932		
275	0.7145	0.1782	0.4215	0.3881	0.6947	0.5267	1.0000	1.0000		
276	0.3411	1.0000	0.2484	0.8504	0.8504	0.2116	0.8712	0.1741		
277	0.7145	0.8504	0.8504	0.9404	0.9404	1.0000	0.8712	0.8712		
278	0.3411	0.2116	0.9404	0.7145	0.8644	0.5267	0.7145	0.1216		
279	0.8644	0.3554	1.0000	0.1741	0.8644	0.1932	0.2136	0.8504		
280	1.0000	0.8644	0.5267	0.5267	0.8712	0.2508	0.3881	0.2409		
281	0.1741	0.4463	0.8712	0.2484	0.8504	0.2409	0.9404	1.0000		
282	0.8712	0.8504	0.4457	1.0000	0.4215	0.3145	0.9404	1.0000		
283	0.8644	0.8712	0.3554	0.3554	0.3554	0.4215	0.5267	0.3554		
284	0.6947	0.6947	0.1373	0.1741	0.8712	0.1782	0.3145	0.6947		
285	0.2484	0.2116	0.8712	0.1216	1.0000	0.1782	0.8644	0.2484		
286	0.2116	0.2484	0.1741	0.3145	1.0000	0.1288	0.4215	0.5267		
287	0.2484	0.8644	0.8504	0.2484	0.4215	0.2116	0.1373	0.6947		
288	0.9404	0.2116	0.1710	0.4215	1.0000	0.2116	0.3554	0.1216		
289	0.5267	0.5267	0.1888	0.2484	0.8712	0.4215	0.8504	0.2457		
290	0.2136	0.3145	0.8644	0.2484	0.8504	0.3554	0.4215	0.3554		
291	0.1216	0.8504	0.4463	0.2484	0.2136	0.2136	0.1782	0.4457		
292	0.7145	0.2409	0.6947	0.8504	0.6947	0.5267	0.7145	0.2508		
293	0.7145	0.1741	0.7145	0.1492	0.8644	0.1741	0.5267			
294	0.7145	0.9404	0.4215	0.4767	0.7145	0.8712	0.3554			
295	0.1373	1.0000	1.0000	0.8644	0.3554	0.8644	0.4215			
296	0.8504	0.4215	0.1782	0.8712	0.1782	0.8644	0.1373			
297	0.8712	1.0000	0.0872	0.4215	0.8504	0.3775	0.7145			
298	0.6947	1.0000	1.0000	0.2020	0.2116	0.1492	0.8712			
299	0.1782	0.8504	0.8644	0.5267	0.4215	0.2116	0.8504			
300	0.8504	0.9404	1.0000	0.1492	0.3554	0.1932	0.4767			
301	0.5267	1.0000	0.2116	0.8504	0.1782	0.6947	0.8504			
302	0.3881	0.8504	0.8712	0.7145	0.1492	0.5267	1.0000			
303	1.0000	0.8644	0.6947	0.4215	0.2116	0.8712	0.1373			
304	0.6947	0.6947	0.7145	0.1373	0.3554	0.4457	0.2484			
305	0.3554	0.1492	0.4215	0.4767	0.1741	0.8644	0.1782			
306	0.2136	0.9404	0.8644	0.8504	1.0000	0.1492	0.9404			
307	0.2116	0.1373	0.4767	0.5267	0.3881	0.2020	0.4463			
308	0.8712	1.0000	0.3554	0.2484	1.0000	0.3881	0.8504			
309	1.0000	0.4767	0.3554	0.1710	0.6947	0.2136	0.2484			
310	0.8504	0.5267	0.1216	0.5267	0.3145	0.8504	0.2116			
311	0.2136	0.1710	0.5267	0.4767	0.4215	0.2136	0.2409			
312	0.0872	0.2116	1.0000	0.4767	0.8644	0.7145	0.5267			
313	0.9404	0.2484	0.2484	0.3145	0.1373	0.6947	0.2484			
314	0.6947	0.3554	0.5267	0.6947	0.3554	0.3554	0.6947			
315	0.8644	0.2484	0.4215	0.8504	0.5267	0.8504	0.3554			
316	0.3145	0.4215	0.8712	0.4767	1.0000	0.2484	0.2136			
317	0.3554	0.1492	0.4457	0.3145	0.8504	0.2136	0.8712			
318	0.8712	0.1782	0.1782	0.2136	0.8504	0.8644	0.7145			
319	0.6947	0.1373	0.8504	0.5267	0.8712	0.4457	0.7145			
320	0.4215	0.3554	1.0000	0.4215	0.1492	0.1278	0.8644			
321	0.8644	0.9404	0.6947	0.2484	0.4463	0.2457	0.4215			
322	0.2116	0.9404	0.7145	0.1710	0.1782	0.2508	0.5267			
323	0.8504	0.2484	0.1741	0.5267	0.1741	0.8644	0.2409			
324	0.5267	0.9404	0.1741	0.2484	0.1741	0.6947	0.8644			
325	0.1492	0.8504	0.4215	0.5267	0.3554	0.3554	0.7145			
326	0.4215	0.5267	0.1216	0.2484	0.8504	0.1199	0.1782			
327	0.2116	0.6947	0.3554	0.8504	0.3145	0.3554	0.5267			
328	0.5267	0.6947	0.8712	0.2116	0.8712	0.2116	0.8712			
329	0.1373	1.0000	0.1080	0.3554	0.1782	0.2116	0.8712			
330	0.4463	0.9404	0.8712	0.1710	0.2136	0.8644	0.6947			
331	0.1373	0.4767	0.3881	0.1710	0.1741	0.7145	1.0000			
332	0.1932	0.9404	0.2484	0.2116	0.3145	0.1278	0.4215			
333	0.2136	0.8644	0.6947	0.2457	0.1741	0.2484	1.0000			
334	0.5267	0.5267	0.8712	0.8504	0.8712	0.3411	0.9404			
335	1.0000	0.4215	1.0000	0.4215	0.4463	0.1492	0.3554			
336	0.3145	0.5267	0.8644	0.8712	0.4463	0.2116	0.8504			
337	0.2484	1.0000	1.0000	0.1782	0.5267	0.1216	0.4215			
338	0.1492	1.0000	0.3775	0.4767	0.6947	0.3881	0.3554			
339	0.1782	0.8712	0.7145	0.3145	0.4463	0.1278	0.5267			
340	0.2136	0.8712	0.8644	0.3554	0.8504	0.8712	0.9404			

Site	secD	rpsA	dnaA	lamB	tufA	lacI	ompA	araC	rplA	trpR
341	0.9404	0.8712	0.2484	0.1710	0.2116	0.7145	0.6947			
342	0.2484	0.4215	0.8712	0.3411	0.4215	0.4457	0.4463			
343	0.4215	0.1373	0.2457	0.0872	1.0000	0.1216	0.2136			
344	0.3002	0.8644	0.4215	0.4215	0.8644	0.5267	0.1782			
345	0.2020	0.8504	0.1216	0.4767	0.1782	0.2508	0.2136			
346	0.5267	0.8644	0.2484	0.1932	1.0000	0.1288	0.7145			
347	0.1932	0.3554	0.1216	0.2116	0.8504	0.4767				
348	0.7145	0.2136	0.2484	0.6947	0.6947	0.2136				
349	0.8504	0.2409	0.1741	0.4767	1.0000	0.8644				
350	0.8504	0.3554	0.2116	1.0000	0.4767	0.7145				
351	0.2484	0.7145	0.1888	0.4215	0.6947	0.8712				
352	0.4215	0.2484	0.0784	0.8504	0.4767	0.2136				
353	0.4767	0.1782	0.7145	0.3145	0.1782	0.9404				
354	0.3881	0.1710	0.4215	0.5267	0.8504	0.1373				
355	0.2484	0.2136	0.2116	0.2484	0.5267	0.8712				
356	0.1741	0.2136	0.4215	0.2457	0.2484	0.8644				
357	0.4463	0.1741	0.5267	1.0000	0.4215	1.0000				
358	0.3554	0.7145	0.1741	0.1373	0.3554	0.1932				
359	0.5267	1.0000	0.6947	0.2136	0.4767	0.3775				
360	0.2484	0.2116	0.8712	0.8712	0.9404	0.2136				
361	0.4215	0.1492	1.0000	0.2116	0.9404	0.0000				
362	0.8504	0.2484	0.7145	0.8504	0.2116					
363	0.3554	0.3554	0.8644	0.5267	0.8644					
364	0.1782	0.8504	0.8712	0.3554	0.4215					
365	0.4767	0.5267	0.5267	0.2484	0.1492					
366	0.7145	0.8712	0.4457	0.2484	0.1782					
367	0.2116	0.9404	0.8644	0.2136	0.4215					
368	0.8644	1.0000	0.7145	0.3145	0.7145					
369	0.1741	0.8504	0.4457	0.3554	0.4767					
370	0.6947	0.3554	0.2136	0.4215	0.5267					
371	1.0000	0.4215	1.0000	0.2116	0.5267					
372	0.3145	0.3554	0.3554	0.2020	0.8504					
373	0.3554	0.3881	0.8644	0.7145	0.8644					
374	0.5267	0.4215	0.2457	0.1492	0.8712					
375	0.1932	0.4463	0.2116	0.1492	0.1741					
376	0.8504	0.5267	0.4215	0.1710	0.7145					
377	0.3554	0.1741	0.5267	0.2136	0.4215					
378	0.3554	0.8504	0.2484	0.7145	0.8712					
379	0.5267	0.4215	0.4215	0.8504	1.0000					
380	0.7145	0.1741	0.2136	0.5267	0.8504					
381	0.2484	0.4215	0.3554	0.1932	0.8504					
382	0.8504	0.8504	0.3411	0.4215	0.8712					
383	0.8712	0.4457	0.6947	0.1710	0.2116					
384	0.7145	0.5267	0.7145	0.2508	0.9404					
385	0.9404	0.8504	1.0000	0.8712	0.8504					
386	0.8644	0.8504	0.3145	0.1782	0.7145					
387	0.6947	0.4215	0.3145	0.7145	0.8504					
388	0.3554	0.5267	0.3554	0.4215	0.9404					
389	0.2136	0.8504	0.4215	0.8712	0.9404					
390	1.0000	0.8644	0.3554	0.2457	0.7145					
391	1.0000	0.9404	0.2457	0.1741	0.3554					
392	0.6947	0.1492	0.7145	0.7145	0.9404					
393	0.4215	0.8644	0.5267	0.2116	0.8644					
394	0.2484	0.3881	0.2020	0.3145	0.8504					
395	0.4215	0.5267	0.2020	0.1216	0.0000					
396	0.1216	0.4215	0.1373	0.3554						
397	0.2484	0.1373	0.3554	0.1710						
398	0.4215	0.1710	0.8712	0.5267						
399	0.2136	0.2484	0.8712	1.0000						
400	0.3881	0.9404	0.1373	0.3554						
401	0.8712	0.7145	0.8712	0.1710						
402	0.8644	0.8504	0.3002	0.8504						
403	0.8504	1.0000	0.6947	0.3145						
404	0.2484	1.0000	0.7145	0.5267						
405	0.1932	0.7145	0.8712	0.3145						
406	0.1741	0.9404	0.1782	0.2116						
407	0.8712	0.8712	0.8712	0.8504						
408	0.4215	1.0000	0.2136	0.2484						
409	0.2116	0.3145	0.4767	0.7145						
410	0.8504	0.3554	0.7145	0.5267						
411	0.4215	0.3554	0.4767	0.2484						
412	0.2484	0.8504	0.7145	0.2484						
413	0.2484	0.5267	0.8644	0.7145						
414	0.1782	1.0000	0.7145	0.2484						
415	0.2484	0.4215	0.3554	0.1741						

Site	secD	rpsA	dnaA	lamB	tufA	lacI	ompA	araC	rplA	trpR
416	1.0000	0.7145	1.0000	0.8504						
417	0.1216	0.7145	0.8644	0.3554						
418	0.8712	0.9404	0.4463	0.1216						
419	0.2136	0.9404	0.2484	0.9404						
420	0.8644	0.8644	0.1492	0.2150						
421	0.2508	0.2136	0.1932	0.7145						
422	0.8644	0.9404	0.8644	0.5267						
423	0.8644	0.5267	0.1782	0.1741						
424	0.8644	0.7145	1.0000	0.2484						
425	0.8712	1.0000	0.4215	0.8504						
426	0.1216	0.8712	0.8504	0.8504						
427	0.8504	1.0000	0.5267	0.1932						
428	0.7145	0.8712	0.7145	0.1741						
429	0.4457	0.4215	0.1741	0.8504						
430	0.4215	0.1373	0.8504	0.8712						
431	0.7145	0.8644	0.8504	0.8504						
432	0.1782	0.8504	0.8712	0.5267						
433	0.4215	0.9404	0.5267	0.1932						
434	0.2136	0.3554	0.1492	0.5267						
435	0.4215	0.2136	0.3411	1.0000						
436	0.9404	0.2020	0.3411	0.1710						
437	1.0000	0.7145	0.6947	0.2116						
438	1.0000	1.0000	0.2020	0.1741						
439	0.8712	0.5267	0.1492	0.8504						
440	0.2116	0.1782	0.1216	0.1216						
441	0.4215	0.1741	0.2409	0.2136						
442	0.8504	0.2484	0.8712	0.4767						
443	0.0872	0.2484	0.3554	1.0000						
444	0.2116	0.1710	0.4215	0.4215						
445	0.8644	0.9404	1.0000	0.1710						
446	0.8504	0.7145	0.2136	0.1710						
447	0.4767	0.8644	0.4457							
448	0.2136	0.2484	0.8712							
449	0.2484	0.3554	1.0000							
450	0.4215	0.3554	1.0000							
451	1.0000	0.8504	0.1932							
452	0.2136	0.7145	0.1492							
453	0.3775	0.4215	0.5267							
454	0.8644	0.6947	0.4215							
455	1.0000	0.2116	0.3554							
456	0.7145	0.8504	1.0000							
457	0.2409	0.3554	0.5267							
458	0.2020	0.6947	0.1741							
459	0.1216	0.4463	0.2508							
460	0.8504	0.7145	0.2484							
461	0.8644	0.9404	0.1288							
462	0.8644	0.5267	0.4215							
463	0.9404	0.7145	0.1199							
464	0.3881	0.3554	0.2348							
465	0.4215	0.8504	0.4457							
466	0.8644	0.7145	0.2508							
467	0.1741	0.2116	0.3002							
468	0.4767	0.6947								
469	0.4215	1.0000								
470	0.4215	0.8644								
471	0.1741	0.7145								
472	0.3145	0.5267								
473	0.3554	0.8504								
474	0.3554	0.9404								
475	0.1741	1.0000								
476	0.8504	0.8504								
477	0.8644	0.3145								
478	0.4215	0.8644								
479	0.7145	0.8712								
480	0.2116	0.7145								
481	0.1932	0.3881								
482	0.7145	1.0000								
483	0.8644	0.7145								
484	0.4215	0.1373								
485	0.1216	0.8712								
486	0.2484	0.5267								
487	0.4457	0.8712								
488	0.4215	0.9404								
489	0.1288	1.0000								
490	0.4215	0.5267								

Site	secD	rpsA	dnaA	lamB	tufA	lacI	ompA	araC	rplA	trpR
491	0.2457	0.7145								
492	0.8504	0.2116								
493	0.4215	0.8644								
494	0.4767	0.9404								
495	0.3002	0.8644								
496	0.8644	0.1932								
497	0.4457	0.9404								
498	0.0872	0.8504								
499	0.8504	0.5267								
500	0.7145	1.0000								
501	0.3411	0.9404								
502	0.8644	1.0000								
503	0.1932	0.7145								
504	0.4767	0.3554								
505	0.0872	0.1741								
506	0.8504	0.2116								
507	0.4215	0.8504								
508	0.7145	0.9404								
509	0.8504	0.5267								
510	0.4215	0.8712								
511	0.2457	0.3554								
512	0.1288	0.2484								
513	0.2116	0.8712								
514	0.2020	0.7145								
515	0.7145	0.4215								
516	0.6947	0.1932								
517	0.7145	0.8644								
518	0.2457	0.3881								
519	0.5267	0.9404								
520	0.7145	0.8712								
521	0.2484	0.7145								
522	0.6947	0.3554								
523	0.8644	0.5267								
524	0.4215	1.0000								
525	0.2484	0.7145								
526	1.0000	0.5267								
527	0.8712	1.0000								
528	0.4215	0.3554								
529	0.3554	0.5267								
530	1.0000	0.7145								
531	1.0000	0.4215								
532	0.4457	0.7145								
533	0.1932	0.4463								
534	0.2484	0.9404								
535	0.1888	0.2484								
536	0.8712	0.3554								
537	0.4463	0.2136								
538	0.9404	1.0000								
539	0.1492	0.5267								
540	0.2136	0.7145								
541	0.7145	0.2484								
542	0.4215	0.1741								
543	0.5267	0.1373								
544	1.0000	0.2484								
545	0.8504	0.2484								
546	0.3145	0.7145								
547	0.8712	0.4767								
548	0.8504	0.7145								
549	0.7145	1.0000								
550	0.1741	0.7145								
551	0.1932	0.1741								
552	0.3881	0.3554								
553	0.4215	0.7145								
554	0.1741	0.7145								
555	0.5267	0.3554								
556	0.7145	0.8504								
557	0.2484	1.0000								
558	0.4215	0.0000								
559	0.2116									
560	0.3411									
561	0.8644									
562	0.4215									
563	0.3554									
564	0.2457									
565	0.4215									

Site	secD	rpsA	dnaA	lamB	tufA	lacI	ompA	araC	rplA	trpR
566	0.4215									
567	0.8644									
568	0.3145									
569	0.7145									
570	0.6947									
571	0.8504									
572	0.2116									
573	0.3775									
574	0.7145									
575	0.4215									
576	0.3554									
577	0.3775									
578	0.1741									
579	0.7145									
580	0.4215									
581	0.4463									
582	0.2116									
583	0.8504									
584	0.4215									
585	0.8504									
586	0.6947									
587	0.7145									
588	0.3411									
589	0.3002									
590	0.4767									
591	0.1741									
592	0.2116									
593	0.7145									
594	0.4215									
595	0.2457									
596	0.8504									
597	0.3411									
598	0.8712									
599	0.1216									
600	0.4215									
601	0.6947									
602	0.2484									
603	0.8644									
604	0.1080									
605	0.3145									
606	0.8504									
607	0.8504									
608	0.3554									
609	0.8712									
610	0.2457									
611	0.3554									
612	0.3554									
613	0.8644									
614	0.2508									
615	0.4215									

Appendix D

Sample Computer Code

```
#include "lattice.h"
#include "ran2.h"
#include <iostream>
#include <sstream>
#include <fstream>
#include <ctime>
#include <cmath>
#include <string>
using namespace std;

#define PI 3.1415926535898

string itos(int i);
bool FileExists(string fname);

int main(int argc, char *argv[])
{
  if(argc != 9)
  {
    cout << "Incorrect parameters...Stopping program.\n";
    cout << "Correct syntax is:\n";
    cout<< argv[0] << " L1 L2 L3 Alpha Beta N_tot Nruns N*\n";
    return 0;
  }
  //Declare constant parameters
  const int L1 = atoi(argv[1]);
  const int L2 = atoi(argv[2]);
  const int L3 = atoi(argv[3]);
```

```
const int MT = 1000000;
const int SS = 100000;
const int interval = 100;
const int MI = MT/interval;
const double pa = atof(argv[4]);
const double pb = atof(argv[5]);
int N_star = atoi(argv[8]);
const int Mrun = atoi(argv[7]);
const int n = atoi(argv[6]);
//Declare variables
int N1_t;
int N2_t;
int N3_t;
int value;
double rho1[Mrun];
double rho2[Mrun];
double rho3[Mrun];
double J1_in[Mrun];
double J2_in[Mrun];
double J3_in[Mrun];
double J1_out[Mrun];
double J2_out[Mrun];
double J3_out[Mrun];
double profile1[L1];
double profile2[L2];
double profile3[L3];
double pae;
int rs;
int N_res;
long idum;
string line;
ofstream fileout;
ifstream filein;
//Build filenames to include L, n, alpha, and beta
string filename1 = "density";
string filename2 = "N_t";
string filename3 = "profile";
string laststate = "last-state";
string fileend = "-1L";
fileend += itos(L1);
fileend += "-2L";
fileend += itos(L2);
```

```
fileend += "-3L";
fileend += itos(L3);
fileend += "-N";
fileend += itos(n);
fileend += "-A";
fileend += itos((int)(pa*100.0+0.1));
fileend += "-B";
fileend += itos((int)(pb*100.0+0.1));
fileend += ".txt";
filename1 += fileend;
filename2 += fileend;
filename3 += fileend;
laststate += fileend;
cout << L1 << "\n";
cout << L2 << "\n";
cout << L3 << "\n";
cout << pa << "\n";
cout << pb << "\n";
cout << n << "\n";
cout << Mrun << "\n";
//Initialize lattice, arrays, and random number generator
Lattice lat1(L1, pa, pb);
Lattice lat2(L2, pa, pb);
Lattice lat3(L3, pa, pb);
idum=-1*(long)time(NULL);
for(int i=0; i<Mrun; i++)
{
  rho1[i] = 0.0;
  rho2[i] = 0.0;
  rho3[i] = 0.0;
  J1_in[i] = 0.0;
  J2_in[i] = 0.0;
  J3_in[i] = 0.0;
  J1_out[i] = 0.0;
  J2_out[i] = 0.0;
  J3_out[i] = 0.0;
}
for(int i=0; i<L1; i++)
{
  profile1[i] = 0.0;
}
for(int i=0; i<L2; i++)
```

```
{
  profile2[i] = 0.0;
}
for(int i=0; i<L3; i++)
{
  profile3[i] = 0.0;
}
cout << "Initialization done.\n";
//Start runs
//Reach Steady-state
if(FileExists(laststate))
{
  filein.open(laststate.c_str());
  for(int s=0; s<L1; s++)
  {
    getline(filein, line);
    value = atoi(line.substr(0, 1).c_str());
    lat1.SetSite(s, value);
    if(s<L2)
    {
      value = atoi(line.substr(2, 1).c_str());
      lat2.SetSite(s, value);
    }
    if(s<L3)
    {
      value = atoi(line.substr(4, 1).c_str());
      lat3.SetSite(s, value);
    }
  }
}
if(!FileExists(laststate))
{
  N_res = n;
  lat1.Reset();
  lat2.Reset();
  lat3.Reset();
  pae = pa*tanh((double)N_res/(double)N_star);
  lat1.SetAlpha(pae);
  lat2.SetAlpha(pae);
  lat3.SetAlpha(pae);
  for(int t=0; t<SS; t++)
  {
```

```
    for(int i=0; i<L1+L2+L3+3; i++)
    {
      rs = (int)(ran2(&idum)*(L1+L2+L3+3));
      if(rs <= L1)
      {
        lat1.Move(rs);
      }
      if((rs > L1) && (rs <=L1+L2+1))
      {
        lat2.Move(rs-L1-1);
      }
      if(rs > L1+L2+1)
      {
        lat3.Move(rs-L1-L2-2);
      }
      N_res = n - lat1.GetN() - lat2.GetN() - lat3.GetN();
      pae = pa*tanh((double)N_res/(double)N_star);
      lat1.SetAlpha(pae);
      lat2.SetAlpha(pae);
      lat3.SetAlpha(pae);
    }
  }
}
N_res = n - lat1.GetN() - lat2.GetN() - lat3.GetN();
pae = pa*tanh((double)N_res/(double)N_star);
lat1.SetAlpha(pae);
lat2.SetAlpha(pae);
lat3.SetAlpha(pae);
cout << "Steady-state reached.\n";
lat1.SetSS(true);
lat2.SetSS(true);
lat3.SetSS(true);
if(FileExists(filename2))
{
  fileout.open(filename2.c_str(), ios::app);
}
if(!FileExists(filename2))
{
  fileout.open(filename2.c_str());
  fileout << "L1=" << L1 << "\n";
  fileout << "L2=" << L2 << "\n";
  fileout << "L3=" << L3 << "\n";
```

```
  fileout << "MCS=" << MT << "\n";
  fileout << "SS=" << SS << "\n";
  fileout << "Interval=" << interval << "\n";
  fileout << "Alpha=" << pa << "\n";
  fileout << "Beta=" << pb << "\n";
  fileout << "N_tot=" << n << "\n";
  fileout << "N*=" << N_star << "\n";
  fileout << "run,t,N1,N2,N3" << endl;
}
//Start collecting data
for(int r=0; r<Mrun; r++)
{
  cout << "Starting run " << r << ".\n";
  lat1.ResetJ();
  lat2.ResetJ();
  lat3.ResetJ();
  for(int t=0; t<MT; t++)
  {
    for(int i=0; i<L1+L2+L3+3; i++)
    {
      rs = (int)(ran2(&idum)*(L1+L2+L3+3));
      if(rs <= L1)
      {
        lat1.Move(rs);
      }
      if((rs > L1) && (rs <= L1+L2+1))
      {
        lat2.Move(rs-L1-1);
      }
      if(rs > L1+L2+1)
      {
        lat3.Move(rs-L1-L2-2);
      }
      N_res = n - lat1.GetN() - lat2.GetN() - lat3.GetN();
      pae = pa*tanh((double)N_res/(double)N_star);
      lat1.SetAlpha(pae);
      lat2.SetAlpha(pae);
      lat3.SetAlpha(pae);
    }
    if(t%interval == 0)
    {
      N1_t = lat1.GetN();
```

```
      N2_t = lat2.GetN();
      N3_t = lat3.GetN();
      for(int s=0; s<L1; s++)
      {
        profile1[s] += (double)lat1.GetSite(s);
      }
      for(int s=0; s<L2; s++)
      {
        profile2[s] += (double)lat2.GetSite(s);
      }
      for(int s=0; s<L3; s++)
      {
        profile3[s] += (double)lat3.GetSite(s);
      }
      fileout << r << "," << t << "," << N1_t;
      fileout << "," << N2_t << "," << N3_t << endl;
      rho1[r] += (double)N1_t/(double)(MI*L1);
      rho2[r] += (double)N2_t/(double)(MI*L2);
      rho3[r] += (double)N3_t/(double)(MI*L3);
    }
  }
  J1_in[r] = (double)lat1.GetN_in()/(double)MT;
  J1_out[r] = (double)lat1.GetN_out()/(double)MT;
  J2_in[r] = (double)lat2.GetN_in()/(double)MT;
  J2_out[r] = (double)lat2.GetN_out()/(double)MT;
  J3_in[r] = (double)lat3.GetN_in()/(double)MT;
  J3_out[r] = (double)lat3.GetN_out()/(double)MT;
}
fileout.close();
for(int s=0; s<L1; s++)
{
  profile1[s] /= (double)(Mrun*MI);
}
for(int s=0; s<L2; s++)
{
  profile2[s] /= (double)(Mrun*MI);
}
for(int s=0; s<L3; s++)
{
  profile3[s] /= (double)(Mrun*MI);
}
//Write file
```

```
if(FileExists(filename1))
{
  fileout.open(filename1.c_str(), ios::app);
}
if(!FileExists(filename1))
{
  fileout.open(filename1.c_str());
  fileout << "L1=" << L1 << "\n";
  fileout << "L2=" << L2 << "\n";
  fileout << "L3=" << L3 << "\n";
  fileout << "MCS=" << MT << "\n";
  fileout << "SS=" << SS << "\n";
  fileout << "Interval=" << interval << "\n";
  fileout << "Alpha=" << pa << "\n";
  fileout << "Beta=" << pb << "\n";
  fileout << "N_tot=" << n << "\n";
  fileout << "N*=" << N_star << "\n";
  fileout << "run,rho1,rho2,rho3,J1_in,J2_in,J3_in,";
  fileout << "J1_out,J2_out,J3_out\n";
}
for(int r=0; r<Mrun; r++)
{
  fileout << r << "," << rho1[r] << ",";
  fileout << rho2[r] << "," << rho3[r] << ",";
  fileout << J1_in[r] << "," << J2_in[r] << ",";
  fileout << J3_in[r] << "," << J1_out[r] << ",";
  fileout << J2_out[r] << "," << J3_out[r] << "\n";
}
fileout.close();
if(FileExists(filename3))
{
  fileout.open(filename3.c_str(), ios::app);
}
if(!FileExists(filename3))
{
  fileout.open(filename3.c_str());
  fileout << "L1=" << L1 << "\n";
  fileout << "L2=" << L2 << "\n";
  fileout << "L3=" << L3 << "\n";
  fileout << "MCS=" << MT << "\n";
  fileout << "SS=" << SS << "\n";
  fileout << "Interval=" << interval << "\n";
```

```
    fileout << "Alpha=" << pa << "\n";
    fileout << "Beta=" << pb << "\n";
    fileout << "N_tot=" << n << "\n";
    fileout << "N*=" << N_star << "\n";
    fileout << "i,rho1_i,rho2_i,rho3_i\n";
  }
  for(int s=0; s<L1; s++)
  {
    fileout << s+1 << "," << profile1[s];
    if(s < L2)
    {
      fileout << "," << profile2[s];
    }
    if(s < L3)
    {
      fileout << "," << profile3[s];
    }
    fileout << "\n";
  }
  fileout.close();
  fileout.open(laststate.c_str());
  for(int s=0; s<L1; s++)
  {
    fileout << lat1.GetSite(s);
    if(s<L2)
    {
      fileout << "," << lat2.GetSite(s);
    }
    if(s<L3)
    {
      fileout << "," << lat3.GetSite(s);
    }
    fileout << "\n";
  }
  fileout.close();
  cout << "File written.\n";
  return 0;
}

string itos(int i)
{
  stringstream s;
```

```
  s << i;
  return s.str();
}

bool FileExists(string fname)
{
  ifstream fin;
  fin.open(fname.c_str());
  if(fin.good())
  {
    fin.close();
    return true;
  }
  else
  {
    fin.close();
    return false;
  }
}
```